ENERGY TRANSFORMED FLAGSHIP
www.csiro.au

Environmental Impacts of Amine-based CO_2 Post Combustion Capture (PCC) Process

Deliverable 4.2: Determination of the fate of PCC emissions into the atmosphere

Dennys Angove, Stephen White, Anne Tibbett, Ian Campbell, Kathryn Emmerson, Martin Cope, Michael Patterson, Paul Feron, Merched Azzi

5 July 2013

Prepared for Australian National Low Emissions Coal Research and Development

4-0910-0067

Australian National Low Emissions Coal Research & Development

Citation

Angove DE, White SJ, Tibbett AR, Campbell I, Emmerson KM, Cope ME, Patterson MP, Feron PMH, Azzi M (2013). Deliverable 4.2: Determination of the fate of PCC emissions into the atmosphere. Prepared for: ANLEC R&D. CSIRO, Australia.

Copyright and disclaimer

Important disclaimer

Contents

Figures

Tables

Acknowledgments

The authors wish to acknowledge financial assistance provided through Australian National Low Emissions Coal Research and Development (ANLEC R&D). ANLEC R&D is supported by Australian Coal Association Low Emissions Technology Limited and the Australian Government through the Clean Energy Initiative.

The authors would like to thank the appointed ANLEC Reviewers Geoff Bongers and Peter Nelson for their detailed comments.

The authors extend their gratitude to Qi Yang (CSIRO Materials Science and Engineering) and Chris Fookes (*Ret.* CSIRO Energy Technology) for helpful discussions.

Summary

This report is concerned with research performed as one of the five activities of the project funded by ANLEC R&D entitled "*Environmental Impacts of Amine-based CO_2 Post Combustion Capture (PCC) Process".*

This report is project deliverable 4.2 which details research undertaken as Activity 4: *Determination of the fate of PCC emissions in the atmosphere*. Outcomes from this work were used to perform a dispersion modelling scenario (deliverable 4.3) for the anticipated emissions from a black coal-fired power station retrofitted with an MEA-based CO_2 capture plant.

MEA and piperazine (PZ) smog chamber experiments were performed over a range of initial conditions. Sampling techniques, analytical procedures and instrumental developments were investigated for the determination of priority compounds formed while carrying out smog chamber experiments. The successful implementation of a number of these methods provided valuable quantitative and qualitative information for evaluation of chamber experiments.

Sorbent collection techniques enabled frequent sampling over the period of the chamber experiment and also served to stabilise reactive analytes and/or concentrate trace species without the requirement for additional isolation techniques. Liquid chromatography (HPLC) of derivatised analytes provided highly sensitive analysis of polar and reactive compounds. Gas chromatography using both chemical ionisation and electron ionisation modes of mass spectrometry provided a highly selective and sensitive tool for quantitative analysis and qualitative characterisation of a range of photolysis products.

MEA/NOx smog chamber experiments were carried out over a range of MEA and NOx concentrations. The results generated from these experiments were used to investigate product and ozone formation from MEA photooxidation and to provide data to assist in the development of a chemical mechanism for MEA. Supplementary experiments were performed with MEA in the presence of HNO_3, NO_3, O_3, HCHO and glycolaldehyde. Results from these experiments, along with findings from published works, were also used in the development of the MEA mechanism. Additionally, reaction rate constants were calculated for the reaction of MEA with formaldehyde and glycolaldehyde.

Based on the experience gained from the MEA experiments performed, a restricted set of piperazine (PZ) experiments were completed. In comparison with MEA photooxidation, PZ generated higher yields of aerosol, reacted rapidly with ozone and generated nitrosamines and nitramines. For the conditions used in these experiments, both MEA and PZ produced high aerosol yields.

A chemical mechanism was developed for MEA (CSIMEA) based on existing knowledge and acquired results from this study. To ensure that photooxidation products of interest were simulated accurately across the MEA/NOx experiments, yields from important reactions were representatively fitted. This mechanism was embedded into the CSIRO Chemical Transport Model to simulate the potential air quality impacts of emissions from an MEA-based PCC plant treating the flue gas from a black coal-fired power plant performed as deliverable 4.3.

The upper limit of the tropospheric lifetime of MEA and PZ determined by consideration of the OH radical chemistry for MEA was ~2.4 hours and for PZ, was estimated to be ~1.2 hours.

Recommendations for further study have been made.

This page is intentionally blank

Part I Introduction and Experimental

This page is intentionally blank

1 Preamble

This report is associated with the collaborative research agreement between Australian National Low Emissions Coal R & D (ANLEC) and CSIRO to undertake the research project entitled "*Environmental Impacts of Amine-based CO_2 Post Combustion Capture (PCC) Process"*.

The project consisted of the following 5 research tasks.

1. Carry out analysis of legislative, regulatory and permitting requirements for the use of PCC in Australian power stations in a national and international context.
2. Develop mass balance and life cycle analysis of candidate liquid absorbents when used in PCC.
3. Provide detailed assessment of the amount and nature of harmful degradation products from candidate liquid absorbents for PCC.
4. Determine the fate of PCC emissions into the atmosphere.
5. Develop a test Procedure for Post-Combustion Capture Amines.

The work presented in this report is one of two reports (deliverables 4.2 and 4.3) which are concerned with Task 4: *Determination of the fate of PCC emissions in the atmosphere*.

This report (deliverable 4.2) presents research associated with the experimental investigation performed under Task 4 and is concerned primarily with sampling and analytical method developments as well as the application of these methods to the investigation of the atmospheric chemistry of 2-aminoethanol, also called ethanolamine or monoethanolamine (MEA), and piperazine (PZ).

Results from this study were used to carry out the regional dispersion study (deliverable 4.3) which was undertaken for a black coal-fired power station scenario employing an MEA-based PCC process.

2 Introduction

It is expected that widespread use of amines for PCC capture during coal-fired electricity production will result in amine emissions to the atmosphere. Up until recently, amine research has been limited because ambient amine concentrations were generally believed to be low and therefore, not problematic in an environmental context. Consequently, knowledge of the atmospheric chemistry of amines, such as MEA and piperazine (PZ) which may be used for PCC, is also limited.

Reviews on the atmospheric chemistry of PCC-amines have been published by Bråten *et al.* (2009) and Angove *et al.* (2010b). A number of relevant documents are also available on the same website as the latter. Recent experimental studies of MEA atmospheric chemistry (Nielsen *et al.* 2010; Karl *et al.* 2012; Onel *et al.* 2012) are included in this report.

The rationale for undertaking Task 4 is that more relevant knowledge is needed of the atmospheric chemistry of the selected solvents MEA and PZ. This will be facilitated using CSIRO experimental methods and supplementing CSIRO results from the findings of other research laboratories as they become available. The original aim of this study was to develop a new chemical reaction scheme which describes the atmospheric degradation of MEA and PZ that could be embedded into the CSIRO chemical transport model to predict the ground level concentrations of pollutants of concern.

There were 5 scientific objectives which are summarised below.

1. To further investigate the development of gas phase sampling and analytical methods that can be reliably used to determine major products formed during the atmospheric decomposition of MEA and PZ during smog chamber experiments.
2. To investigate the atmospheric chemistry of MEA and PZ in the CSIRO smog chamber by varying the concentrations of amines and NO_x (See Table 1).
3. To develop a chemical mechanism for the atmospheric decomposition of MEA and PZ using available literature data and results from experiments performed in Task 4.
4. To develop an empirical scheme based on the amine chemical mechanisms for MEA and PZ that can be embedded into a predictive model which can be used for screening scenarios within a short time frame to address urgent regulatory matters.
5. To perform an air quality study using a predictive model for MEA that employs the amine chemical mechanism arising out of objective 4.

Achievements were made on all objectives except for the development of a PZ mechanism which could not be initiated due to the demanding requirements needed to address the photo-chemistry of the MEA system. However, PZ/NOx and supplementary PZ experiments were performed the results of which are presented in this report.

The dispersion study performed using a predictive model employing the MEA mechanism (CSIMEA) developed in this study is the subject of deliverable 4.3.

3 Experimental

3.1 Smog chamber operation

The CSIRO smog chamber located in Sydney was used to support the experimental investigation undertaken as part of Task 4. It has been described previously by Hynes *et al.* (2005), Lee *et al.* (2009) and White *et al.* (2010). A system schematic is presented in Lee *et al*. (2009). In brief, the chamber has a volume of 18.1 m^3 and is lined with FEP Teflon film. The chamber is illuminated by 80 black-light tubes (Sylvania BLB 350, 36W) which emit radiation over the UVA range 350-390 nm, with peak intensity occurring at 366 nm. The smog chamber was used to:

1. Develop amine injection methods,
2. Assist in the development of sampling and analytical methods by allowing the setup of trace level amine concentrations in the gas phase
3. Investigate artefact formation during sampling and analysis
4. Assist in the preparation of IR calibration spectra
5. Perform dark-only loss and chemistry experiments, as well as photochemical experiments. The latter experiments were used primarily for mechanism development and modelling purposes.

The UVA light intensity, J_{NO2}, was set to the required level before each experiment using a PCE-UV34 radiation meter, in-conjunction with a calibration curve previously prepared using a series of NO_2 photolysis measurements performed using a certified 0.4% NO_2/He mixture (BOC Gases). The NO_2 mixture was also used for the NOx/amine photochemical experiments, along with a 1.09±0.05% NO/N_2 mixture (BOC Gases). The amines used in these experiments were ethanolamine (MEA; Sigma-Aldrich, 99+%) and piperazine (PZ; Fluka, Bioultra, anhydrous). They were stored at ~4°C under N_2.

Dark chemistry experiments were performed with formamide, formaldehyde and glycolaldehyde vapours. Formamide vapour was produced by injecting a known mass of formamide (Sigma-Aldrich, deionised, 99.5%) into a small glass vessel attached to chamber wall, which was heated at ~70°C to produce the vapour which was carried into the chamber in N_2 at ~2 litres min^{-1} over ~30 minutes. Formaldehyde vapour was produced by gentle heating of ~100 mg of paraformaldehyde (Aldrich, powder, 95%) at ~50°C in a small glass cell and carried into the chamber in N_2 at ~2 litres min^{-1}. Glycolaldehyde vapour was produced in a similar manner to that of formaldehyde using glycolaldehyde dimer (Aldrich). Formaldehyde and glycolaldehyde mixing ratios were monitored by long-path FTIR.

In trial MEA experiments, MEA carryover was significant if the mixing ratio was greater than ~500 ppbv or if experiments were performed daily. As experience was gained, carryover could only be controlled if two full days were left for cleaning between each experiment. After each experiment the chamber was flushed with scrubbed air at ~800 litres min^{-1} with all UV lights on for ~4 hours then ~8 hours with lights off. The chamber was then sealed and a ~6 hour propene/NOx experiment was performed followed by another light on/off 6/24 hour scrubbed air cycle. If the particle number concentration was persistently greater than 20 particles cm^{-3} at the start of the second cleaning day, then another propene/NOx experiment was

performed. This method was also used after PZ experiments, although an additional cleaning day was required for some PZ experiments.

Ozone was measured using a API M400E ozone analyser which was calibrated prior to each run with an ozone calibrator (API M700). NOx was measured using a Monitor Labs Chemiluminescent 9841B analyser which was calibrated prior to each run using a certified NO/N_2 mixture (100 ppmv), with further calibration checks made occasionally after some runs. An SMPS system (TSI 3071A impactor employing a 0.71 mm impactor jet connected to a TSI 3022A condensation particle counter) was used to measure particle distributions over a diameter range of 13 to 685 nm. Aerosol number concentrations were corrected for wall loss (Singh-Peterson, 2007). The density of the aerosol was assumed to be 1 g cm^{-3}.

3.2 Amine injection

The amines used in amine-based PCC are problematic with regard to their study in the gas phase due to their low vapour pressures. At 25°C, the vapour pressure for MEA is 0.46 Torr and for PZ it is 4.1 Torr. In addition, PZ is a solid which is highly hygroscopic. In preparation for this project, a number of trial MEA injections were performed with a glass cell of volume 90 cm^3. The cell was attached directly to the smog chamber interface panel and the carrier/reactant gas control panel. Both the interface and gas control panels had been pre-purged. A known mass of MEA was injected into the cell in the dark, and the cell was then partly immersed in hot water. Pre-heated nitrogen (~55°C) flowing at ~2 litres min^{-1}, was passed over the MEA and carried into the chamber. In some cases, particle distributions of low mass were observed after injection. If the temperature of the glass cell exceeded 60°C for even a short time, significant loss occurred in the cell made obvious by a residual deposit. If external heating of the cell was applied by a heat gun, a particle distribution occurred in the chamber in every case. At this time, the formation of particles was thought to occur as a result of MEA condensation. This injection technique was repeated and optimised until MEA FTIR absorbance features were maximised. A reference spectrum for MEA was obtained during this process. MEA calibrations using this spectrum have been verified and FTIR measurements agree with those obtained using the NITC sampling and analytical method to within 7%.

However, this injection method could not be used for the main body of the MEA experiments used in this study because it took ~4 hours for an injection to be completed, which meant experiments could take up to 14 hours to complete. Consequently a new injection cell and method was developed in attempt to reduce injection times.

The new cell had a volume of ~30 cm^3 and a reduced path length into the smog chamber. A known mass of MEA was injected into the cell before NO_x reactants. The cell was insulated with fibreglass tape and heated by the nitrogen carrier to ~55°C. The carrier flow rate was set to ~10 litres min^{-1} for 30 minutes and then reduced to ~2 litres min^{-1} for 30 minutes. This technique was systematic but still produced cell loss which was more noticeable as the MEA mass was decreased. Using this method, small particle distributions still sometimes occurred on injection. The formation of these small distributions was eventually determined to be caused by trace NO_x left in the injection pathway. This effect was in the main overcome by much more rigorous purging of the injection pathway and all valve dead spaces with nitrogen prior to cell installation.

The injection method used for PZ was similar to the aforementioned for MEA, except that PZ was dissolved in fresh Milli-Q water to a concentration of ~100 mg cm^{-3} and injected into the cell as a known mass of PZ solution. The cell was heated with a heat gun to ~70°C continually throughout the injection. PZ was less susceptible to aerosol formation in the smog chamber during injection.

3.3 Analytical methods

Research Objective 1 of ANLEC task 4 was the development of gas phase sampling, analytical and instrumental methods applicable to the quantitative and qualitative monitoring of chamber experiments for MEA, piperazine and photolysis products. A number of collection and isolation techniques were developed for instrumental analysis using gas chromatography-mass spectrometry (GCMS) and high performance liquid chromatography (HPLC). Outcomes from the development phase were detailed in the interim report and further work undertaken in validation of methodologies is described in Appendix A and Appendix B.

The sections that follow provide an overview of the methodologies implemented and investigations undertaken for the determination of MEA, piperazine, formamide, formaldehyde and other carbonyl compounds, 2-nitroaminoethanol, and other minor nitrated and oxygenated photolysis products.

3.3.1 THERMAL DESORPTION (TD) GCMS TECHNIQUES

The sorbent collection and thermal desorption GCMS method (TD-GCMS) was implemented for the analysis and characterisation of major priority compounds and trace organic products from the chamber experiments. This work focused on nitrogenous and oxygenated organics which were likely to be amenable to this technique.

A Markes Unity 2™ desorption unit and Ultra 2™ autosampler (Markes International Ltd) were interfaced to a Varian 450-GC gas chromatograph and 240-MS ion trap mass spectrometer (Varian Corporation, now Agilent Technologies Ltd). Chamber air was drawn through sorbent tubes containing the selected sorbent (Markes International) at a calibrated mass flow controlled flow rate for the required time period, generally 100 ml min^{-1} for 15 minutes. Samples were taken to monitor at least four phases of each experiment, from dark through to the UV.

Sorbent combinations of different selectivity were tested for application to the range of compounds likely to be present in the chamber samples, as reported in Appendix A. Tenax TA® was implemented for routine monitoring as it provided excellent reproducibility of the major products and an adsorption range which covered even the smaller nitrated and oxygenated compounds of interest. Tenax/Unicarb® showed greater affinity for a few compounds but similar or lower affinity for others. The requirement for a higher desorption temperature and its higher background levels translated to lower sensitivity for overall trace product characterisation. The thermal desorption technique was optimised for various parameters which impact on the efficiency of primary desorption, of secondary trapping and desorption and of GC transfer. Of importance in this work is the minimisation of exposure of sensitive compounds to prolonged high temperature. This is an aspect of this technique which has advantages over conventional liquid injection of a solvent extracted sample, where exposure to surfaces at higher temperatures can be experienced by the sample over a more sustained period.

The GCMS was optimised for chromatographic resolution across the expected compound range, including higher oxygenated and nitrated compounds expected to be found as products in the chamber samples. The mass spectrometer was operated under both chemical ionisation (CI-MS) and electron ionisation modes (EI-MS). Quantitative analyses was undertaken using the methanol positive ion CI-MS, due to the superior sensitivity and specificity of this mode particularly for oxygenated and nitrated compounds. Recollection of

desorbed analytes from each sample tube allowed subsequent re-analysis under EI-MS mode immediately after the CI-MS analysis.

The knowledge of a compound's molecular weight, obtained from CI-MS, together with its EI mass spectra allowed structural elucidation and characterisation of a specific identity or an organic class for each compound found in the chamber samples. Mass spectral search software assisted in this process, for those compounds included in the NIST database. The ability of the ion-trap mass spectrometer to run both CI and EI-MS modes simultaneously, which cannot be achieved using quadrupole MS instrumentation, provided a power tool for characterisation of nitrated and oxygenated compounds relevant to this project.

MEA was deprioritised as a candidate for the TD-GCMS technique after various issues encountered in the development phase, which were fully described in the interim report, could not be overcome. Whilst GCMS itself was able to adequately resolve and identify MEA from sorbent collection of MEA headspace, the collection and desorption process proved quantitatively inefficient when applied to chamber sampling. The successful development of HPLC methodology for determination of MEA using *in-situ* derivatisation, as described in a Section 3.3.2, was implemented for quantitation of MEA in chamber samples. Derivatisation effectively overcomes issues associated with this compound's basicity and inherent activity that can occur on surfaces of various components used for collection and instrumental analysis using GC techniques. The TD-GCMS method was used for qualitative monitoring of MEA to assess its progress relative to product formation in samples from the chamber experiments.

The use of headspace TD-GCMS was implemented for evaluation of the integrity of pure MEA used for preparation of the chamber for MEA experiments. Minor components present as impurities or decomposition products were evaluated by CI-MS and EI-MS to provide information important in determining the origin of compounds observed in chamber experiments. Analysis by CI and EI-MS found a number of compounds in the MEA headspace which also occur as photolysis products. These include oxazoline (4,5-dihydro-oxazole), 1,3-oxazolidine, 2-methyloxazolidine, pyrazine and formamide. In all cases these compounds were at significantly lower concentration, relative to the MEA, in the headspace than in chamber samples indicating minimal concentration as artefacts of pure MEA used in the chamber. This is discussed further in Section 4.2.

Piperazine was monitored in all PZ chamber experiments using Tenax sorbent tube and TD-GCMS analysis. Validation included analytical aspects, as described in Appendix A, however full validation using standard gas phase chamber atmospheres was not achievable under the experimental program of work. Piperazine was adequately resolved and reproducible by TD-GCMS analysis, however it showed a non-linearity in its response over the required concentration range. This was found to be due to reactivity and adsorption effects more likely associated with GC transfer and column components than the desorption process. Despite this, its reproducibility at each concentration level enabled its calibration provided certain constraints in the data set were upheld. Piperazine measurements were made on all PZ experiments to provide a semi-quantitative comparison to data obtained from the FTIR result.

Formamide, a major photolysis product, was routinely monitored and accurately quantified using the TD-GCMS method. For all chamber experiments, samples were taken at four or more phases during each experiment and clean chamber background and system blanks were routinely included. Under nominal conditions of sampling and analysis a method detection limit of 0.02 ppbv in chamber air was achieved, with linearity over the range 0.2 to 40 ppbv. A full description of the TD-GCMS methodology and its validation for formamide can be found in Appendix A.

A full characterisation of minor photolysis products was undertaken for certain experiments. Section 4.2 of this report includes results from that assessment for Experiments 750 MEA, E807 ^{13}C isotopically labelled MEA, E753 MEA/Formaldehyde (dark), E773 MEA/Formaldehyde and E785 MEA/Glycolaldehyde. Results for piperazine E787 and E789 are discussed in Section 5. The process of evaluation of CI-MS data for molecular weight determination followed by elucidation of EI-MS spectra is detailed in Appendix A. The characterisation yielded up to 40 nitrogenous and oxygenated organic products from around 80 compounds searched as likely candidates of photolysis. Oxazolines, oxazolidines and related compounds, amides, aldehydes, nitrosamines and nitramines were identified.

CI-MS was used to monitor experiments where isotopically labelled ^{13}C-MEA or PZ/^{15}NO was used. The ability to use CI data to determine molecular weight and hence the proportion of native and labelled component for each compound proved invaluable in evaluating the distribution of the label in the reactant and its products.

3.3.2 SORBENT COLLECTION AND HPLC TECHNIQUES

MEA using NITC derivatisation and HPLC analysis

Analysis of the monoethanolamine (MEA) concentration in the experimental chamber was carried out by in-situ derivatisation using 1-naphthylisothiocyanate (NITC) and analysis by High Performance Liquid Chromatography (HPLC). The method was based on the US OSHA Method PV2111 (1988) for determining ethanolamine in ambient air. To date the OSHA method is only partially validated and guidance was also obtained from Levin *et al*. (1989) who makes certain modifications which are more amenable to aspects of the desorption and HPLC analysis. These methodologies were used as a basis for further development and were optimised and validated for the requirements of this project, as described in detail in Appendix B.

In-situ derivatisation was performed by drawing gas from the experimental chamber through a sampling tube containing in 10% NITC on a polystyrene XAD-2 adsorbent (SKC Incorporated). An optimum flow rate of ~0.05 l min^{-1} for a sampling time of ~60 minutes was used. The adsorbent is ultrasonically extracted into 2 ml of acetonitrile and analysed by HPLC. An Agilent Technologies 1200 series HPLC was used with detection using diode array operated at 230 nm. Chromatographic separation was carried out on a C8 column (Restek) under isocratic mobile phase of water/acetonitrile. Full scan diode array provided a spectrum where the NITC-MEA derivative shows UV absorption at λ_{max} = 222 nm with ε_{max} = 6056 L mol^{-1} cm^{-1}. A less intense peak at λ_{max} = 285 nm is also seen.

MEA quantitation was performed using the external standard method and multipoint calibration using standards prepared from MEA and an excess of NITC. Calibration over the concentration range 0.05 to 10 µg ml^{-1} was linear using least squares regression analysis with a correlation coefficient of ≥ 0.999. An instrument detection limit of 0.015 µg ml^{-1} was achieved which, under nominal conditions of sampling and analysis, was equivalent to a method detection limit of 2 ppbv of MEA in the chamber atmosphere.

Diethanolamine using NITC derivatisation and HPLC analysis

The NITC method for determination of diethanolamine (DELA) was investigated based on similar principles to that of MEA outlined above. OSHA method PV2018 (1987), which has been only partially validated provided some guidance.

It has been confirmed that DELA can be readily derivatised with 1-NITC when dissolved in ACN and separated by reversed phase HPLC on a C8 column with a solvent mix of 30% ACN in water at a flow of

1.5 ml min^{-1}. The NITC-DELA derivative gave UV absorptions at λ_{max} = 220 nm with ε_{max} = 1933 L mol^{-1} cm^{-1} and a less intense peak at λ_{max} = 278 nm. The derivative elutes slightly later than the MEA derivative indicating they can be distinguished and quantified with the current system with the limitation that major concentration differences may impact on the accuracy of peak integration. An instrument detection limit of ~0.1 µg ml^{-1} has been estimated.

The validation of the method for gas phase chamber sampling was not within the scope of this project and the retention and desorption efficiency associated with this aspect of the methodology should be assessed before its implementation for DELA analysis.

Piperazine using NITC derivatisation and HPLC analysis

An investigation was made into the determination of piperazine based on similar principles to that used for MEA. An OSHA in-house method indicates that this is possible although no actual methodology is provided. The method was not successful despite a number of modifications made to the method which are described in Appendix B. This method would require significant further effort in its development and validation.

Carbonyl compounds using DNPH derivatisation and HPLC analysis

Carbonyl compounds formed during the decomposition of MEA and related systems and of piperazine were sampled using *in-situ* 2,4-dinitrophenylhydrazine (DNPH) derivatisation and HPLC analysis. The method is based on US EPA Method TO-11A "Determination of Formaldehyde in Ambient Air Using Adsorbent Cartridge Followed by High Performance Liquid Chromatography (HPLC)" (1999).

The DNPH/HPLC method was implemented for the analysis of the following 11 carbonyl compounds in chamber experiments.

- Glycolaldehyde
- Formaldehyde
- Acetaldehyde
- Acetone
- Acrolein
- Propionaldehyde
- Methacrolein
- Methylvinylketone
- Benzaldehyde
- Glyoxal
- Methylglyoxal

This method has routinely been used by our laboratory for priority aldehydes and ketones in ambient and emissions samples and as such provided an efficient and sensitive means of analysing for primary photolysis products from chamber experiments, such as formaldehyde and acetaldehyde. Its optimisation focussed on other non-standard compounds likely to be specific to the chamber experiments such as glycolaldehyde, glyoxal etc. Optimisation for glycolaldehyde made reference to the publication by Zhou *et al.* (2009).

The DNPH/HPLC method is fully validated for major carbonyls and as such the full development process is not included in the Appendix, but is available on request. An outline of the method and its performance under validation follows.

Chamber samples were drawn through a DNPH sampling cartridge (Waters Sep-Pak® XpoSureTM aldehyde samplers) under mass flow controlled rate of ~2.0 litres min^{-1} for a nominal sampling time of 45 minutes, or a shorter time if analyte mass was expected to be high. The carbonyl-DNPH derivatives were desorbed from the sampling cartridges into 5 ml of acetonitrile and filtered before analysis by HPLC. An Agilent Technologies 1200 series HPLC system was used with a diode array detector operated at 365 nm. The column used for the chromatographic separation was a C8 column (Restek Ultra 4.6 mm id x 250 mm, 5 µm). 20 µL of sample was injected under a gradient elution programme of water/methanol followed by water/acetonitrile/tetrahydrofuran. Quantitation was performed using the external standard method and multipoint calibration using primary standard containing a priority carbonyl mixture (Supelco CARB Method 1004 DNPH Mix 2) and a glycolaldehyde-DNPH standard (Restek Corporation). Blank samples were prepared with each batch of samples.

Calibrations over the concentration range 0.1 to 10 µg ml^{-1} were linear using least squares regression analysis with a correlation coefficient of ≥ 0.999. It had been previously determined that the method delivered an instrument detection limit of 0.003 µg ml^{-1} (average for CARB compounds), derived at the 99% confidence interval using five replicate analyses of a 0.01 µg ml^{-1} standard solution and an injection volume of 20 µl. This is equivalent to a method detection limit of 0.14 ppbv (for formaldehyde) as the gas phase chamber concentration under nominal sampling and analytical parameters.

Calibrations for methylvinylketone (MVK), glyoxal and methylglyoxal were calculated from the ratios of their response factors to that of methacrolein with reference to data from Wang *et al.* (2009), since commercially available standards are not available for these compounds. Their measurement was therefore considered as semi-quantitative.

Nitroaminoethanol using underivatised and derivatised collection for HPLC analysis

An investigation was carried out to determine if 2-nitroaminoethanol (NAE) could be detected directly by HPLC without derivatisation and, if detected, to assess if it could be efficiently collected and quantified in chamber samples by HPLC. Based on these results further investigation was undertaken to determine whether *in-situ* derivatisation could be used for the determination of this compound.

The results clearly showed that underivatised NAE was sufficiently chromaphoric and could be easily resolved and detected at concentrations down to ~0.2 µg ml^{-1} in standard solution by the HPLC. However the results from its collection onto, and desorption from, Florisil sorbent cartridges indicated its adsorption or reaction with the collection media. In addition, other co-collected polar compounds affected chromatographic performance in the resolution of this compound.

Derivatisation using NITC (based on amine functionality) and using DNPH (from NO_2 functionality) also proved unreliable and significant further work would be required if NAE were to be effectively collected and analysed in the chamber gas phase using sorbent collection and liquid chromatography.

4 MEA experiments

4.1 Literature summary of relevant MEA photochemistry research

Given the importance of MEA to the PCC industry, a number of studies in recent years have focussed on MEA photochemistry. Its photochemistry is similar to that of amines in general, with removal in the atmosphere primarily occurring by reaction with radicals (Nielsen *et al.* 2012a; Lee and Wexler, 2013) and partitioning into aerosol (Ge *et al.* 2011).

The presence of a hydroxyl substituent means the photochemistry of MEA is more complex than for alkylamines, for which much of the atmospheric amine research before 2008 had been performed (Pitts *et al.* 1978; Schade and Crutzen 1995). Experimental studies of MEA photochemistry which have been performed include the particle phase smog chamber study by Murphy *et al.* (2007), the Maximum Incremental Reactivity (MIR) smog chamber study by Carter (2008), the ADA study in the EUPHORE chamber (Nielsen *et al.* 2010; Karl *et al.* 2012), a Norsk Energi project in the CSIRO chamber (Angove *et al.* 2010a), a formamide/MEA study (Angove *et al.* 2012) and reaction rate constant determination by Onel *et al.* (2012).

With the exception of the reaction rate constant determination by Onel *et al.* (2012), these studies have looked at the photochemistry and/or particle formation of MEA in the presence of NOx. MEA was identified by Carter as a species that promotes ozone formation to a small degree. The major products observed from the reaction of MEA with the OH radical are formamide and formaldehyde, with aminoacetaldehyde, oxoacetamide and *N*-nitro-2-aminoethanol identified as minor products. Particle formation from MEA photooxidation in the presence of NOx is high, however no studies been performed on aerosol formation properties under limited NOx conditions.

The quantification of MEA has proven difficult or illusive in some studies. Where MEA concentrations have been calculated, determining the reaction or particular method of degradation relies on estimates of the reaction rates of different removal pathways, for example removal by OH, NO_3 and HNO_3. Direct calculation of the reaction rate constant of MEA with OH has been performed recently, with various estimates and calculated values summarised in Table 1.

The reaction rate constants of MEA with other radicals are less certain. Estimates of the reaction rate constant of MEA with the NO_3 radical are around 1-2 x 10^{-13} cm^3 $molecule^{-1}$ s^{-1} (Carter, 2008; Karl *et al.* 2012) which is relatively high for the reaction of NO_3 with a volatile organic gas.

One major area of health concern from amine photooxidation is the formation in the atmosphere of nitrosamines and nitramines. The nitramine which is most likely to form as a result of MEA photooxidation, *N*-nitro-2-aminoethanol, has been observed using PTR-TOF-MS in the EUPHORE chamber. The most likely nitrosamine which could form, *N*-nitroso-2-aminoethanol, has not been observed. As it is a primary nitrosamine, it is likely to be unstable in atmospheres containing oxygen (Angove *et al.* 2010b; Tang *et al.* 2012). The formation of secondary nitrosamines from MEA photochemistry in the atmosphere is a possibility, however none have been observed to date.

Table 1. Calculations of reaction rate constant for MEA + OH

Reference	Theory / Expt	Rate constant (10^{-11} cm^3 $molecule^{-1}$ s^{-1})	Notes
Carter 2008	Theory	4.41	Using group additivity estimates for amines as per SAPRC mechanism protocol
Nielsen *et al.* 2010	Theory	3.1	Estimated, presumably from Structure-Activity Relationship (SAR)
Jackson and Attalla 2010[a]	Theory	11.4	Calculated using state-of-the-art hybrid meta-density functional theory with a large basis set (M06-2X/cc-pVTZ)
Lambropoulous 2010[a]	Theory	25.6	Calculated using the Perdew-Wang GGA-PW91 generalized-gradient approximation functional in combination with a double-numerical-with-polarisation (DNP) basis set
Karl *et al.* 2012	Theory	3.58	SAR calculations as per Kwok and Atkinson (1995)
Karl *et al.* 2012	Experimental	9.2 ± 1.1	Calculated relative to the reaction of 1,3,5-trimethylbenzene
Onel *et al.* 2012	Experimental	7.61 ± 0.76	Absolute determination of MEA + OH rate by monitoring OH concentration with laser induced fluorescence.

[a] Presented in Angove *et al.* (2010b)

4.2 Results of MEA/NOx reaction experiments

4.2.1 MEA + NO_X

A total of 12 smog chamber experiments were performed to support the objectives of this study, including the development of the MEA mechanism and experimental modelling which are discussed in Section 6 of this report. A copy of the experimental gas phase and aerosol phase profiles of these experiments is presented in Appendix C.

Before each experiment, on-line instruments were calibrated and a fresh FTIR baseline obtained. MEA was then injected over ~40-60 minutes and allowed to mix for 20 to 40 minutes. NO_2 was then injected and mixed, followed 10 to 15 minutes later by the NO injection. FTIR was used to determine MEA and NH_3 mixing ratios, DNPH/HPLC was used for HCHO and Tenax/GCMS was used for $HCONH_2$. The chamber was

then mixed vigorously and left in the dark for 2 hours. The lights were turned on and set for a J_{NO2} of 0.50±0.03 min^{-1}. The initial temperature was 22±2°C and the relativity humidity was <5%.

The initial mixing ratios of MEA, NO and NO_2 used in these experiments are summarised in Table 2 along with the final mixing ratios for O_3, NH_3, HCHO and $HCONH_2$ obtained at, or near the end of the 4 hour UV stage. Also included in Table 2 are the final aerosol mass concentrations as determined by SMPS.

Table 2. Initial and final mixing ratios for reactants and key products observed in the 12 MEA/NOx experiments

	Initial concentrations				Final concentrations (at/near to 4 hours)				
Expt	MEA/ NOx	MEA (ppbv)	NO (ppbv)	NO_2 (ppbv)	O_3 (ppbv)	NH_3 (ppbv)	HCHO (ppbv)	$HCONH_2$ (ppbv)	Aerosol (µg m^{-3})
723	24.2	424	15	3	77	63	13.4	18.9	166
748	12.0	289	21	3	78	58	15.8	17.4	218
746	4.5	109	18	6	26	19	7.6	6.8	48
750	9.4	412	40	4	85	77	14.8	29.0	359
727	6.6	283	35	8	58	50	9.3	19.6	161
736	2.4	119	41	8	15	17	5.6	6.3	29
688	4.7	427	80	11	21	30	9.2	14.2	62
731	2.8	251	81	9	19	33	9.0	11.8	89
738	1.3	127	10	90	35	16	6.1	5.9	127
691	3.1	444	121	21	13	32	9.3	16.0	59
733	1.9	261	120	21	12	29	8.7	10.8	58
725	1.0	464	410	53	3	21	7.2	10.9	27

In all experiments, except E738, NO and NO_2 were injected in the ratio ~9:1 which after 2 hours in the dark decreased to an average ratio of 6.4:1. In E738, the NO:NO_2 injected ratio was ~1:9. Similar to Nielsen *et al.* (2010), this experiment was performed with NO_2 as the predominant NOx species to investigate the effect of NO_2 on the formation of aerosol in the dark and its subsequent effect on aerosol formation while under UV.

Except for E738 which is a special case, for NOx mixing ratios above ~40 ppbv the most active systems were those with the highest MEA/NOx ratios since they recorded the highest O_3 and HCHO mixing ratios. Ozone and HCHO production was constrained as the MEA/NOx ratio increased for NOx mixing ratios in the range 18-24 ppbv.

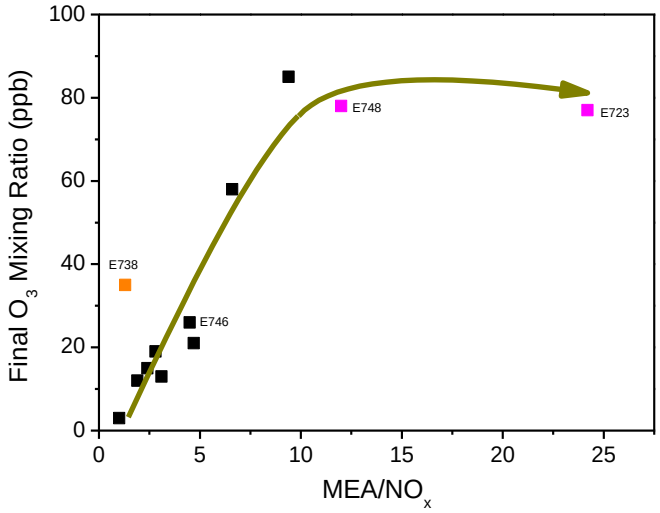

Figure 1. Plot of O_3 mixing ratios at 4 hours against initial MEA/NOx

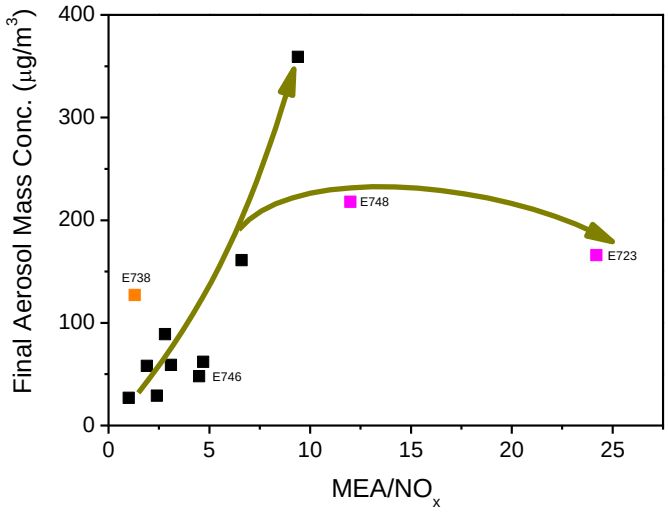

Figure 2. Plot of aerosol mass concentration at 4 hours against initial MEA/NOx

Figure 1 is a graph of final O_3 mixing ratios measured for each experiment plotted against the MEA/NOx ratio. The dark yellow trace is a construction to facilitate discussion. The low NOx experiments are show as magenta points, and E738 as an orange point.

The formation of O_3 was constrained in E723 by the low initial NOx mixing ratio. Ozone production in the high initial NO_2 experiment 738 was greater than that observed for E688 and E731, both of which had larger MEA/NOx ratios but similar NOx. The final O_3 in E738 is a reflection of the high ozone equilibrium concentration (32 ppbv) established at the start of the experiment resulting from the high initial NO_2 concentration.

Figure 2 is a graph of the final aerosol mass concentration plotted against the MEA/NOx ratio. The traces have been constructed and are indicative only. The magenta (E723/E748) and orange (E738) points are for the same experiments represented in Figure 1.

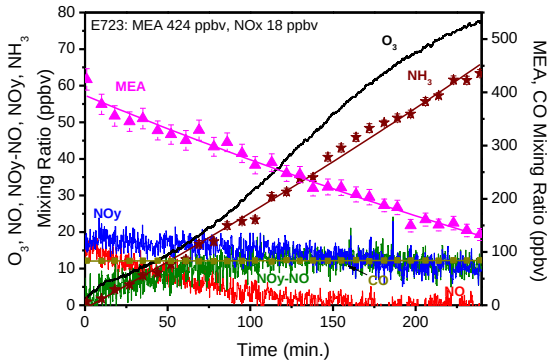

Figure 3a. UV gas-phase profiles E723

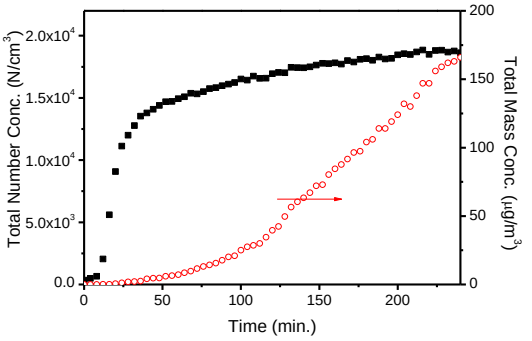

Figure 3b. UV aerosol profile E723

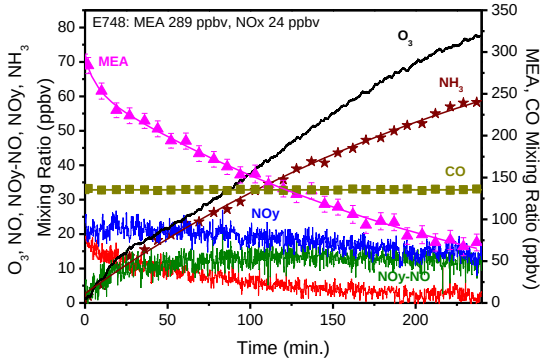

Figure 3c. UV gas-phase profiles E748

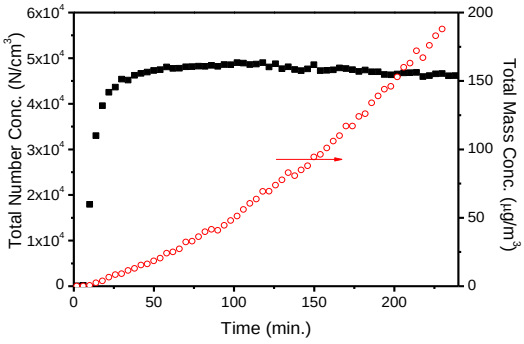

Figure 3d. UV aerosol profile E748

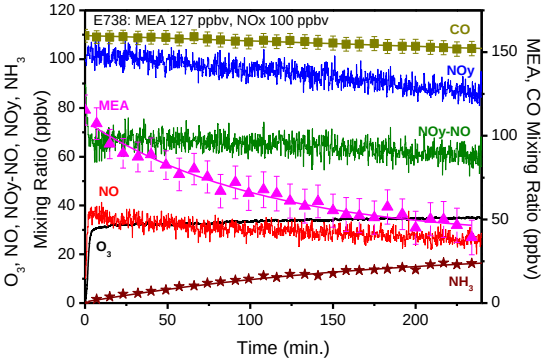

Figure 3e. UV gas-phase profiles E738

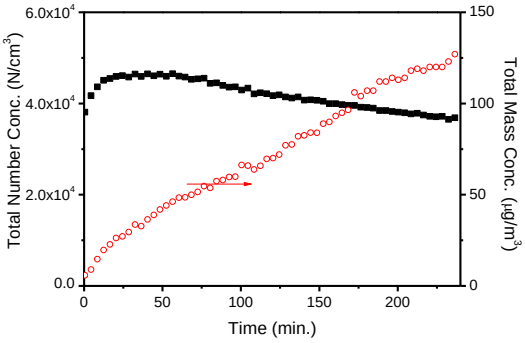

Figure 3f. UV aerosol profile E738

Figure 3. UV gas and aerosol profiles for E723, E748 and E738

Below a MEA/NOx ratio of ~5, the production of aerosol appears limited to a mass concentration less than 100 µg m^{-3}, above which the increase in aerosol mass concentration appears sustained up to a MEA/NOx of ~10. The one exception to this was E738 with high NO_2, which had an aerosol mass of 127 µg m^{-3}. In Figure 1, O_3 formation is constrained for MEA/NOx greater than ~10. In Figure 2, it can be seen that aerosol formation is also constrained for MEA/NOx greater than ~10.

This observation indicates that in the MEA/NOx system used in this study, the production of aerosol precursors is dependent upon two factors. The first of these is an active RO_2 to RO radical pathway controlled by the presence of NO. The effect of this is shown in Figure 3, where the supply of NO becomes limited well before the end of E723 and just limited at the end of E748, resulting in sharp growth to the

amount of aerosol. The second factor is related to the high aerosol growth observed in E738. The higher initial NO_2 concentration used in this experiment will give rise to much higher nitrate radical concentrations at the beginning of the experiment compared to experiments with higher initial NO. For experiments with high initial NO, the nitrate radical mixing ratio is much lower than that in E738 until later in the experiment, after which time the concentrations of NO_2 and ozone have increased.

Aerosol production in gas phase amine systems can form as inorganic aerosol or a combination of both inorganic and organic aerosol. If MEA in the dark is in the presence of HNO_3 then the aerosol that forms is inorganic (see Section 4.3.1). As observed in this study, rapid aerosol formation does not appear to occur in the presence of NO only in the dark. It is concluded that in the UV experiments presented in Table 2 it is likely that the aerosol formed is a combination of inorganic and organic forms.

Ammonia formation has been observed in these experiments as well as experiments performed by Nielsen *et al.* (2010). From later experiments on alkylamines, Nielsen *et al.* (2011a) postulated that the formation of ammonia may occur by the condensation of a primary amine and a primary imine to form a secondary imine and ammonia. If this path were to proceed, then it is likely that the subsequent product formation arising from the imine would be incorporated into the organic aerosol component of the aerosol. In these experiments, the formation of ammonia occurred only when the lights were on, and ceased immediately after the lights were turned off.

Figure 4 is a graph of aerosol mass concentration versus the mixing ratio of ammonia measured at the end of the twelve experiments listed in Table 2.

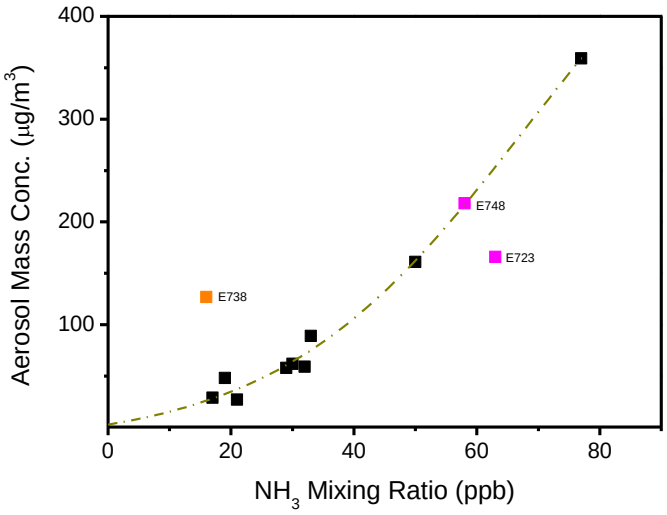

Figure 4. Plot of aerosol mass concentrations against observed NH_3 mixing ratios after 4 hours

For convenience, a sigmoidal growth model fit was applied to that data where NO was not limited. The outliers E723 and E738 were not included in the fit. The plot suggests that at the end of each experiment there is a relationship between the total aerosol mass concentration and the ammonia formed, as long as the supply of NO is not limited.

As shown in Figure 1, in the case of E723, the production of aerosol was constrained. A similar effect is observed in Figure 5, where ammonia formation was also constrained at high MEA/NOx. One interpretation of this observation is that the formation of organic aerosol in the MEA/NOx system is linked directly to ammonia formation.

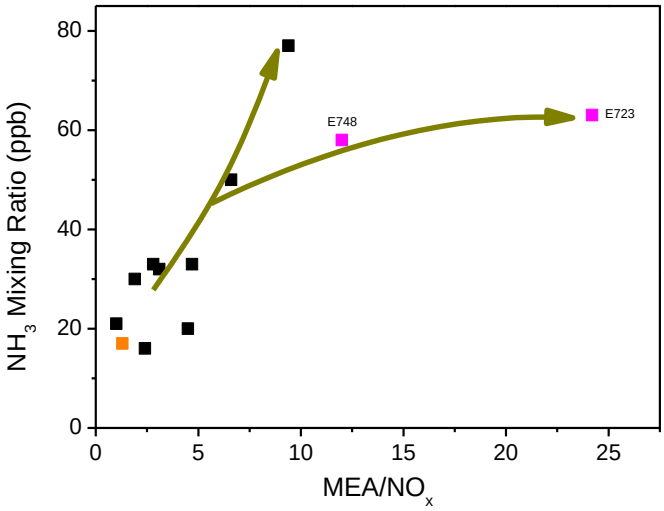

Figure 5. Plot of NH_3 mixing ratio at 4 hours against initial MEA/NOx

In E738, the final aerosol mass concentration was much greater than that expected for a MEA/NOx ratio of 1.3. In this experiment the initial NOx condition was reversed where NO_2>>NO. Consequently, under these conditions, the aerosol formed in E738 is expected to have a higher proportion of inorganic aerosol, the formation of which is independent of ammonia formation.

Since formamide and formaldehyde were considered to be major products formed during the photooxidation of MEA, a significant effort was made to accurately quantify them in the twelve experiments listed in Table 2. Formamide was sampled using Tenax® sorbent tubes and analysed using GCMS with final mixing ratios falling in a range of ~6 to 30 ppbv. Although MEA in headspace was adequately resolved by GCMS, it could not be quantified in experimental samples due to inefficiencies in sorbent sampling and/or the desorption process. Formaldehyde was analysed using DNPH/HPLC, with final mixing ratios between ~5 to 16 ppbv. DNPH/HPLC was also used to determine the final mixing ratios for glycoladehyde and acetaldehyde which in all experiments were less than 3 ppbv and 2 ppbv, respectively.

Nielsen *et al.* (2010) detected nitraminoethanol in their MEA/NOx experiments performed in the EUPHORE facility. In this study, HPLC and GCMS methods were investigated for the analysis of nitraminoethanol. Whilst this study found that the HPLC method can be used to sensitively detect this compound using standard preparations, the sampling media has proven to be ineffective, as discussed in Section 3.3.2. The use of GCMS to analyse for nitraminoethanol has also proven unsuccessful since the nitramine appears to breakdown before or during analysis, or does not desorb from the sorbent, as discussed in Section 3.3.1. Consequently, the formation of nitraminoethanol during any of the experiments listed in Table 2 cannot be confirmed.

As well as being used to quantify formamide, GCMS was used to identify products formed during the photo-oxidation of MEA in the presence of NOx, as described in Section 3.3.1. The results of an analysis of E750 is given in Table 3, where it is compared against an analysis of stock MEA, determined by headspace analysis and, for convenience, results from experiments where MEA was reacted with carbonyls (see Sections 4.3.3 and 4.3.4).

Table 3. Tenax/GCMS results for MEA headspace, MEA/NOx E750, MEA/formaldehyde E773 and MEA/glycolaldehyde E785

Compound (retention time)	MW	MEA headspace	E750 MEA + NOx: Dark	E750 MEA + NOx: Light (relative to dark)	E773 MEA + HCHO: MEA only	E773 MEA + HCHO: MEA + HCHO (relative to MEA)	E785 MEA+Glycol: MEA + Glycol (1 Glyd inj)	E785 MEA+Glycol: MEA + Glycol (3 injs.) (relative to 1 Glyd inj)
MEA	61	Large	Large	<	Large	<	Large	gone
formamide	45	Small	Med	++++	Small	=	NA	NA
MW 156 (20.78)	156	Trace	Med	++++	Small	+++	NA	NA
1,3-oxazolidine	73	Med	Med	+++	Med	++++	Large	gone
oxazoline	71	Small	Med	+++	Med	=	Med	<
pyrazine	80	Small	Small	+++	Small	<	Small	<
morpholin-2-one	101			+++			Small	++
MW 89; $C_3H_7NO_2$ (18.40)	89	Small	Small	++	Med	+++	Med	<
2-oxoacetamide	73		Trace	++	Trace		Trace	+
MW 75 (13.05)	75		Small	++			Trace	<
MW 103; C_7H_5N (15.44)	103	Trace	Small	++	Small	=	Small	<
MW 56 (8.35)	56	Small	Small	+			Small	<
MW 75 (13.89)	75		Trace	+				
MW 102 (15.12)	102		Trace	+	Trace	++		
N-ethylformamide	73		Small	+	Trace		Small	<
MW 101; $C_4H_7NO_2$ (16.45)	101		Trace	+	Trace	+++	Trace	+
MW 85; C_4H_7NO (11.15)	85			+				
3-methyl-1,3-oxazolidine	87			+	Trace	+++		
2-methyl-1,3-oxazolidine	87	Small	Small	=	Small	<	Small	gone
N-acetylethanolamine	103					+	Small	<
MW 101 (18.91)	101				Small	=	Small	<
butanoic acid	88						Med	+++
MW 129 (15.09)	129						Small	++
MW 97 (11.56)	97							++
pyridine	79							++

Legend:

Large	Peak size > 10^6	<	lower
Med	10^5 < Peak size < 10^6	=	equal within 25%
Small	10^3 < Peak size < 10^5	+	Peak size increase < 10^4
Trace	Peak size < 10^3	++	10^4 < Peak size increase < 10^5
	tentative identification	+++	10^5 < Peak size increase < 10^6
	unknown compound	++++	Peak size increase > 10^6
NA	Not observable using this method	gone	Below detection limit

A relative measure of the peak area response of substances is listed in Table 3 for E750 before lights on, with a change in the maximum observed peak area for the samples taken during lights on shown relative to the dark peak area response. It should be noted in all cases that the scaling in Table 3 is based on peak area response as measured by GCMS in chemical ionisation (CI) mode, which can vary significantly depending upon the properties of the compounds being ionised. Hence the relative intensities provided are indicative only, and with the exception of formamide, are not quantitative measures (see Appendix A for details).

The compounds found are listed in Table 3; six of which have confirmed identities, six with tentative identifications and 12 unknowns. Compounds were identified where possible using their molecular weight obtained from CI data and by examination of their electron ionisation (EI) spectra. In some cases identification against standard compounds was possible. Due to the low concentrations of some analytes, it was not always possible to generate a EI mass spectrum, and hence their elucidation using mass spectra was compromised or not available.

Although the peak response for formamide in the dark is medium (Med) for E750, this corresponds to gas phase formamide mixing ratio of just 0.8 ppbv. For all experiments listed in Table 2**,** the average formamide mixing ratio measured just prior to the lights being turned (Dark) was less than 2 ppbv.

Compounds which were found in MEA headspace include formamide, 1,3-oxazolidine, oxazoline, pyrazine, and 2-methyl-1,3-oxazolidine. In experiment 750, the compounds detected just prior to the lights being turned on, which was ~200 minutes after MEA injection and ~120 minutes after NO_2/NO injection, are listed in Table 3 under the column labelled “Dark”.

All the compounds detected in the MEA headspace were identified in the E750 dark sample, along with six additional compounds. After the lights were turned on, the concentration of all compounds increased except for MEA which decreased due to photooxidation, and 2-methyl-1,3-oxazolidine which did not change. The latter is probably formed as a result of ethanolamine reacting with acetaldehyde, which is present in low concentrations (< 2 ppbv) in the dark chamber.

In addition to the six new compounds observed in the E750 dark sample, a further three more new compounds were observed after the lights were turned on. Excluding formamide, the 5 most significant products observed by GCMS that were formed in E750 were:

1. An unidentified compound with a molecular weight of 156 g mol^{-1}.
2. 1,3-oxazolidine formed as condensation product with formaldehyde.
3. Oxazoline; formation presumably initiated by hydrogen abstraction by OH from 1,3-oxazolidine.
4. Pyrazine formed by the condensation of 2 molecules of MEA.
5. Morpholin-2-one postulated to be formed by a reaction between MEA and glycolaldehyde.

4.2.2 MEA + $^{15}NO_X$

Nitrous oxide has a global warming potential of 310 (100 years), and has been proposed as a potential product of amine photooxidation (Schade and Krutzen, 1995). It was important therefore to determine if N_2O is formed from MEA photooxidation, and if so, determine its yield.

Using ^{15}NO and diethylamine (DEA), it was previously reported in ANLEC Deliverable 4.1, that the formation of N_2O (as $^{14}N^{15}NO$ or $^{15}N^{14}NO$) was not observed in experiment 646 during the photo-oxidation of DEA. A

null result was also obtained for E649 in which MEA (~490 ppbv) was photo-oxidised in the presence of ^{15}NO (~50 ppbv).

After close examination of IR spectra obtained for the experiments listed in Table 2 and as a result of the MEA+^{15}NO experiment 649, it is concluded that N_2O is not formed during MEA photooxidation in the presence of NOx under the experimental conditions used in this study.

4.3 Results of supplementary MEA experiments

In the atmosphere MEA can be removed by reaction with OH, NO_3 and condensation reactions with carbonyls. It can also removed by partitioning into the particle phase as inorganic aerosol generated by reaction with HNO_3 or as organic aerosol, most likely in complex combination with the inorganic form, produced as result of hydrogen abstraction reactions with OH and NO_3. It is likely that deposition onto surfaces also occurs.

Investigations of the reaction of MEA with the OH radical (Karl *et al.* 2012; Onel *et al.* 2012) indicate that reaction with the OH radical is likely to be an important MEA loss process in the atmosphere. No data presently exists for its reactivity with NO_3 and O_3, although estimates have been made by comparison with other amines (Carter, 2008).

Since there is a lack of data, the purpose of the supplementary experiments was to investigate the reactions of MEA with HNO_3, O_3 and the NO_3 radical. Also included are experiments with two carbonyls: formaldehyde, since it is a major product of MEA photo-oxidation; and glycolaldehyde, which is an expected MEA photooxidation product (Bråten *et al.* 2009). Problematically, glycolaldehyde was not observed in mixing ratios above 3 ppbv in the MEA+NOx experiments listed in Table 2.

4.3.1 MEA + HNO_3

As MEA is a basic compound, in the gas phase it will react with acids in the atmosphere, such as nitric acid (HNO_3), to form aerosol. Similarly to ammonium salt aerosol formed by the reaction of ammonia with atmospheric acids, the formation of MEA salt particles is a reversible process, with the aerosol existing in equilibrium with gas-phase acid and MEA.

High amounts of nitrate have been observed in aerosol arising from MEA photooxidation in smog chamber experiments. In the presence of NO_2, O_3 and propene, ethanolamine reacts to form aerosol containing high amounts of nitrate (Murphy *et al.* 2007). A similar result has been observed for MEA in the presence of high concentrations of NO_2 (Nielsen *et al.* 2010). In the presence of more favourable conditions for photooxidation (lower NOx, higher NO to NO_2 ratio and lower O_3 concentrations) the nitrate component of the aerosol formed from MEA photooxidation was considerably lower, with the organic component comprising over two thirds of the total observed aerosol (Karl *et al.* 2012).

The objective of these experiments was to investigate the nature of aerosol formation from the reaction between MEA and HNO_3 in the dark in the smog chamber.

Injection of nitric acid into the chamber was accomplished by injection of a known quantity of nitric acid, diluted with Milli-Q water, into a heated glass cell through which nitrogen gas was passed at 2 litres min^{-1}. Nitric acid was injected into the chamber already containing gas phase MEA, in some cases multiple injections of HNO_3 were performed. The full list of experiments is listed in Table 4, with time normalised to

the first HNO_3 injection. Unless otherwise noted, the injection of HNO_3 into the chamber and subsequent reaction occurred under dark conditions. The amount of nitric acid injected is inferred from measurement of the mass of dilute acid injected, assuming full volatilisation.

Table 4. MEA + HNO_3 experiments. Time of injection is given relative to the first nitric acid injection

Expt	Relative time (min)	Injection (Number)	Amount (ppbv)	Notes
696	-92	MEA	54*	-
	0	HNO_3 (1)	1.5	-
	94	HNO_3 (2)	4.4	-
	189	HNO_3 (3)	9.1	Expt ended at 276 min.
698	-108	MEA (1)	51*	-
	0	HNO_3	1.6	-
	102	MEA (2)	90*	Expt ended at 280 min.
702	-199	MEA	470	Initial water concentration of about 1.1 x 10^6 ppbv present in clean air.
	0	H_2O (1)	4 x 10^4	Done to verify that aerosol growth was not due to Milli-Q water.
	29	H_2O (2)	1.5 x 10^5	-
714	-89	MEA (1)	10.7*	MEA dissolved in water to make dilute
	0	HNO_3 (1)	4.1	-
	99	HNO_3 (2)	4.1	-
	170	HNO_3 (3)	10.1	-
	204	HNO_3 (4)	10.5	-
	228	MEA (2)	11.4*	Expt ended at 290 min.

* Estimated MEA injection given measured liquid volume.

Unlike other experiments in this report, the aerosol measurements for HNO_3 experiments were not corrected for wall loss. The aerosol formed from these experiments was inorganic aerosol which was inherently different from the aerosol formed from MEA/NOx experiments, which is believed to be mostly organic in nature. This is evident in the particle number measurements of these experiments, where the number of particles does not vary substantially in the MEA/NOx experiments (Appendix C), but can change rapidly in the nitric acid experiments (Figure 6).

The theoretical mass has been calculated assuming full injection of nitric acid and MEA given quantified liquid volumes used for injections. The values in the figures have been multiplied by a factor of 2.4, for reasons explained below.

Within 15 minutes of the injection of nitric acid, aerosol formation occurred for almost all injections, as shown in Figure 6. The one exception to this was in experiment 714 (Figure 7), where aerosol formation did not occur after the third and fourth nitric acid injections. This was because the gas phase concentration of MEA had been depleted, as confirmed by aerosol growth upon a subsequent second injection of MEA.

Nitric acid was not observed by FTIR in the gas phase in any experiment, with a detection limit of approximately 15 ppbv. One exception was experiment 714, where some features consistent with nitric acid absorption were possibly observable after the fourth injection of nitric acid, but were not observed

after the second MEA injection. This is a tentative observation as the peaks were not sufficiently above baseline noise to provide positive identification.

For experiment 714, the lower than expected aerosol growth after the second injection and lack of aerosol growth after the third injection indicate that the amount of MEA in the chamber was considerably less than expected from the injection. This was also true of the second MEA injection.

Table 5 shows the impact of each HNO_3 injection, and a single MEA injection for experiment 714, on total aerosol mass (PM). The theoretical measurements assume full injection of nitric acid, or in the case of experiment 714, full injection of both nitric acid and MEA.

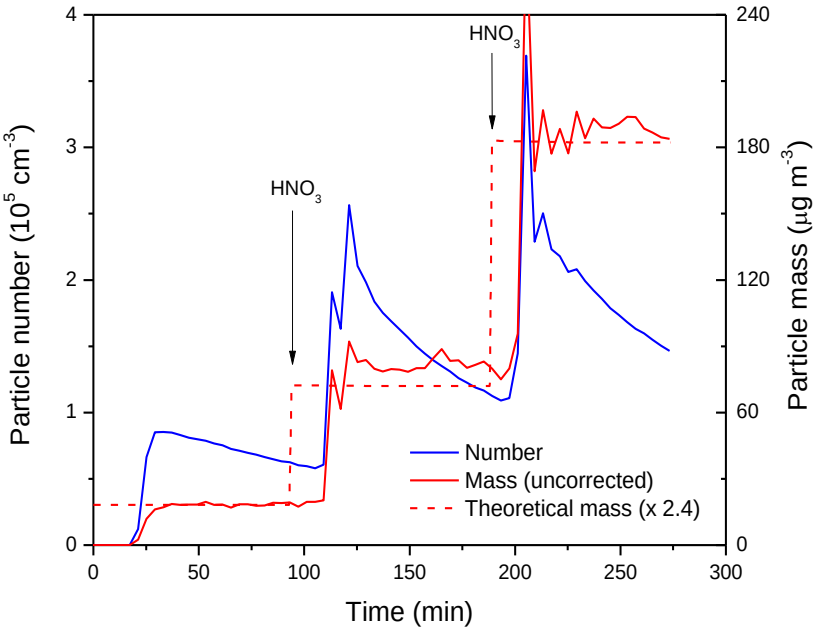

Figure 6. Particle measurements from experiment 696 (MEA + HNO_3); first HNO_3 injection at time zero

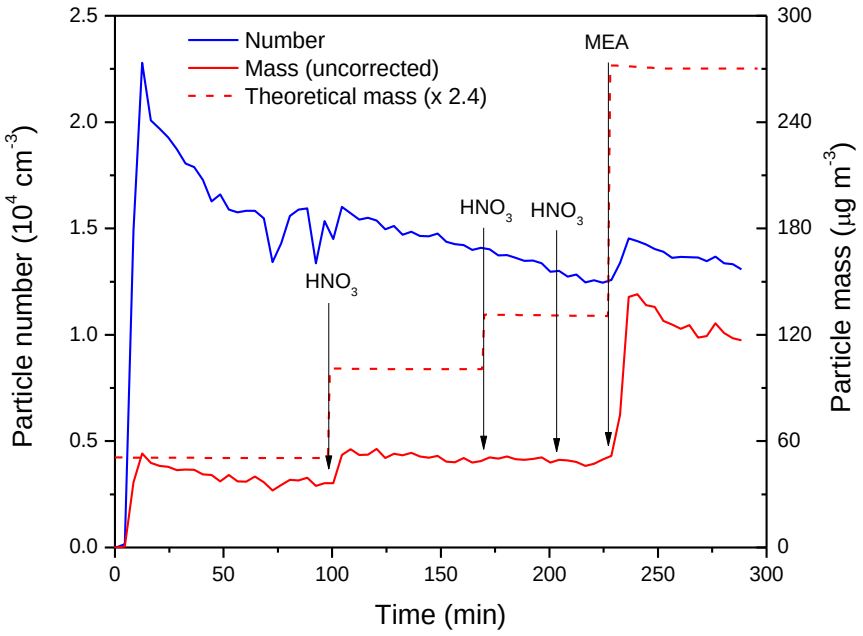

Figure 7. Particle measurements from experiment 714 (MEA + HNO_3); first HNO_3 injection at time zero

Table 5. Change observed in aerosol (PM) due to injections of nitric acid

HNO_3 Injection	HNO_3 injected ($\mu g\ m^{-3}$)	Theoretical ΔPM ($\mu g\ m^{-3}$)	ΔPM ($\mu g\ m^{-3}$)	Observed / Theory (%)
696-1	3.8	7.6	18.4 ± 0.7	243
696-2	11.4	22.5	63.5 ± 3.0	282
696-3	23.4	46.1	107 ± 5	233
696-total	38.6	76.0	189 ± 4	249
698	4.2	8.3	19.6 ± 0.8	235
714-1	10.7	21.0	36.8 ± 2.1	175
714-2	10.6	21.0	11.9 ± 2.4	57
714-3	25.8	12.6*	0.9 ± 2.4	-
714-4	26.9	-0.1*	-1.0 ± 2.4	-
714-MEA	28.6 (MEA)	57.5*	71.7 ± 4.3	125
714-total	74.0	111.8	120 ± 4	108

* Theoretical measurements for E714 are determined assuming full MEA injection. Negative growth for aerosol for the fourth injection is due to slight dilution of the chamber due to injection.

For each nitric acid injection where the gas phase MEA concentration was not limited, which is experiments 696 and 698, the amount of aerosol growth observed was much higher than that calculated from the injected amount of HNO_3. On average, the change in aerosol mass observed was two to three times what was expected given the injected amount of nitric acid. In one example, E696, the amount of aerosol observed (189 ± 4 $\mu g\ m^{-3}$) was 10% higher than the combined injected amounts of HNO_3 (38.6 $\mu g\ m^{-3}$) and MEA (130 $\mu g\ m^{-3}$). This increased observed mass relative to theoretically calculated mass implies one or more of the following possibilities:

1. Reaction between MEA and nitric acid occurs in a yield different than 1:1
2. The density of the aerosol observed is less than 1 $g\ cm^{-3}$
3. The SMPS is over-reading
4. There is an uptake of other compounds into the aerosol (such as water or CO_2).

Due to the low concentrations of nitric acid injected, and the uncertainty in MEA measurements, it has proven difficult to assess how much MEA is lost due to each nitric acid injection. As such the amount of MEA is lost to the aerosol phase was not able to be quantified. Given results observed for reaction of nitric acid with hydrazines in the gas phase (Tuazon *et al.* 1982), the reaction with MEA and nitric acid is believed to be 1:1, so it is unlikely but still possible that this increased mass can be explained by MEA uptake to the aerosol phase.

The density of MEA-nitrate aerosol has not been directly measured, however it is likely to be similar to the density calculated for other amine nitrates at ~1 $g\ cm^{-3}$ (Murphy *et al.* 2007), and the density measured for aerosol arising from MEA photooxidation at 1.3 $g\ cm^{-3}$ (Nielsen *et al.* 2010). The uptake of water to the aerosol phase cannot be discounted as a possibility, however for this to be accurate the aerosol would need to be comprised of 60% water (by weight) to explain the observed result. This is unlikely at the relative humidity of less than 5% used in the smog chamber.

If the observed high aerosol mass is due to the SMPS over-reading, the reasons for this are unclear, and it is uncertain as to whether this problem extends to organic aerosol which is formed in other MEA experiments in this report. This effect needs to be examined further.

To verify the cleanliness of the Milli-Q water which was used to dilute HNO_3, water was injected into a chamber containing MEA in experiment 702. A small particle distribution was observed upon injection of MEA of ~500 particles cm^{-3}, with total aerosol mass less than 0.1 µg m^{-3}. This distribution was not affected by injection of water (up to 2 ml), and the mass remained constant until the end of the experiment. We can therefore rule out the effect of Milli-Q water directly impacting upon aerosol formation with MEA alone, given the amount of water used in dilution and injection of nitric acid was a lot less than in present already in the smog chamber.

The reaction between MEA and nitric acid in the chamber forms aerosol rapidly, and has different behaviour from the organic aerosol formed in MEA/NOx experiments. The majority of the aerosol which is observed in MEA/NOx experiments is most likely not explained by the formation of HNO_3 and subsequent nitrate aerosol formation.

4.3.2 MEA + O_3 AND MEA + NO_3

A single experiment, experiment 706, was performed to observe the reaction of MEA with both ozone and the nitrate (NO_3) radical. The experiment was performed in the dark to eliminate the reactions of MEA with OH and $O(^3P)$ radicals. In the dark, the nitrate radical will form through the reaction of ozone and nitrogen dioxide:

$$O_3 + NO_2 \rightarrow NO_3 + O_2$$

It is expected that MEA would react rapidly with the NO_3 radical but slowly with O_3, given results observed for other primary amines (Malloy *et al.* 2009; Tang *et al.* 2013). The objective of this work was to investigate the impact of the nitrate radical on MEA.

The lights were not used at all during this experiment. Three injections were performed to assess the impact of the nitrate radical on MEA.

First injection	Approximately 240 ppbv ozone was injected between -213 and -118 minutes.
Second injection	MEA (116 ± 10 ppbv) was injected between -72 and -32 minutes.
Third injection	Approximately 50 ppbv NO_2 was injected at 0 minutes, however the amount could not be determined accurately due to faulty NOx analyser.

MEA + O_3

MEA was injected into the chamber containing 240 ppbv of O_3, which was generated by passing clean air past a mercury lamp O_3 generator. Upon injection of MEA, a small particle distribution was observed which was consistent with the similar distributions occasionally observed after the injection of MEA into a clean chamber. The total number of particles was less than 150 cm^{-3}, with a mean particle diameter of less than 50 nm.

Over 30 minutes, approximately 1.5 ppbv of ozone was lost (from an initial amount of 224 ppbv). If the wall loss rate for ozone (1×10^{-6} s^{-1}) is incorporated into this loss, the reaction rate of ozone and MEA was estimated to be 8.5×10^{-19} cm^3 $molecule^{-1}$ s^{-1}. This is an order of magnitude higher than 6.58×10^{-20} cm^3 $molecule^{-1}$ s^{-1} predicted by Carter (2008), but only slightly lower than 1.1×10^{-18} cm^3 $molecule^{-1}$ s^{-1} measured by Borduas *et al.* (2013).

As chamber mixing of MEA after injection was likely still proceeding during the dark period, the calculated MEA + O_3 reaction rate constant is likely to have a high uncertainty, particularly if the reaction of MEA and ozone produces radicals. Although the data is limited, it does suggest that the reaction of ozone and MEA is slow, and therefore is unlikely to be a major source of MEA loss in the chamber experiments.

MEA + NO_3

Upon injection of NO_2, depletion of ozone was registered instantly by the ozone analyser. Within 11±4 minutes, which was the time taken of the first full FTIR scan to be completed after the injection of NO_2, the concentration of MEA had decreased by approximately 20 ppbv (Figure 8). The reaction of MEA also led to the formation of NH_3 at 19±3 % yield across the experiment. This yield is consistent with that observed for NH_3 from the photooxidation of MEA with NOx.

The formation of NH_3 ceased once gas phase MEA had been consumed, which shows that NH_3 is either a first generation product of MEA reaction with NO_3, or is formed through one or more rapid reactions of first generation products under the conditions used.

Aerosol formation from this experiment was substantial, with 500 µg m^{-3} of aerosol formed after 2 hours reaction time (Figure 9). The amount of aerosol formed was in excess of the amount of MEA (294 µg m^{-3}) and NO_2 (95 µg m^{-3}, or 128 µg m^{-3} as NO_3) injected, giving an aerosol yield of approximately 170% relative to total reacted MEA. If it is assumed that all the injected gases (NO_3 and MEA which did not form NH_3) were completely contained in the aerosol phase, the remaining amount (20%) would have to be comprised of oxygen or water.

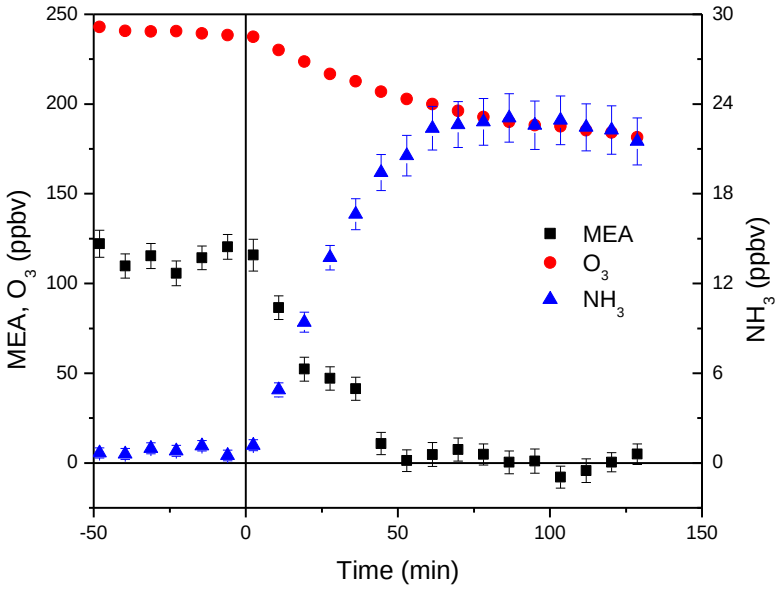

Figure 8. Gas phase concentrations for experiment 706 (MEA + O_3 + NO_2); NO_2 injection at time zero

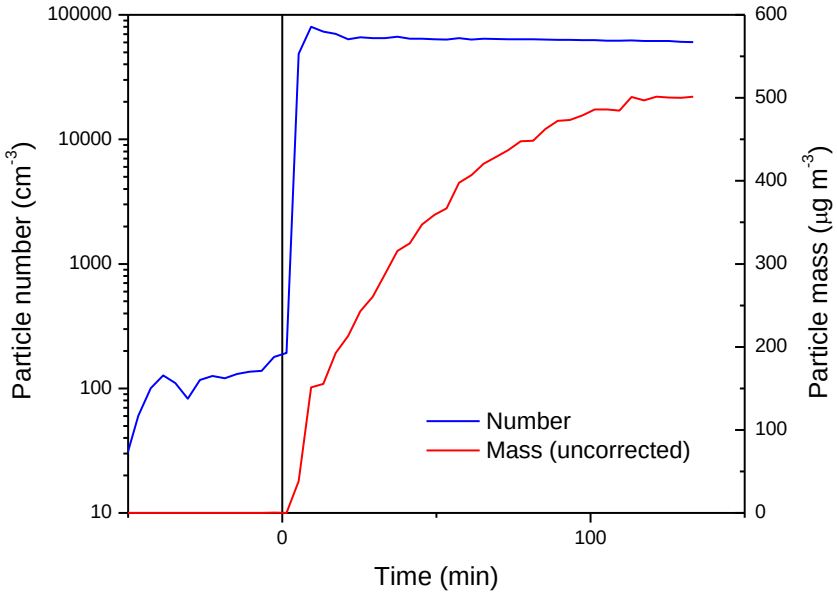

Figure 9. Particle number and mass from experiment 706 (MEA + O_3 + NO_2)

Aerosol yields of up to 115% have been observed for the reaction of alkylamines with the NO_3 radical (Silva *et al.* 2008; Malloy *et al.* 2009; Tang *et al.* 2013), with the aerosol phase comprised of a mixture of inorganic and organic phases. The inorganic aerosol arises at least in part from the reaction of HNO_3 with the amine, with nitric acid formed by hydrogen extraction from the initial nitrate radical reaction with the amine:

$$R\text{-}NH_2 + NO_3 \rightarrow RNH^{\cdot} + HNO_3$$

$$R\text{-}CH_2\text{-}NH_2 + NO_3 \rightarrow R\text{-}C^{\cdot}H\text{-}NH_2 + HNO_3$$

The presence of ozone in this experiment may have increased the potential aerosol yield, because although MEA reacts with ozone slowly, some of the reaction products may react quickly with ozone. The reaction mechanism for MEA with NO_3 also has the potential to form other radicals, such as the OH or HO_2 radicals. As such, it cannot be confirmed that the loss of MEA was entirely due to reaction with NO_3 or HNO_3, which means no recommendation can be made as to the reaction rate constant of MEA with the NO_3 radical.

Similarly, the high aerosol responses observed from the reaction of MEA with HNO_3 reaction, which may possibly be attributed to the instrument over-reading nitrate aerosol, may also have affected this experiment. Given results observed in other studies, it is reasonable to conclude that the aerosol yield from the reaction of MEA with NO_3 in the presence of ozone is much higher than that which arises from the largely OH-initiated photooxidation of MEA with NOx.

4.3.3 MEA + FORMALDEHYDE

During the course of this study it became apparent that when samples which contained MEA, including those taken from MEA headspace, were analysed by GCMS, 1,3-oxazolidine was always present.

In solution, 1.3-oxazolidine can be formed by the reaction between MEA and formaldehyde (HCHO) to form a Schiff base which subsequently cyclises to 1,3-oxazolidine (Bergmann *et al.* 1953). It has also been observed to form *N,N'*-methylenebisoxazolidine (MW 156.7 g mol^{-1}) with formaldehyde in excess (Gafarov *et al*. 1978). This latter compound, or similar compound, is a candidate for the unknown compound (20.78) listed in Table 3. Other compounds detected include 3-methyl-1,3-oxazolidine and three unknowns at MW 89 (18.40), MW 101 (16.45) and MW 102 (15.12).

In the MEA+NOx experiments HCHO is a major product and therefore it is expected that it will react with MEA to form 1,3-oxazolidine which, by way of example, was observed to increase in concentration in E750. However, its analysis was complicated by the variability in Tenax media. Even though the sampling Tenax tubes were the same type, one batch systematically produced significantly larger peak areas for 1,3-oxazolidine than another. This effect only appeared to be an issue for 1,3-oxazolidine.

The purpose of this experiment was to clarify the relationship between 1,3-oxazolidine and HCHO by investigating the reaction that occurs between them in the gas phase.

Two trial experiments were performed to optimise injection and sampling methodology and establish an experimental protocol. The results presented here and in Table 3 arose out of experiment 773 which was performed over two days at 25±1°C, mostly in the dark. The initial MEA mixing ratio prior to HCHO injection was 384±12 ppbv. Four injections of HCHO were performed using the warmed paraformaldehyde method. The first three were monitored using FTIR. The last injection was adjusted to cause an excess of HCHO in the chamber and allowed to react with residual MEA overnight.

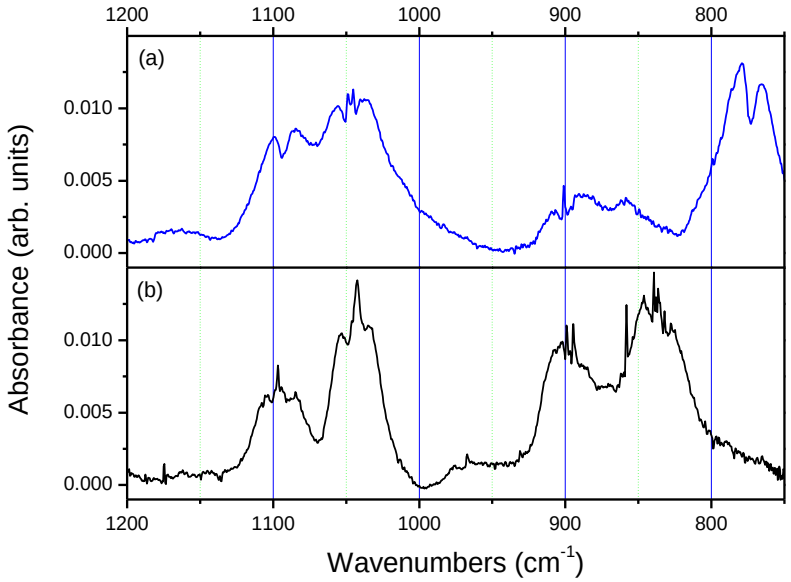

Figure 10. FTIR spectra (1 cm^{-1}) obtained in E773 for (a) unreacted MEA and (b) after complete reaction of MEA with HCHO in the gas phase

Figure 10 compares the FTIR spectrum (1 cm^{-1}) obtained for MEA in the chamber prior to the injection of HCHO with a spectrum taken of the product formed in the dark overnight.

There are obvious differences between the spectrum of MEA in Figure 10a and the product spectrum in Figure 10b**.** The most prominent difference being the lack of the NH_2 wagging feature and accompanying C^2H_2 rocking features below 800 cm^{-1} in the product spectrum. This suggests that the amine group has been modified but it is unclear if the spectrum represents 1,3-oxazolidine. According to Bergmann (1953) the oxazolidine ring, in the liquid phase, is "characterised by a triplet of bands in the 1080-1200 cm^{-1} region". In the product spectrum there are only two obvious bands in this region. Spectral assignments for this spectrum are yet to be finalised. Evidence for the product being 1,3-oxazolidine is given in Table 3, where the GCMS results for a sample taken at the start of the second day indicates that the predominant species was 1,3-oxazolidine.

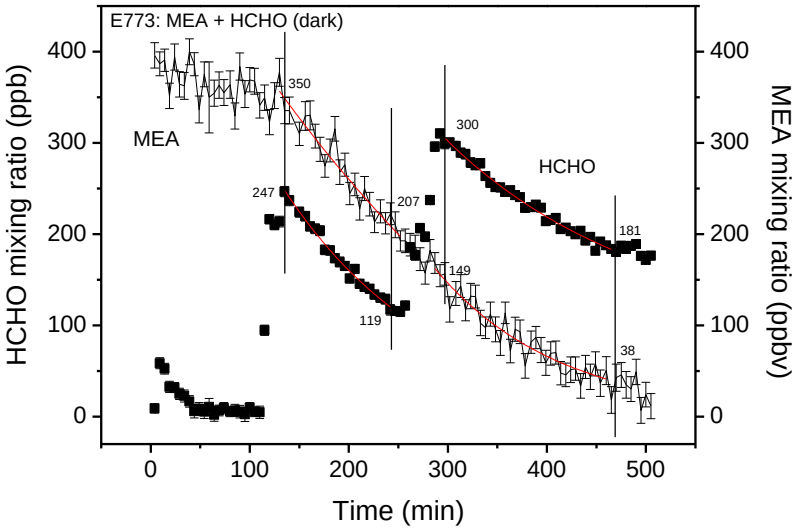

Figure 11. Reactant profiles for MEA and HCHO observed in E773

As shown in Figure 11, after the first HCHO short duration injection at time zero, there was a small decrease in the MEA mixing ratio as all the HCHO was consumed. At ~120 minutes a second larger injection was performed which resulted in loss of both HCHO and MEA. This reaction was allowed to proceed until at ~250 minutes a third injection was performed.

In order to estimate a rate constant for this reaction, it was assumed that the reaction between MEA and HCHO was second order overall but first order in MEA and HCHO where,

$$\text{MEA} + \text{HCHO} \rightarrow \text{1,3-oxazolidine} + H_2O$$

Both reaction transitions shown in Figure 11 were analysed by application of the second order differential rate law for a non-stoichiometric ratio,

$$\frac{dx}{dt} = k([A(0)] - x)([B(0)] - x)$$

Where the initial reactant concentrations $A(0)$ and $B(0)$ are not equal, k is the rate constant and x is reactant consumed.

Figure 12 is a graph of the linear form of the second order differential law as applied to the two reaction transitions shown in Figure 11 where the slope of each graph is the rate constant, $k_{\text{MEA + HCHO}}$.

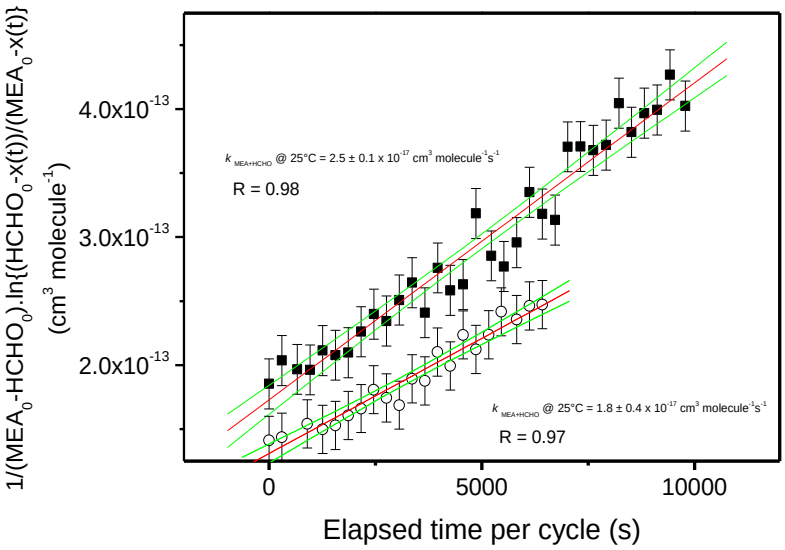

Figure 12. MEA+HCHO rate constant determination for experiment 773

In Figure 12, the 95% confidence limits are shown in green. The value of the rate constant obtained for the first transition was 2.5±0.1 x 10^{-17}cm^3 molecule^{-1} s^{-1} and for the second transition was 1.8±0.4 x 10^{-17} cm^3 molecule^{-1} s^{-1}.

It is concluded that the reaction between MEA and HCHO to form 1,3-oxazolidine is first order in each reactant. The average value of the rate constant, $k_{\text{MEA+HCHO}}$ was calculated to be ~2.1 x 10^{-17} cm^3 molecule^{-1} s^{-1} at 25±1°C.

The reaction between MEA and formaldehyde has been included in the MEA photooxidation mechanism developed in this study.

4.3.4 MEA + GLYCOLALDEHYDE

A single experiment (E785) was performed to investigate the reaction between glycolaldehyde and MEA. Trials were not able to be performed for this experiment so the experimental protocol used was similar to that used for the formaldehyde experiment. The MEA and glycolaldehyde concentrations were monitored using FTIR. The reference spectrum used for glycolaldehyde was generated by Montserrat Martín Reviejo from work done in the EUPHORE chamber, and were kindly provided to CSIRO for another project in 2005 (Magneron *et al*. 2005, Wirtz 2005).

MEA was injected into the chamber first and allowed to settle for ~130 minutes, at which time the mixing ratio was 436±14 ppbv. Three injections of glycolaldehyde were performed by warming the glycolaldehyde dimer at the same carrier rate for different periods. The last injection was made long enough to ensure that glycolaldehyde was in excess and that all the MEA had reacted.

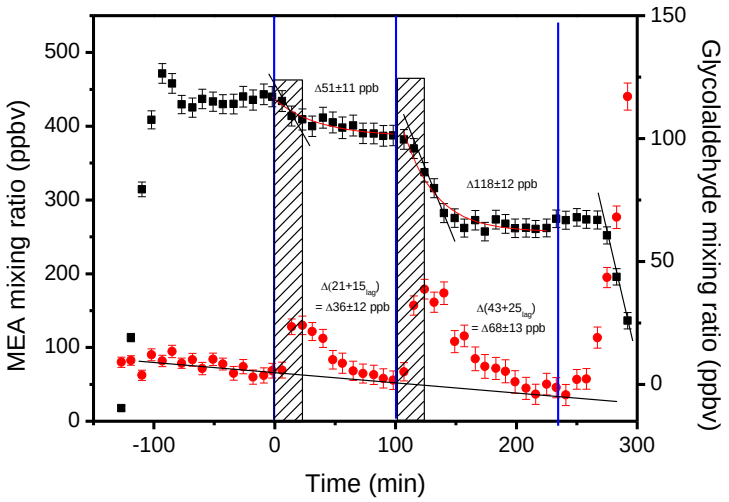

Figure 13. Mixing ratio profiles for MEA and glycolaldehyde obtained in E785

Figure 13 shows the MEA (black) and glycolaldehyde (red) mixing ratio profiles over the course of the experiment. The glycolaldehyde reacted much more quickly with MEA than formaldehyde. The reaction was so much faster that there was a lag time (hatching) between the MEA and glycolaldehyde as the glycolaldehyde reacted whilst being injected.

On the assumption that the reaction was first order in both glycolaldehyde and MEA, the second order differential rate law was applied to the data in a similar manner to that used for the MEA + HCHO reaction. The initial glycolaldehyde mixing ratio was calculated to be 114 ppbv based on the disappearance of MEA. The result of this analysis indicated that it was likely that the reaction was not second order overall.

The reaction was then assumed to be third order overall and second order in MEA and is described by the reaction,

2MEA + glycolaldehyde (GLYD) → products

Data for MEA was applied to the integrated rate expression for a nonstoichiometric starting mixture derived from the differential rate law:

$$-\frac{1}{2}\frac{d[MEA]}{dt} = -\frac{d[GLY]}{dt} = k[MEA]^2[GLY]$$

Figure 14 is a graph of the results obtained from the third order integrated rate expression plotted against time. According to third order reaction theory, the slope of the line obtained is equal to $0.5k$ where k is the rate constant. The rate constant, $k_{MEA+GLY}$ obtained from a linear fit of the data in Figure 14 was ~2.0 x 10^{-29} cm^6 $molecule^{-2}$ s^{-1}.

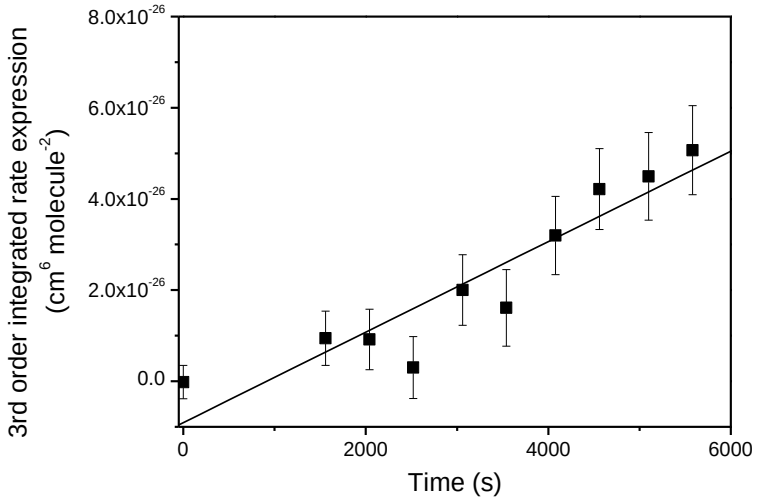

Figure 14. MEA+glycolaldehyde rate constant determination for experiment 785

It is postulated that for such a reaction to proceed, the most likely scenario would be that MEA and glycolaldehyde would form a carbonyl+amine transition product which is stabilised by hydrogen bonding between the hydrogen on the glycolaldehyde hydroxyl group and the carbonyl oxygen located on the neighbouring α-carbon. It is expected that this would leave the α-carbon open to nucleophilic attack by the amino group or possibly, the hydroxyl group of an additional MEA molecule. It is unclear at this stage what the final product(s) would be but this sequence can be represented by two reactions, where the second reaction is thought to be faster than the first, such that $k_2 > k_1$.

$$\text{MEA + GLY} \xrightarrow{k_1} \text{product 1}$$

$$\text{MEA + product 1} \xrightarrow{k_2} \text{product 2}$$

A similar observation was made by Tuazon *et al.* (1994) for the reaction between diethylamine and formaldehyde, which also proceeded in a 2:1 molecular ratio to form *N,N,N',N'*-tetramethyl-diaminomethane.

The GCMS results presented in Table 3 indicate that after the first glycoladehyde injection, MEA was present as well as 1,3-oxazolidine, both of which were depleted after the third injection. Compounds that appear to be associated with the MEA/glycolaldehyde reaction and not with the other reactions in Table 3 are butanoic acid, pyridine and two unknowns with molecular weights of 97 (11.56) and 129 (15.09) g mol^{-1}. Compounds common to the MEA+NOx experiment 750 are morpholin-2-one, 2-oxoacetamide and unknown MW 101(16.45).

The reaction between MEA and glycolaldehyde has been included in the MEA photo-oxidation mechanism developed in this study.

5 Piperazine (PZ) experiments

5.1 Literature summary of relevant PZ photochemical research

In contrast to the work performed for MEA, only a single experimental study has been publicly reported on piperazine (Nielsen *et al.* 2012b). Products observed from the photooxidation of piperazine in NOx include 1,2,3,6-tetrahydropyrazine, 1-nitrosopiperazine, 1-nitropiperazine, dihydropyrazine, pyrazine, formamide, ammonia, formaldehyde and acetaldehyde. As a secondary amine, the main nitrosamine (1-nitrosopiperazine) is expected to be stable enough to be observed in the atmosphere, as observed by Nielsen *et al.* (2012b). They showed however that this nitrosamine was more reactive than other secondary nitrosamines, probably due to the second amine atom present in piperazine. The same was also true for the equivalent nitramine (1-nitropiperazine).

The reaction rate of PZ with OH has not been determined, but is expected to be fast as piperazine contains two amine atoms and four carbon atoms directly adjacent to an amine, all of which are known to react rapidly with OH. The structure-activity relationship (SAR) method (Kwok and Atkinson 1995), used to estimate unknown reaction rate constants of VOCs with the OH radical, predicts a reaction rate constant for PZ with OH of 1.69 x 10^{-10} cm^3 $molecule^{-1}$ s^{-1}. Similar predictions are made by the SAPRC SAR method (1.86 x 10^{-10}) (Carter 2008) and the updated SAR parameters described by Nielsen *et al.* (2012a) (1.58 x 10^{-10}). These calculations must be used with caution, as the effect of two amine nitrogens on a single compound has not been evaluated using this approach, and the reactivity of diamines may be affected in ways not accounted for by the current SAR protocol.

As a secondary amine, piperazine will react with ozone and the nitrate radical at non-negligible rates. Using the SAR expression for the reaction of amines with ozone generated by Carter (2008), an estimate for the reaction of piperazine with ozone of 2.1 x 10^{-16} cm^3 $molecule^{-1}$ s^{-1} is generated. The calculated ozone reaction rate for PZ is more rapid than any reaction rate experimentally determined to date for amines and ozone. This is because the SAR method for ozone relies on a correlation to the OH reactivity of carbon atoms adjacent to an amine, for which piperazine has four.

5.2 Results of PZ/NOx reaction experiments

5.2.1 PZ + NO_X

A total of four PZ/NOx experiments were performed to investigate the photooxidation of PZ in NOx and identify reaction products. Given the number of experiments performed, it was not possible to develop a mechanism for PZ photooxidation as a component of this report. The experimental procedure, including sampling and analysis, was the same as that used for the MEA experiments (Section 4.2.1).

A reference infrared spectrum of PZ was generated for this study, but its quantitative validation is still proceeding. Consequently, the PZ concentrations presented are an upper limit determined using a reference spectrum produced by a known mass injection of PZ assuming 100% recovery.

The initial mixing ratios used in these experiments are shown in Table 6, along with the final mixing ratios for key species.

Table 6. Initial and final mixing ratios for reactants and key products observed in the four PZ/NOx experiments and single PZ/^{15}NOx experiment

Exp	Initial Conditions				Final concentrations at/near to 4 hours				
	PZ/NOx	PZ (ppbv)	NO (ppbv)	NO_2 (ppbv)	O_3 (ppbv)	NH_3 (ppbv)	HCHO (ppbv)	Aerosol ($\mu g\ m^{-3}$)	Aerosol Yield
789	8.9	381	39	4	16	38	15.4	703	0.52
791	1.6	70	39	6	13	8.5	8.3	148	0.69
793[a]	2.7 ± 1	393	-	-	31	36	13.7	1466	1.12
800	1.2	60	41	9	15	10	9.6	137	0.66
803[b]	9.0	376	42	0	6	37	13.1	544	0.44

[a] Final concentrations for E793 were taken at 3 hours. Initial NOy difficult to determine, but should be around 200 ppbv given injection volume (measured > 106 ppbv).

[b] Exp 803 was performed using ^{15}NO instead of ^{14}NO. See Section 5.2.2.

Ozone growth was inhibited in PZ experiments, with a maximum of 31 ppbv observed for the four experiments completed (Figure 15 through Figure 18). The maximum O_3 concentration observed for MEA/NOx experiments was 85 ppbv for E750, for the equivalent PZ experiment (E789) it was merely 16 ppbv. This was despite a more rapid reaction of PZ and more rapid conversion of NO to NO_2. The logical conclusion was that PZ, while reacting faster than MEA in the presence of NOx, also inhibited ozone formation. This could occur by uptake of nitrogen to organic compounds such as nitramines, or depletion of ozone by reaction with PZ. Both of these processes occur for PZ photooxidation, as shown by the formation of nitramines (Section 5.1.3) and rapid reaction of PZ and its reaction products with ozone (Section 5.2.1).

The maximum yield of ammonia observed was 10 ± 1 % in the high PZ experiments, with equivalent but higher yields (within experimental uncertainty) observed for the low PZ experiments: 13 ± 2 % for E791 and 14 ± 5 % for E800. This is lower than the ammonia yield observed for MEA experiments (>20%) after 4 hours.

The formation of formaldehyde was confirmed for PZ, but as observed with MEA in the gas phase, it is expected that formaldehyde will react with PZ. A product which could be consistent this expectation was observed by Nielsen *et al.* (2012b), and a compound of the same molecular weight was observed with GCMS in these experiments. This compound was tentatively identified as piperazine-1-carbaldehyde. To form the carbaldehyde ($C_5H_{10}N_2O$) from the reaction of piperazine and formaldehyde ($C_4H_{10}N_2$ + CH_2O = $C_5H_{12}N_2O$) requires the loss of two hydrogen atoms, so it is possible that this compound arises from the reaction of formaldehyde with a reaction product of PZ.

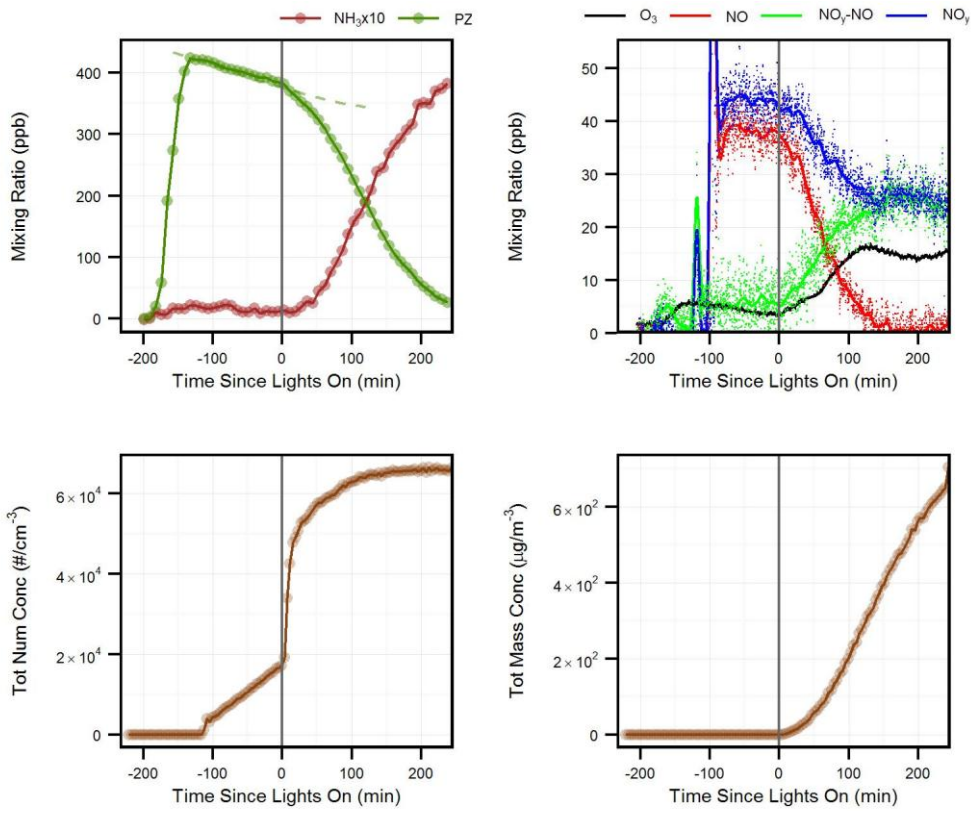

Figure 15. Gas and particle phase results from E789 (PZ + NOx)

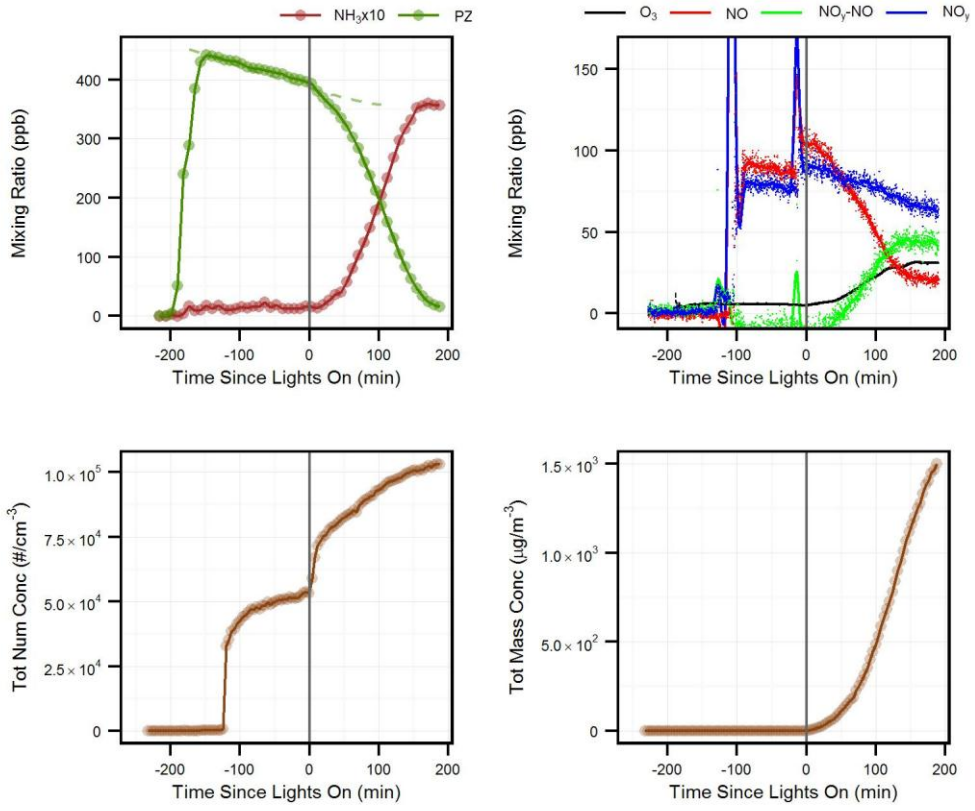

Figure 16. Gas and particle phase results from E793 (PZ + NOx)

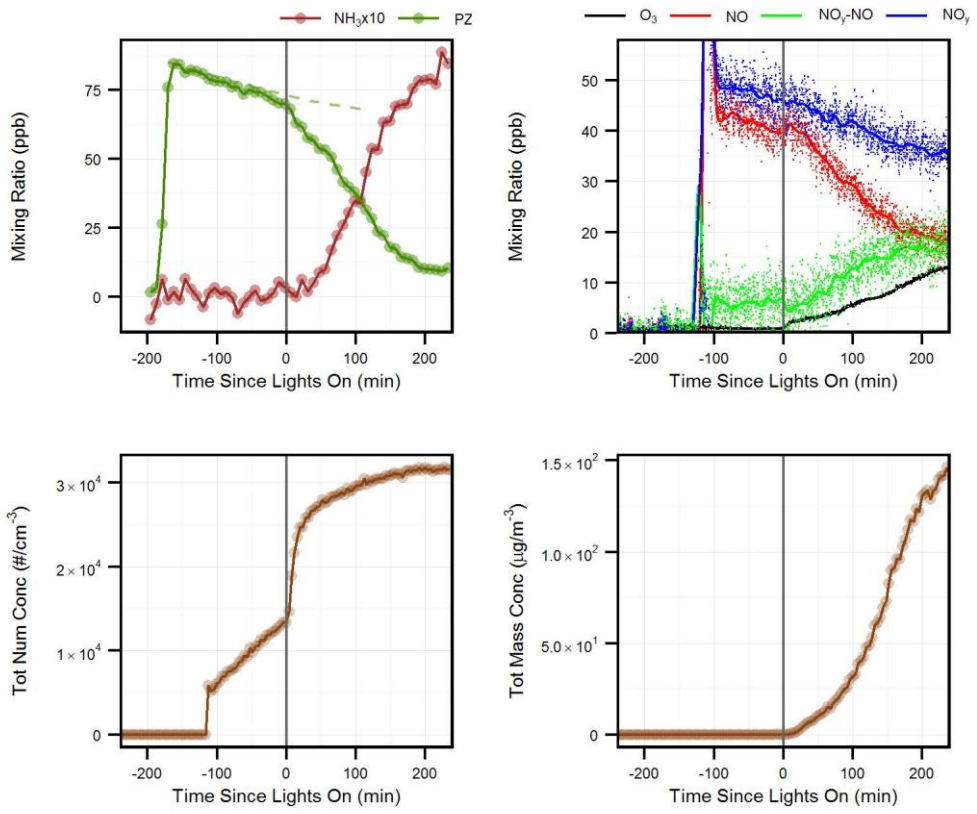

Figure 17. Gas and particle phase results from E791 (PZ + NOx)

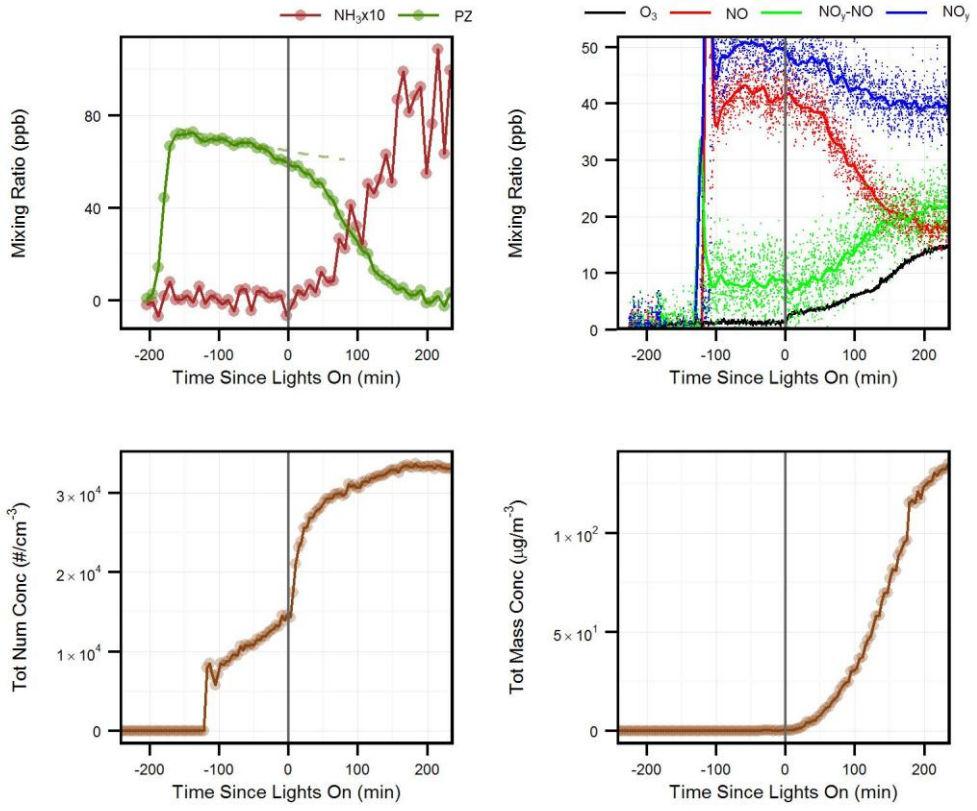

Figure 18. Gas and particle phase results from E800 (PZ + NOx)

The photooxidation of PZ produces large amounts of aerosol, with yields ranging from 52% in E789 after four hours to in excess of 110% for E793 after three hours. The yields are significantly higher than MEA NOx photooxidation experiments at 4 hours, which for experiments with initial NO greater than NO_2, had aerosol yields between 7% and 40%.

The highest aerosol yields for both piperazine and MEA were those which contained the highest mixing ratio of NO_2 across the experiment. For piperazine, this was the high NOx E793, which was halted early due to exceptionally high aerosol mass. For MEA, the experiment which contained high initial NO_2 (E738) had an aerosol yield of 50%. In contrast, another MEA experiment E725 which had an NO_2 concentration of between 50 and 80 ppbv across all four hours, less than 30 µg m^{-3} of aerosol formed after four hours. These results would suggest that a significant formation route for aerosol production in amine chamber experiments is directly or indirectly related to NO_2, such as reactions of amines with the nitrate radical, or reactions of NO_2 with amine photooxidation products.

5.2.2 PZ + ^{15}NOX

Two PZ/NOx experiments were performed using nitrogen-15 labelled nitric oxide (^{15}NO), instead of unlabelled (natural isotopic) nitric oxide. The first of these experiments, E795, was excluded due to high carryover of organic material from the previous high NOx experiment (E793). The initial conditions for the other experiment (E803) are shown in Table 6, with the gas phase profile shown in Figure 19. The injection of NO_2 was not performed for either experiment as ^{15}N-labelled nitrogen dioxide was not available.

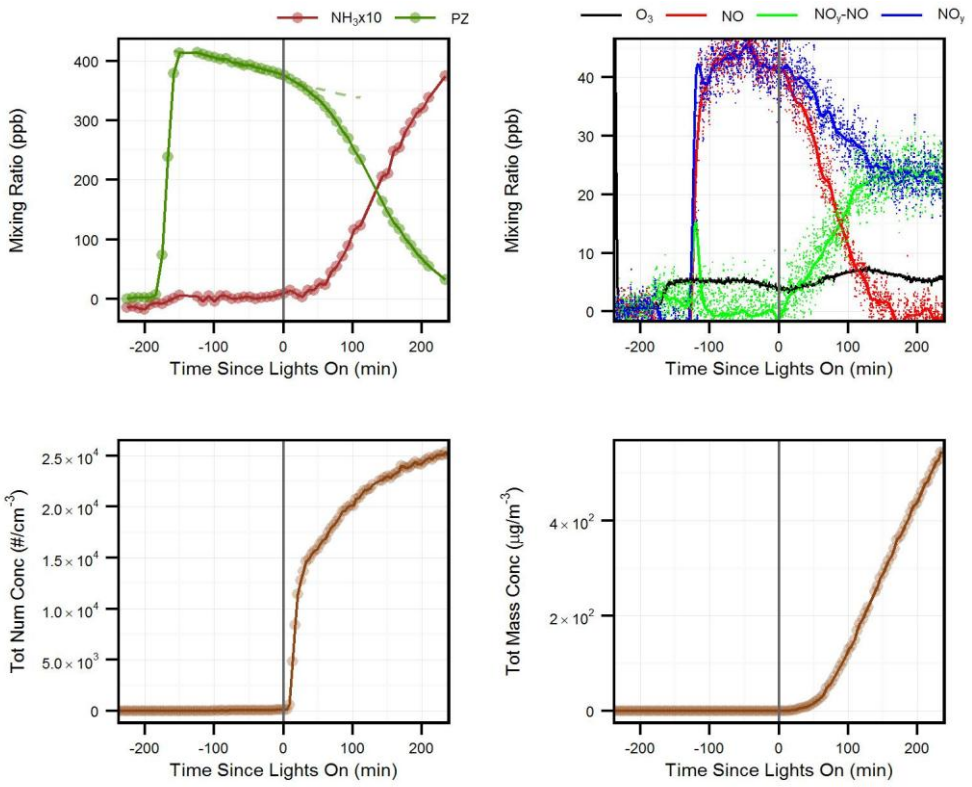

Figure 19. Gas and particle phase results from E803 (PZ + ^{15}NO)

The purpose of these experiments was to confirm the presence of nitrosamine and nitramine as photooxidation products of PZ, and to observe any other products which arose from the uptake of NOx to

amine compounds. The nitrosamine and the nitramine were confirmed, however no additional products containing NOx were observed.

The ozone and aerosol formation from E803 was lower than that of E789. Both of these experiments had similar initial conditions, except that NO_2 was not injected in E803. The concentration profiles for PZ across 4 hours were similar also, indicating a similar loss of PZ through reaction and wall loss. So while a kinetic isotope effect due to ^{15}NO cannot be ruled out as a reason for the differences between E803 and E789, the lack of initial NO_2 in E803 is the more likely reason that ozone and aerosol formation was inhibited.

5.2.3 NITROSAMINE AND NITRAMINE FORMATION FROM PZ

The atmospheric degradation of piperazine with NOx will lead to the formation of 1-nitropiperazine (NPZ) and 1-nitrosopiperazine (NitroPZ) (Figure 20).

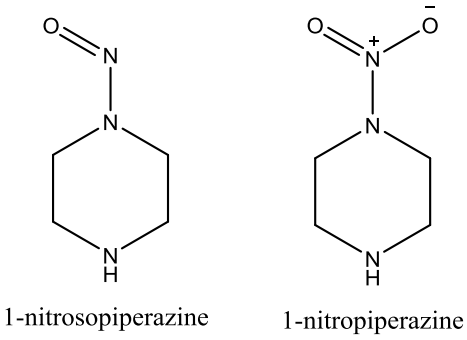

Figure 20. Chemical structures of 1-nitrosopiperazine (NPZ) and 1-nitropiperazine (NItroPZ)

Peaks corresponding to the molecular weight of the nitrosamine (*m/z* 115) and nitramine (*m/z* 131) were observed in the GCMS analysis of collected sorbent tube samples for PZ/NOx experiments. The nitrosamine was confirmed by retention time and mass spectral fragment comparison to the standard. For the nitramine, the base peak (*m/z* 86; M-44) was unlabelled, and corresponded to the loss of the NO_2 substituent from the nitramine.

Gas phase concentrations of the nitrosamine and peak area responses for the nitramine are provided for E789 in Figure 21. The gas phase concentrations provided for NPZ are tentative only, and are based on the response of the nitrosamine standard.

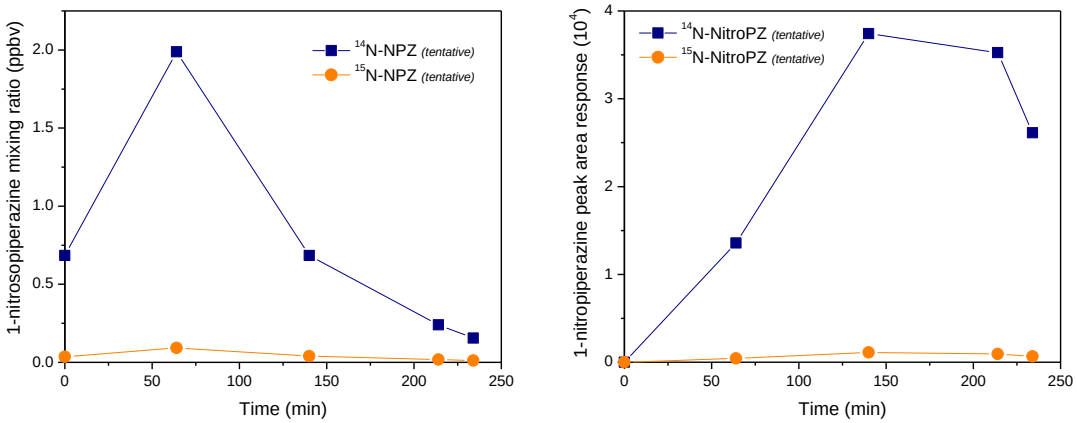

Figure 21. Tentative NPZ mixing ratio and area peak response for NitroPZ from E789

The profile of both the nitrosamine and the nitramine are consistent with expectations, with the concentration of NPZ higher for samples taken when NO was present in the chamber. As NO was depleted and converted into NO_2, the concentration of the nitramine increased while the nitrosamine decreased. NPZ was observed in the dark TD sample in E789, despite the fact that minimal PZ had reacted. It is possible that NPZ observed at or before time zero is a degradation product arising due to sampling or injection of PZ.

For experiment 803, where ^{15}NO was used instead of unlabelled nitric oxide, the nitrosamine formed during the experiment will be ^{15}N-labelled at *N*-nitroso atom following hydrogen abstraction at the amine atom (Figure 22). The nitramine will be ^{15}N-labelled at the nitro position, formed by equivalent reaction of the aminyl radical with $^{15}NO_2$ rather than ^{15}NO.

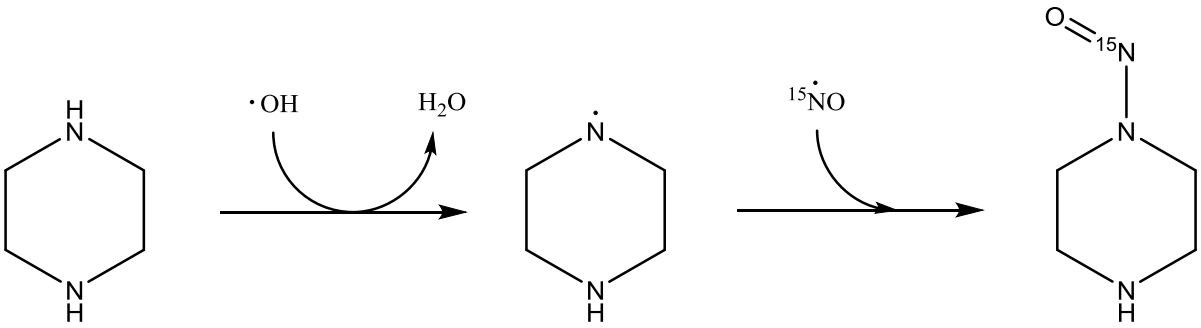

Figure 22. Formation of 1-(nitroso-^{15}N)piperazine (^{15}N-NPZ) from piperazine and ^{15}NO

The uptake of reactive nitrogen to the amine to form nitrosamine and nitramine was confirmed by the presence of peaks which correspond to the labelled compounds (Figure 23). The response of these peaks was much higher than the response for the equivalent unlabelled isotopologue. For the nitramine, the base peak arising from the loss of the $^{15}NO_2$ substituent in the labelled experiment (m/z 86) was the same as in the unlabelled experiments.

In E789, the base peak areas of the ^{15}N nitrosamine and nitramine isotopologues relative to the base peak areas of ^{14}N and ^{15}N isotopologues combined were 5% and 3% respectively. This can be attributed to naturally occurring isotopologues of these compounds. It is not clear though why the nitramine isotopic ratio is lower than the nitrosamine.

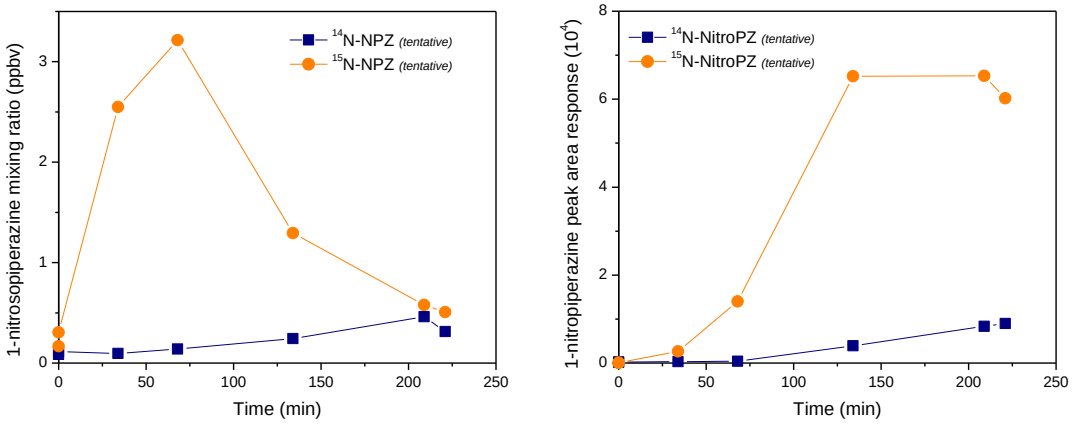

Figure 23. Tentative NPZ mixing ratio and area peak response for NitroPZ from E803

For E803, the relative peak area of the ^{15}N nitrosamine ranged between 56% and 96% of the total peak area for both isotopologues. For the ^{15}N nitramine, this proportion was between 87% and 97%. The unlabelled NPZ was present in the dark before the lights were turned on, with peak area approximately 30% of the total NPZ response. At least 65% of the NPZ can therefore be attributed to injected ^{15}NO, either during equilibration and reaction in the chamber, sampling or analysis.

Over time in E803, the proportion of ^{14}N-nitrosoamine and ^{14}N-nitramine increases relative to the isotopologues containing ^{15}N. Some of this might be attributed to partitioning of extant organic material from previous experiments off the chamber walls, or nitrosamine formation where the *N*-nitroso nitrogen atom arises from a nitrogen atom in PZ.

5.3 Results of supplementary PZ experiments

5.3.1 PZ + O_3

A single experiment (E787) was performed to evaluate the reaction of PZ with ozone. To avoid photolysis of ozone, the experiment was performed in the dark, except for a single hour photolysis at the end of the experiment (Figure 24).

Approximately 245 ppbv of ozone was injected into the chamber, followed after equilibration by an injection of PZ. Reaction occurred almost instantly upon injection of PZ, and as such the initial PZ concentration could not be measured. The initial PZ concentration estimated by liquid volume injection mass was 117 ppbv. Ammonia was generated by the reaction of PZ with ozone, with a yield of at least 9% assuming full injection of PZ, consistent with that observed by PZ/NOx experiments.

During the reaction of PZ and ozone, approximately 200 ppbv of ozone had reacted. This amount was in excess of the maximum amount of piperazine likely to be in the chamber, but as PZ is a diamine it was not in excess of the total molecular amine concentration. As the reaction of ozone with PZ is unlikely to be termolecular, it can be concluded that ozone also reacts with at least some of the first generation products of piperazine.

Irradiation of the products arising from PZ and O_3 in the presence of 40 ppbv ozone resulted in additional growth of aerosol and ammonia. A small increase in ozone concentration was also observed during this time. This reaction to form aerosol and ammonia during irradiation implies either that some of the products formed by PZ and O_3 photolyse to form reactive products, or that the $O(^3P)$ radical which is formed by photolysis of ozone leads to further reaction of PZ products.

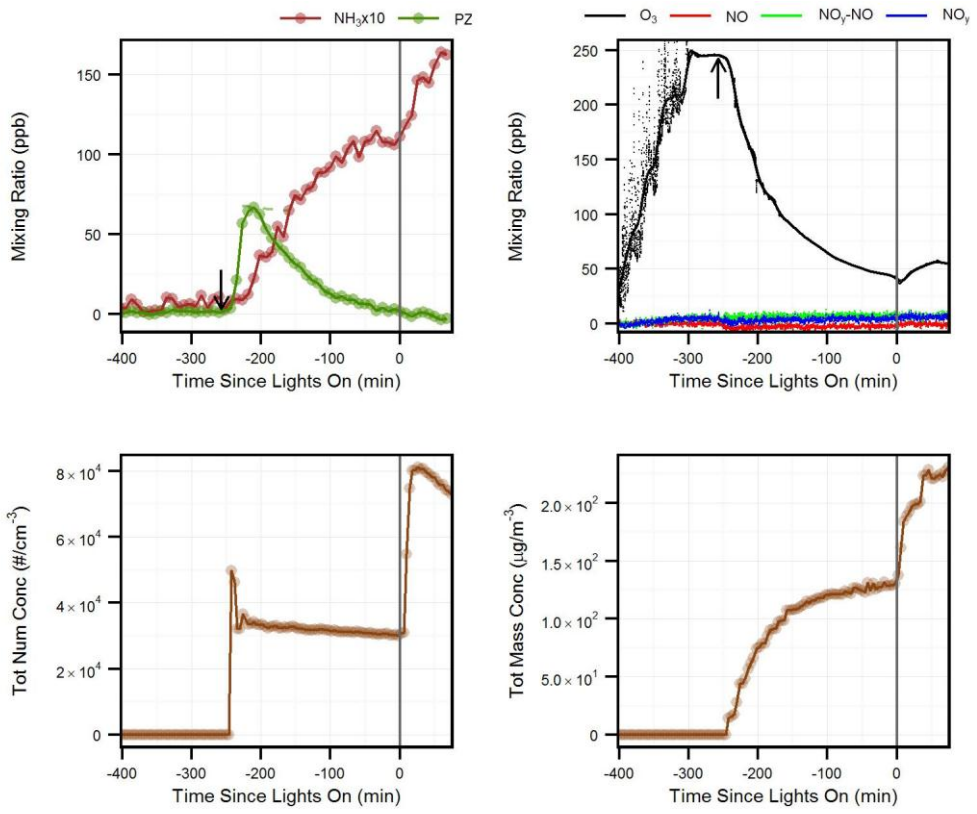

Figure 24. Dark and UV profiles for E787. PZ injection at -257 mins (arrow)

5.3.2 PZ + HNO_3

A single experiment (E783) was performed to evaluate the reaction between nitric acid and PZ in the smog chamber. Similar to the experiments with MEA, each injection of nitric acid gave rise to an increase in total aerosol mass (Figure 25) which was greater than what should have occurred given the amount of HNO_3 injected. The factor increase was higher than that observed for MEA, with a factor of 3.2 for the first injection as calculated in Table 7.

Table 7. Change observed in aerosol (PM) due to nitric acid injections for experiment 783.

Injection (Number)	HNO_3 injection ($\mu g\ m^{-3}$)	Theoretical ΔPM ($\mu g\ m^{-3}$)	ΔPM ($\mu g\ m^{-3}$)	Observed / Theory (%)
HNO_3 (1)	5.6	13.3	43.0 ± 1.2	324
HNO_3 (2)	12.3	29.0	108 ± 2	374
HNO_3 (3)	47.8	113.1	355*	314*
HNO_3 (combined)	65.4	154.8	507*	327*

* Aerosol mass did not equilibrate, still increasing.

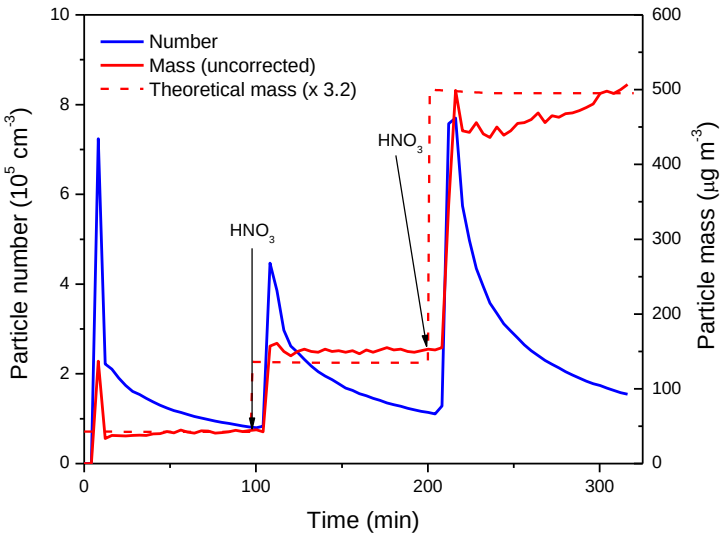

Figure 25. Particle measurements from experiment 783 (PZ + HNO_3). First injection of HNO_3 occurred at 0 minutes

As the PZ concentration could be determined more precisely than MEA, the variation in gas phase concentration due to the injection of nitric acid could be observed (Figure 26). The three injections of nitric acid (equivalent to 2.2, 4.8 and 18 ppbv) resulted in changes of greater than 4 ppbv in the concentration of PZ each time. The accuracy of PZ mixing ratios as fit by FTIR is till yet to be confirmed at these concentrations, so no quantitative analysis can be performed until a reference spectrum has been verified.

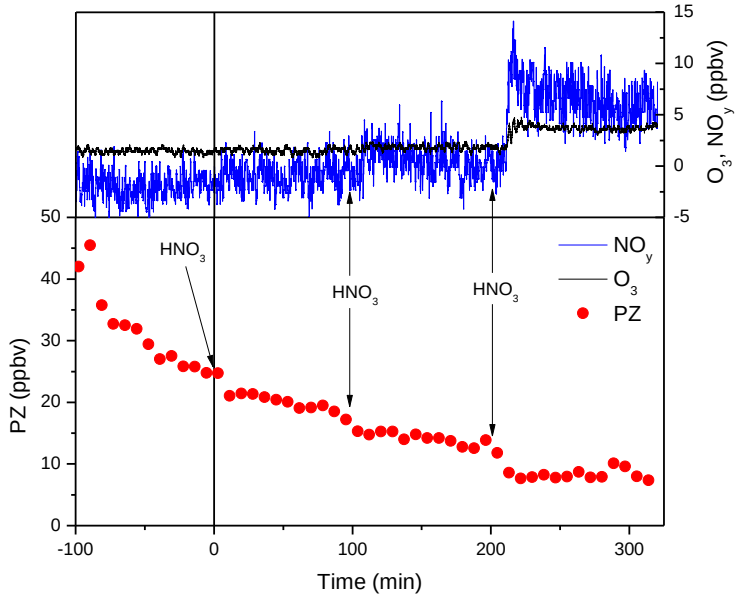

Figure 26. O_3, NOy and (tentative) PZ mixing ratios for E783

After the final injection of nitric acid, the NOy concentration increased. This would imply either that the gas phase PZ concentration is limited leaving excess nitric acid in the gas phase; or that the dissociation constant of piperazine nitrate under these conditions is such that for these concentrations of PZ and nitric acid, they are present in significant concentrations in both the gas and particle phases.

As with MEA and other amines, the reaction of nitric acid with PZ in the smog chamber yields particles that exist in equilibrium with the gas phase. Given the poor accuracy of PZ mixing ratios determined under these conditions, it cannot be ascertained if nitric acid reacts once with PZ to form a nitrate salt, or twice to form a dinitrate salt.

Part II Chemical Mechanism Modelling

This page is intentionally blank

6 Chamber modelling

6.1 Introduction

To support the objectives of this study, a mechanism was developed to describe the photooxidation of MEA. This mechanism was developed using experimental results from the MEA smog chamber experiments, and was designed in such a way that it could be implemented into an air quality model to assess potential MEA effects in the atmosphere.

The chemical mechanism developed was built on knowledge from the two existing chemical mechanisms (Carter 2008; Karl *et al.* 2012), as well as data from experiments performed in the CSIRO smog chamber. The Karl MEA mechanism has been used as a starting point for the mechanism development, with alterations made to provide more accurate simulations of chamber data. In particular, this new mechanism aims to improve predictions of total MEA loss, and to accurately predict formamide, formaldehyde and ammonia production formed during MEA photooxidation.

In this section, the ability of the updated chemical mechanism (CSIMEA) in predicting the formation of key products from MEA photooxidation in the smog chamber was assessed. In some circumstances, the ability of the SAPRC and Karl mechanisms in predicting key product formation was also assessed. Due to time constraints a chemical mechanism for piperazine was not able to be developed as part of this project.

For all analysis in this section, the formation of ozone was represented by $\Delta(O_3\text{-NO})$, which includes ozone formation as well as the conversion of NO to NO_2, by factoring in initial NO concentrations (Johnson, 1983):

$$\Delta(O_3\text{-NO}) = \{[O_3]_t - [O_3]_0\} - \{[NO]_t - [NO]_0\}$$

6.2 Existing MEA chemical mechanisms

Two MEA gas-phase chemical mechanisms have been developed and made publically available. Both of these used data from smog chamber experiments to generate important reaction rate and product yields. The first mechanism was developed as a component of the SAPRC-07 mechanism, using smog chamber experiments performed in the presence of a surrogate hydrocarbon mixture (Carter, 2008). As with other VOCs in the SAPRC mechanism, MEA was represented by its explicit reactions with atmospheric radicals rather than lumping to an analogue species, although this latter method is also available. The individual reactions of MEA with radicals and species in the chamber produce lumped analogue speices with reactivity approximately equivalent to the expected reaction products. The yields of these lumped species are altered to produce accurate simulations of ozone from chamber experiments.

The major constraint from these experiments was that the amine mixing ratios were not able to be quantified. In order to fit the results, it was assumed that the initial MEA mixing ratio was between 5% and 70% of the expected concentration calculated from the injected liquid volume of amine. These experiments indicated that MEA is a species which has a positive ozone formation potential.

The second mechanism is described in Karl *et al.* (2012), which was used to determine yields of products from reaction with MEA with OH from smog chamber experiments performed in the presence of NOx

(Nielsen *et al.* 2010). This mechanism, as published by Karl *et al.* (2012), was comprised of 17 reactions and 17 compounds and is based on quantum chemical calculations (Bråten *et al.* 2009). The model simulations were constrained to measured NO_2 and O_3 concentrations as a method of determining the reaction rate constant of MEA with OH, which was calculated to be 9.2 x 10^{-11} cm^3 $molecule^{-1}$ s^{-1}.

To our knowledge, neither mechanism has been assessed in their ability to predict MEA degradation against quantified experimental data where key products have not been constrained. Additionally, neither mechanism is able to predict ammonia formation from MEA as written, which is formed at 21 ± 6 % yield in the MEA/NOx experiments in this work, measured as a component of total MEA loss. Some assumptions have been made as to the fate or concentration of MEA in the published results, which may also affect mechanism results.

In the Karl mechanism it was assumed that all of the reaction of MEA with OH proceeded to gas phase products. In their published report, only 20% of the reaction yielded gas phase products, with the other 80% assumed to be semi-volatile species which partition into the aerosol phase. In this work, we found much more accurate results were obtained by assuming that 100% of the reaction at k_{OH} (3.58 x 10^{-11} cm^3 $molecule^{-1}$ s^{-1}) proceeded to gas phase products.

As the Karl mechanism has been altered due to differences in experimental equipment and MEA loss assumptions and calculations between the smog chambers, the analysis here is not considered a robust evaluation of the Karl mechanism. The same is true for the SAPRC mechanism, and the analysis provided below is for comparative reasons.

6.3 Model operation

CSIMEA was developed using the Master Chemical Mechanism protocol (Jenkin *et al.* 1997). As the MCM protocol does not currently factor in the reactions of amines, assumptions were made as to the yields of products using the Karl mechanism as a basis. The MCM mechanism was used to describe the reactions of radicals and non-amine organic species such as formaldehyde and glycolaldehyde. The mechanism was run using the FACSIMILE software package.

The Karl mechanism was operated also using the Facsimile software package. The SAPRC-07 mechanism was run using the SAPRC chemical mechanism software (Carter, 2013).

6.4 Chamber characterisation

Wall effects need to be accounted for to accurately simulate chamber photooxidation experiments. This was achieved by using the established chamber auxiliary mechanism for the CSIRO chamber (White *et al.* 2010). This has been updated to represent a higher observed wall loss of ozone (1 x 10^{-6} s^{-1}) and NO_2 (1.7 x 10^{-6} s^{-1}) in more recent experiments.

The MEA wall loss in the dark has been carefully determined in the CSIRO chamber to be no greater than 4 x 10^{-6} s^{-1} at 23 °C. This rate is lower than that calculated for the EUPHORE chamber (pre-2011), which was ~20-30 x 10^{-6} s^{-1}. MEA is very difficult to work with and as such, this latter determination may have been affected by carryover due to the rapid turnaround of experiments as well as MEA affinity for surfaces.

6.5 MEA loss processes

MEA is consumed or 'lost' in the smog chamber through a variety of processes. MEA is lost during the injection process, presumably due to incomplete volatilisation. The measured initial gas-phase MEA concentrations are used in the chamber model simulations, and therefore this injection loss is not a factor in the model.

For aromatic hydrocarbons such as toluene, the loss processes in the smog chamber are limited to reaction with OH, with very minor losses due to reaction with other radicals, direct wall loss or direct particle partitioning. In addition to loss through reaction with OH, as well as higher propensity for aerosol formation than aromatics, there are many additional potential sinks for MEA. The propensity of amines and their reaction products to condense and polymerise adds another layer of complexity over hydrocarbons.

A thorough review of potential amine losses in the atmosphere is provided by Nielsen *et al.* (2012a) and Lee and Wexler (2013). Highlighted in Table 8 are the potential gas phase reaction loss processes relevant to MEA, with their estimated importance in the smog chamber. For the MEA chemical mechanism, the gas phase loss processes which were included are reaction of MEA with OH, NO_3, HNO_3, formaldehyde (HCHO) and glycolaldehyde ($HOCH_2CHO$).

Loss of MEA to the aerosol phase is also expected to be important, including uptake into aqueous phase, reactions with atmospheric acids leading to aerosol, and potentially partitioning of MEA directly onto existing aerosol.

MEA has a high calculated Henry's law coefficient of 6.18 x 10^6 mol kg^{-1} atm^{-1} at 25°C (Ge *et al.* 2011). The high solubility of MEA and almost all oxygen-containing amines in water means that loss of amines into aqueous phases could be a major loss process in the atmosphere. In the smog chamber however, it is expected that uptake into the aqueous phase will be limited by the low humidity used.

Table 8. Potential gas phase loss reactions for MEA in the smog chamber

Species	Reaction rate constant (cm^3 $molecule^{-1}$ s^{-1})	Chamber importance	Notes
OH	7.61×10^{-11} (Onel *et al.* 2012)	Major	Rate calculated independently. Temperature dependent reaction rate constant of $7.73 \times 10^{-11} \times (T/295)^{-0.79}$
NO_3	1.35×10^{-13} (est) (Carter, 2008) 1.48×10^{-13} (est) (Karl *et al.* 2012)	Moderate	Potentially a major sink of MEA in the chamber. Increased concentration of NO_3 due to minimal irradiation around 550 nm.
O_3	6.6×10^{-20} (est) (Carter, 2008)	Minor	Reaction rate is low for primary amines. Could be non-negligible in unreactive ambient environments.
$O(^3P)$	-	Unknown	Could be a potential moderate loss process in chamber experiments, but unimportant in ambient atmosphere.
HNO_3	4.0×10^{-11} (est) (Carter, 2008)	Moderate	Reaction of MEA and nitric acid shown to form inorganic aerosol instantaneously. Total nitric acid formation in chamber less than a few ppbv.
N_2O_5	-	Minor	Chamber concentration limited due to temperature of 30 °C.
$HONO/NO_2$	-	Minor	Effect that has been seen with NO_2 and HONO (Hanst *et al.* 1977) is likely to be due to surface induced reactions.
HCHO	1.7×10^{-17} (this work)	Moderate	Moderate loss due to demonstrated gas phase reaction between HCHO and MEA yielding oxazolidine.
$HOCH_2CHO$	~ 2.2×10^{-29} cm^6 $molecule^{-2}$ s^{-1} (third order reaction) (this work)	Moderate-Major	Reaction of glycolaldehyde with MEA shown to proceed quickly in 2:1 yield. If it is assumed that 2-iminoethanol hydrolyses to glycolaldehyde in high yield, then this is a potential major sink in chamber experiments.
Other aldehydes	-	Minor	Concentration of other aldehydes in the chamber negligible.
Imines	-	Unknown	Nielsen *et al.* (2011a) showed primary alkyl imines can react rapidly with amines yielding secondary imines and ammonia. Possible MEA loss.

6.6 CSIMEA overview

6.6.1 REACTION WITH OH

The reaction of MEA with OH represents the major loss process for gas-phase MEA. The rate constant has been measured at (7.73±0.24) x 10^{-11} $(T/295)^{-(0.79\pm0.11)}$ cm^3 $molecule^{-1}$ s^{-1} (Onel *et al.* 2012), which was used in this mechanism.

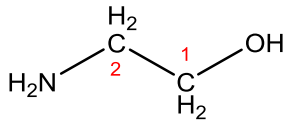

The OH radical acts by abstracting a hydrogen atom from MEA, which can occur at four sites on the MEA molecule (N, C2, C1 or O positions). Nielsen *et al.* (2010) gave approximate yields of reaction at 8% for C1 and O position combined, 84% for the C2 position and 8% for the N position. This was adapted in the Karl mechanism to 5% C1+O, 80% C2 and 15% N.

C1-O pathway

The C1/O pathways were ignored, as no products from abstraction at these positions could be identified, or explained by existing products. This combined pathway was predicted in low yield (<10%) by Nielsen *et al.* (2010). Jackson and Attalla (in Angove *et al.* 2010b) proposed the O position as the major reaction site, yielding methanimine and formaldehyde/formic acid. Formaldehyde is also an expected reaction product of the C2 pathway leading to formamide concentration. Therefore if the C1 pathway occurs in high yield, the concentration of formaldehyde should be greater than that of formamide.

Experimental results in this work show the formaldehyde concentration after 4 hours was between 50-90% of the measured formamide concentration. Formaldehyde is also more reactive than formamide, with the reaction with OH or direct photolysis producing carbon monoxide (CO) as a product. The observed CO concentration did not increase by a quantifiable amount (5 ppbv) in these experiments, and formic acid was only observed in small concentrations in experiments where the nitric oxide concentrations became limited.

This particular C1-O pathway was therefore excluded as a possibility. It is plausible however that reaction with OH does occur at this position, forming products either attributed to a different reaction mechanism, or products as yet undiscovered.

C2-pathway

For the Karl mechanism, the radical formed from OH abstraction at the C2 position reacted with oxygen to form the peroxyl radical at 100% yield (Figure 27). The peroxyl radical was then reduced in NOx-rich environments by NO to yield formamide and the hydroxymethyl radical (CH_2OH).

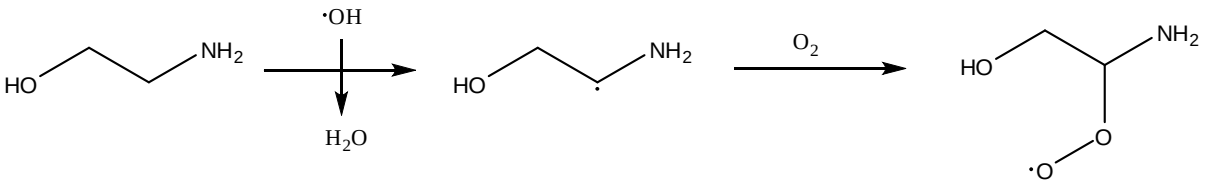

Figure 27. Peroxyl radical formation from MEA-OH reaction at C2 position

The overall product yield of formamide from total MEA loss in the CSIRO chamber is 24±4 % (Angove *et al.* 2012). In the EUPHORE work, the yield of formamide from the OH reaction with MEA was assumed to be 80-85%, however only 16-41% of the MEA loss was attributed to OH loss (Nielsen *et al.* 2011b). Therefore, the overall product yield of formamide from total MEA loss was between 12-35%, which is consistent to that observed in the CSIRO chamber previously. Formamide yields from these experiments however are much lower again, with yields at four hours of 8±2 % relative to total MEA loss. This difference could be attributable to the different experimental conditions used. As formamide reacts slowly with OH (Barnes *et al.* 2010), very little of it is expected to react under chamber conditions, which is consistent with results in this chamber (Angove *et al.* 2012).

Reaction mechanisms observed for other primary amines yield possible alternative pathways not originally considered in the EUPHORE study, which may explain some of the MEA loss which had been attributed to wall effects. Later EUPHORE experiments on methylamine (Nielsen *et al.* 2011a) and ethylamine (Nielsen *et al.* 2012b) show experimental support for a pathway for primary amines whereby abstraction of hydrogen at the adjacent carbon can lead to direct imine formation. For both methylamine and ethylamine, the reaction of this radical with oxygen was calculated to form the imine and HO_2 in greater yield than the peroxyl radical.

Formation of a primary imine in high yield from methylamine photooxidation was predicted by Schade and Crutzen (1995), occurring from the cyclisation of the peroxyl radical, yielding HO_2 and the primary imine (Figure 28).

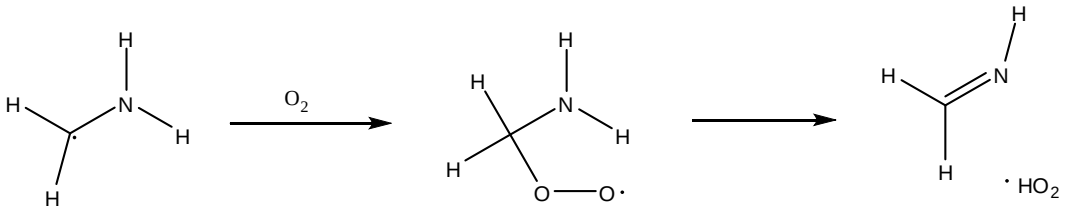

Figure 28. Reaction mechanism of methylamine carbon radical with oxygen yielding methanimine and HO_2

The products which were formed in largest yields from methylamine and ethylamine were secondary imines and ammonia. This reaction proposed to explain this was the reaction of the primary imine with a second molecule of the original amine, yielding ammonia as a product. Condensation reactions yielding products with more carbon than the original amine molecule are common in condensed phase amine mixtures (Gouedard *et al.* 2012), and have been observed in gas phase studies of amines (Pitts *et al.* 1978). Aerosol formed from the reaction of primary amines also shows condensation products as the major component of the organic aerosol phase (Malloy *et al.* 2009).

The formation of 2-iminoethanol and HO_2 from the reaction of the C2-dehydro-MEA radical and oxygen was shown as theoretically possible for MEA by da Silva (2012). This provides a HOx-neutral pathway for the reaction of MEA with OH, and has been included in this mechanism. The same process has been shown experimentally for C2-dehydroglycinyl radicals (da Silva *et al.* 2012). The reactions of 2-iminoethanol will be considered below.

N-position

The aminyl radical differs from carbon-centred radicals in that it can react competitively with species other than oxygen at atmospheric pressure. For aminyl radicals, reaction with NO and NO_2 can form nitrosamines and nitramines respectively (Figure 29). The formation of these has been positively confirmed from the

reactions of secondary aminyl radicals with NOx (Lindley *et al.* 1979; Lazarou *et al.* 1994). Nitramines have also been observed during the reactions of primary amines, including from ethanolamine (Nielsen *et al.* 2010). Nitrosamines arising from primary amines have not been observed in the gas-phase due to their instability. For primary nitrosamines, rearrangement followed by reaction with oxygen can lead to the formation of imines (Angove *et al.* 2010b; Tang *et al.* 2012).

The rate constants for the aminyl radical reactions were defined by the ratios calculated by Lindley *et al.* (1979), with the reaction rate constant for the aminyl radical with NO set to 8.53 x 10^{-14} cm^3 $molecule^{-1}$ s^{-1} (Lazarou *et al.* 1994).

Reaction of the aminyl radical with oxygen will lead to the formation of imines, and this reaction is expected to be the major pathway under limited NOx conditions. Most of the experimental work performed on gas phase aminyl radical reactions has focussed on secondary amines. As it is likely that the primary aminyl radical will be less stable than secondary aminyl radicals, the yield of this reaction with O_2 was increased and fitted to ensure accurate ozone and MEA predictions.

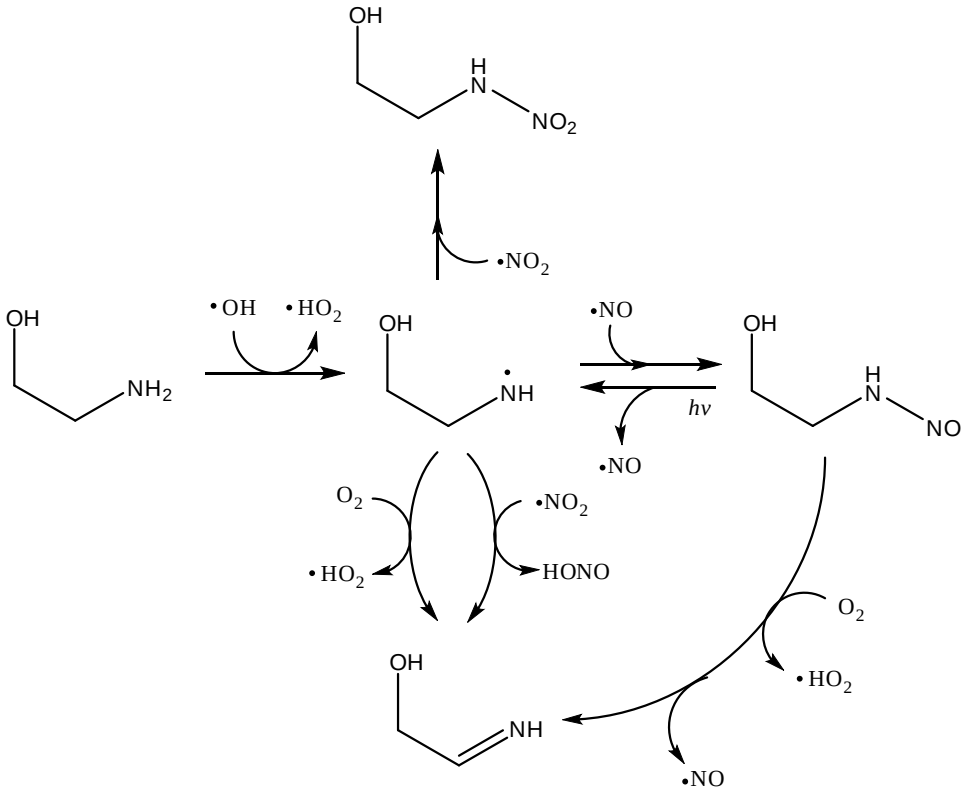

Figure 29. Reaction of ethanolamine aminyl radical (centre), forming nitrosamine (far right), nitramine (top) and 2-iminoethanol (bottom) are shown (adapted from Nielsen *et al.* 2012a)

Nitramines are unreactive with OH, with a calculated reaction rate constant for *N*-nitroaminoethanol of 6.52 x 10^{-12} cm^3 $molecule^{-1}$ s^{-1}, using updated structure-activity relationship (SAR) factors for nitramines (Nielsen *et al.* 2012b). Rather than the formation of the C2-peroxyl-nitramine radical as assumed by Bråten *et al.* (2009), it was assumed that the subsequent reaction of the dehydro-nitramine radical with oxygen proceeds by a second hydrogen abstraction rather than addition to form a peroxyl radical, yielding 2-iminoethanol and NO_2 as products.

Structure-activity relationship estimates for the reaction of amines with OH (Kwok and Atkinson, 1995) indicate that the amine group is a viable site for the abstraction of hydrogen in amine OH reactions,

although the factors for amines remain highly uncertain. In this mechanism, a low yield for the aminyl radical (5%) was fitted. This low yield was required to provide more accurate fits for both high reactivity (high MEA/low NOx) and low reactivity (high NOx) experiments. It is possible that other pathways of the aminyl radical have not been considered, which would increase the yield of this radical from MEA. However as no products that could arise from these were able to be identified, this yield was considered sufficient.

Imine reactions

The reactions of primary imines are a large area of uncertainty in amine photochemistry, as they are a short-lived species which are difficult to measure or isolate. This is especially true for MEA, where the potential imine, 2-iminoethanol, also has a hydroxyl substituent attached.

One possible reaction pathway for this imine would be condensation as postulated by Nielsen *et al.* (2011a; 2012b) from observations of primary amine photooxidation. This reaction proceeds by reaction with the original amine molecule to yield a secondary imine and ammonia. As ammonia is formed in 21 ± 6 % total yield from MEA photooxidation in this chamber, as well as similar yields in the EUPHORE chamber, this is a major potential loss for MEA in chamber experiments. Another possibility is that the imine will hydrolyse rapidly in the chamber to yield ammonia and glycolaldehyde. The reaction of glycolaldehyde and MEA has been shown to occur rapidly in the smog chamber.

The only functional difference between these two pathways as they apply to a smog chamber mechanism is that the 'imine + amine' channel consumes one additional molecule of MEA to generate ammonia, whereas the imine hydrolysis followed by glycolaldehyde reaction with MEA consumes two additional molecules of MEA. As the reaction of glycolaldehyde with MEA has been positively observed in this work, the hydrolysis pathway to glycolaldehyde was selected for all 2-iminoethanol reactions.

The subsequent reactions of products formed as a result of these reactions are much less certain. A reaction mechanism for these lumped products has been included, however this is a highly uncertain component of the mechanism which cannot be solved by chamber experiments of a single amine.

Reaction with OH overview

In this mechanism, the yield of products from the reaction of OH with MEA were 5% N, 40% C2 (peroxy) and 55% C2 (imine). These yields were determined by fitting the full mechanism to ensure minimum ozone error across the entire range of experiments used, as well as maintaining formamide yields to within 40%. The fitting was performed at yield intervals of 2.5%, with the results approaching the best average and lowest standard deviation for $\Delta(O_3\text{-NO})$ across the experiment subset chosen. The fitting also included the relative reaction rate of the aminyl radical with oxygen compared to the three NOx channels.

6.6.2 MECHANISM WITH NO_3

Relatively high reaction rate constants have been measured for the reaction of amines with the NO_3 radical (Nielsen *et al.* 2012a), with values of around 10^{-13} cm^3 $molecule^{-1}$ s^{-1}. For MEA, no reaction rate constant has been determined, however rate constants have been estimated by Carter (2008) to be 1.35 x 10^{-13} cm^3 $molecule^{-1}$ s^{-1}, and by Karl *et al.* (2012), 1.48 x 10^{-13} cm^3 $molecule^{-1}$ s^{-1}.

In the MEA SAPRC mechanism, the reaction of MEA with NO_3 was predicted to give a product mixture of approximately equal reactivity compared to the reaction with OH. When the SAPRC mechanism is run against these experiments however, the predictions of $\Delta(O_3\text{-NO})$ are inaccurate (Figure 30). The same

feature is observed for the Karl mechanism and the CSIMEA mechanism when a similar reaction rate constant is used for NO_3, using the same product yields as for the reaction with OH.

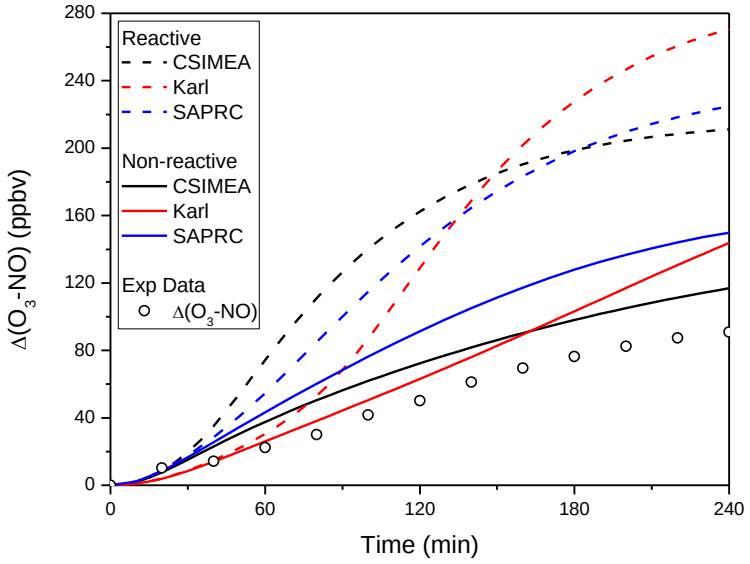

Figure 30. Δ(O_3-NO) predictions for E723 (high MEA/low NOx) for CSIMEA, Karl and SAPRC mechanisms

In order to predict accurate ozone concentrations from MEA experiments, it was determined that the reaction of MEA with NO_3 must give rise to non-reactive products. This ensured that ozone formation was restrained when nitric oxide concentrations became limited, which was consistent with the data (Figure 30). In order to fit ozone as best as possible at both low and high NOx, a fast reaction rate of 1.75 x 10^{-12} cm^{-3} $molecule^{-1}$ s^{-1} was used for $k_{(NO3+MEA)}$. This rate constant is an order of magnitude faster than the rate constants estimated for this reaction (Carter, 2008; Karl *et al.* 2012), however it does correspond to a rate constant calculated in a smog chamber experiment for the reaction of diethylamine with NO_3 (Nielsen *et al.* 2012b). The expected product of this reaction is organic aerosol, given the high aerosol yield observed from the reaction of MEA with NO_3 (Section 4.3.2) and the high yield of organic aerosol observed by the reaction of primary amines with NO_3 (Malloy *et al.* 2009).

6.6.3 MECHANISM WITH HNO_3

As demonstrated in Section 4.3.1, the reaction of even small amounts of nitric acid with MEA in the chamber gives rise to aerosol almost instantaneously. In the SAPRC mechanism, the reaction rate was assumed to be 4 x 10^{-11} cm^3 $molecule^{-1}$ s^{-1}. This rate constant was also used in the CSIMEA mechanism. Tests showed that mechanism predictions were insensitive to changes of two orders of magnitude in this rate constant, with gas-phase nitric acid concentrations limited to less than 0.1 ppbv.

6.6.4 MECHANISM WITH HCHO

The gas phase reaction of HCHO with MEA forms oxazolidine as the primary observed product. Including this reaction in the mechanism improved predictions of formaldehyde, while having a minimal impact upon ozone predictions and only marginal improvements in MEA (Figure 31). As the oxazolidine product is lumped into a secondary amine reaction mechanism scheme which slightly lowers reactivity, the addition of the MEA+HCHO reaction results in a 10% decrease in $\Delta(O_3\text{-NO})$ predictions. This change has been accounted for in the fitting of yield parameters in the MEA + OH reaction as described above.

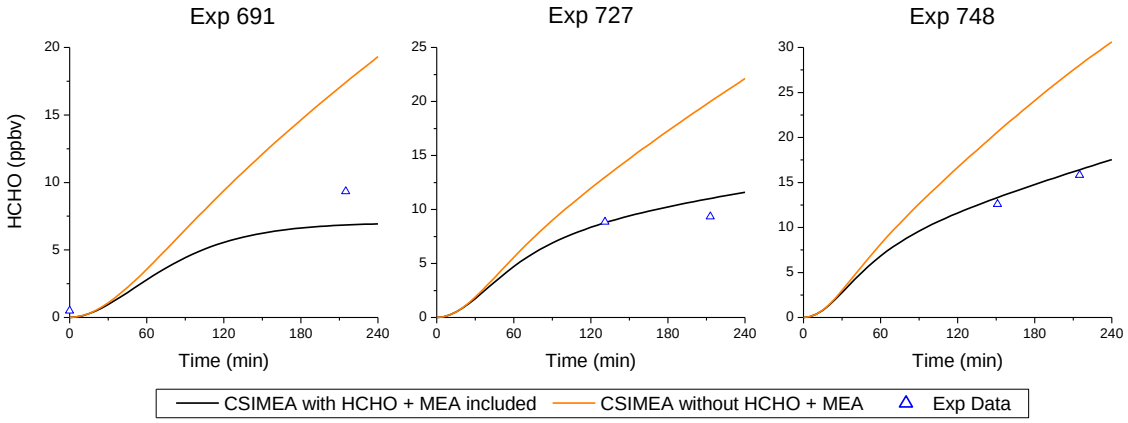

Figure 31. Predictions of HCHO from three MEA/NOx experiments with and without the HCHO+MEA reaction.

6.6.5 MECHANISM WITH GLYCOLALDEHYDE

From the single glycolaldehyde-MEA experiment performed in this study, it was calculated that MEA reacted with glycolaldehyde in 2:1 yield. Unlike the reaction with formaldehyde, where cyclisation to oxazolidine limits the reaction to 1:1 yield, the product formed from the initial reaction is highly susceptible to further reaction with amines. This is equivalent to the reaction of diethylamine with formaldehyde observed by Tuazon *et al.* (1994), which also proceeded in a 2:1 amine:aldehyde yield.

In this mechanism, the reaction of MEA with glycolaldehyde (HOCH2CHO) is implemented as a series of reactions:

MEA + HOCH2CHO → GLYCOLINT

GLYCOLINT + MEA → MEAGLYCOL

As MEA is in excess in all chamber experiments in this work, GLYCOLINT reacts almost entirely with MEA.

In the mechanism, all products arising as a result of condensation reactions, such as GLYCOLINT, MEAGLYCOL and oxazolidine, are lumped to a secondary amine analogue species. A first-step reaction scheme for this was developed for these lumped species equivalent to that expected for a secondary amine containing oxygen, however it is highly uncertain.

6.6.6 ORGANIC AEROSOL

Attempts were made throughout the project to represent the aerosol formation in the mechanism explicitly. However, as the aerosol composition from MEA experiments was not able to be characterised, it was not possible to identify which products in the reaction mechanism were most likely responsible for aerosol formation. Therefore, the two-product Odum approach (Odum *et al.* 1996) was used to simulate organic aerosol formation.

In the Karl mechanism, the formation of organic aerosol was represented by a single-product Odum approach. The organic proportion of the total measured aerosol was measured, which was not possible in these experiments.

Simply fitting an Odum plot to the experimentally determined MEA loss was not sufficient, as loss due to MEA occurs due to a number of reactions (OH, NO_3, HCHO, HNO_3, glycolaldehyde). The role of condensation products arising from the reaction of MEA with aldehydes in organic aerosol formation added additional uncertainty. A simple expression for a two product system from the reaction of MEA with OH was used, and with minor adjustments was found to be sufficient to explain aerosol formation to within 40% for most experiments.

The factors used was $\alpha_1 = 0.1$; $k_1 = 1.0$; $\alpha_2 = 0.5$ and $k_2 = 1 \times 10^{-3}$, assuming an average molecular weight of 126 g mol^{-1} (as used by Karl *et al.* 2012). The initial measured aerosol mass was used as the background aerosol onto which partitioning could occur (minimum of 0.1 µg m^{-3}). The non-reactive product arising from the reaction of MEA and NO_3 was assumed to be organic aerosol. The reason that the aerosol formation was linked to the OH reaction only was that the loss of MEA due to the reaction of formaldehyde and glycolaldehyde were closely linked in the chamber to the OH reaction. No conclusion could be drawn from the data about the equivalent roles in the atmosphere.

Direct particle partitioning of MEA to aerosol was not assumed in the work of Nielsen *et al.* (2010). Attempts to include this pathway in the CSIMEA mechanism resulted in over-predictions of aerosol mass at low MEA/NOx experiments. As these experiments represent the experiments of lowest integrated OH concentration, and therefore the least reactive, it was concluded that the majority of the organic aerosol formed in MEA/NOx experiments was a result of the reaction of MEA with radicals and other species, with minimal amounts of direct partitioning.

The aerosol formation method used does not provide accurate mass balance between the gas and aerosol phases. It is anticipated however that processing of the imine formed in the gas phase, and subsequent MEA condensation is responsible for a large proportion of the aerosol production. The limited first-step reaction pathways attributed to the lumped secondary amine analogues can be justified by assuming that a significant proportion of the condensation products find their way into the aerosol phase.

6.7 Reaction Mechanism

The loss pathways of MEA from two characteristic experiments are shown in Figure 32. The reaction with OH and the condensation reactions involving glycolaldehyde are the predominant loss mechanism of MEA. For the less reactive experiments, such as the high NOx E725, the proportion of MEA lost to the walls relative to total MEA loss is higher. This is reflective only of overall higher MEA concentrations across the four hour experiment in the less reactive higher NOx experiment. The gas phase reaction mechanism in its entirety is shown in Table 9.

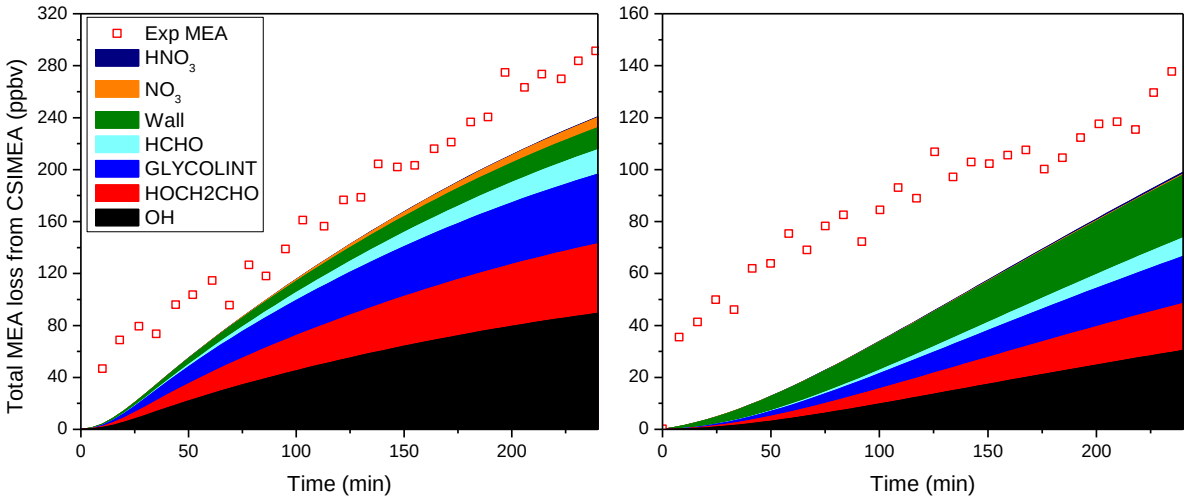

Figure 32. Loss processes of MEA in CSIMEA for (a) E723 (left) and (b) E725 (right)

Table 9. Chemical mechanism for CSIMEA

Rate	Reaction	Products	Reference (rate)
$7.73 \times 10^{-11} (T/295)^{-0.79}$	MEA + OH	0.40 x MEAC2PER 0.05 x $HNCH_2CH_2OH$ 0.55 x $HNCHCH_2OH + HO_2$	Onel *et al.* (2012)
1.75×10^{-12}	MEA + NO_3	MEANO3	This work, fitted
$2.70 \times 10^{-12} e^{(360/T)}$	MEAC2PER + NO	MEAC2OXY + NO_2	MCM protocol
$1.52 \times 10^{-13} e^{(1300/T)}$	MEAC2PER + HO_2	MEAC2HPE	MCM protocol
1.0×10^{6}	MEAC2OXY	$H_2NCHO + HCHO + HO_2$	MCM protocol
J<41>	MEAC2HPE	$H_2NCOCH_2OH + OH$	MCM protocol
$1.90 \times 10^{-12} e^{(190/T)}$	MEAC2HPE + OH	MEAC2PER	MCM protocol
1.70×10^{-10}	MEAC2HPE + OH	$H_2NCOCH_2OH + OH$	SAR
J<22>	H_2NCOCH_2OH	$HNCO + HCHO + HO_2 + HO_2$	MCM protocol
6.59×10^{-12}	$H_2NCOCH_2OH + OH$	$H_2NGLYOX + HO_2$	SAR
1.01×10^{-18}	$HNCHCH_2OH + O_2$	$HNCHCH2OH + HO_2$	This work, fitted
8.53×10^{-14}	$HNCHCH_2OH$ + NO	MEANITROSO	Lazarou *et al.* (1994)
3.95×10^{-13}	$HNCHCH_2OH + NO_2$	0.82 x MEANITRA 0.18 x $HNCHCH_2OH$ + HONO	Lindley *et al.* (1979) relative to above
J<4> x 0.33	MEANITROSO	$HNCHCH_2OH$ + NO	Nielsen *et al.* (2010)
1.00×10^{-17}	MEANITROSO + O_2	$HNCHCH_2OH + HO_2$ + NO	Nielsen *et al.* (2011a)
6.52×10^{-12}	MEANITRA + OH	$HNCHCH_2OH + NO_2$	Nielsen *et al.* (2012b)
1.67×10^{-11}	$H_2NGLYOX + OH$	$HNCO + CO + HO_2$	SAR
$5.60 \times 10^{-12} e^{(-1860/T)}$	$H_2NGLYOX + NO_3$	$HNO_3 + HNCO + HO_2 + CO$	MCM protocol
J<34>	$H_2NGLYOX$	$HNCO + HO_2 + HO_2 + CO$	MCM protocol
4.00×10^{-12}	$H_2NCHO + OH$	$HNCO + HO_2$	Barnes *et al.* (2010)
$1.40 \times 10^{-12} e^{(-1860/T)}$	$H_2NCHO + NO_3$	$HNCO + HNO_3 + HO_2$	MCM protocol
6.00×10^{-12}	$HNCHCH_2OH$ + $HNCHCH_2OH$	SECIMINE + NH_3	This work, estimated
5.00×10^{-10}	$HNCHCH_2OH + OH$	$H_2NCOCH2OH + HO_2$	This work, estimated
1.00×10^{6}	$HNCHCH_2OH + H_2O$	$NH_3 + HOCH_2CHO$	This work, set deliberately fast.
1.00×10^{-18}	$HNCO + H_2O$	NH_3	This work, estimated
1.00×10^{-11}	OXAZOL* + OH	0.80 x LAMINYL 0.20 x NRIMINE + HO_2	This work, estimated
1.00×10^{-13}	OXAZOL* + NO_3	0.80 x LAMINYL 0.20 x NRIMINE + HO_2 1.00 x HNO_3	This work, estimated
3.18×10^{-13}	LAMINYL + NO_2	0.625 x LNITRA 0.375 x NRIMINE 0.375 x HONO	Nielsen *et al.* (2012a) for morpholine (cyclic oxy. amine)
1.81×10^{-13}	LAMINYL + NO	LNITROSO	Nielsen *et al.* (2012a)
3.82×10^{-19}	LAMINYL + O_2	NRIMINE + HO_2	Nielsen *et al.* (2012a)
J<4> x 0.31	LNITROSO	LAMINYL + NO	Nielsen *et al.* (2012a)
3.50×10^{-12}	LNITRA + OH	NRIMINE + $HO_2 + NO_2$	This work, estimated
1.80×10^{-17}	MEA + HCHO	OXAZOL	This work
1.20×10^{-16}	MEA + $HOCH_2CHO$	GLYCOLINT	This work, estimated
5.00×10^{-14}	MEA + GLYCOLINT	MEAGLYCOL	This work, estimated
4.00×10^{-11}	MEA + HNO_3	MEANTR (AEROSOL)	Carter (2008)
1.40×10^{-12}	MEAC2PER + RO2	0.60 x MEAC2OXY 0.40 x H_2NCOCH_2OH	MCM Protocol

Notes

* Same reactions are used for OXAZOL, GLYCOLINT, SECIMINE and MEAGLYCOL

Products not listed by chemical formula:

MEA	$H_2NCH_2CH_2OH$
MEAC2PER	$H_2NCH(OO^{\cdot})CH_2OH$
MEAC2OXY	$H_2NCH(O^{\cdot})CH_2OH$
MEAC2HPE	$H_2NCH(OOH)CH_2OH$
H2NGLYOX	$H_2NC(O)CHO$
MEANITROSO	$ONN(H)CH_2CH_2OH$
MEANITRA	$O_2N(H)CH_2CH_2OH$

Lumped products.

MEANO3	MEA + NO_3 unreactive reaction product
SECIMINE	Secondary imine formed by imine condensation
OXAZOL	Nominally 1,3-oxazolidine
LAMINYL	Aminyl radical arising from lumped secondary amines
NRIMINE	Non-reactive product arising from lumped secondary amines
LNITRA	Nitramine arising from lumped secondary amines
LNITROSO	Nitrosamine arising from lumped secondary amines
GLYCOLINT	MEA + glycolaldehyde intermediate
MEAGLYCOL	2 x MEA + glycolaldehyde product
MEANTR	Inorganic aerosol formed by reaction of MEA with HNO_3

6.8 Mechanism results

6.8.1 METHOD OF COMPARISON

The MEA/NOx experiments were simulated using the CSIMEA mechanism, the modified Karl mechanism and the SAPRC-07 MEA mechanism (Table 10). For the purposes of comparison, E738 was excluded as the NO:NO_2 ratio had been inverted relative to the other experiments, although results for this are shown in Appendix D.

To assess the validity of the three aforementioned chemical mechanisms in accurately simulating the photooxidation of MEA, the predictions of six key products were compared. These products were MEA, $\Delta(O_3\text{-NO})$, ammonia (NH_3), aerosol, formamide ($CHONH_2$) and formaldehyde. The model error for each species *X* at time *t* was defined by:

$$X(t)_{\text{model error}} = 100\% \times \{X(t)_{\text{modelled}} - X(t)_{\text{measured}}\} / X(t)_{\text{measured}}$$

For a fit to be considered accurate, within the high uncertainty regarding amine mechanism predictions, the predicted concentration of a gas phase species should be within 25%. For ease of comparison, the experiments in Table 10 have been ordered by their initial MEA/NOx ratios.

Table 10. Initial concentrations for MEA and NOx for MEA/NOx experiments, as well as change in MEA, $\Delta(O_3\text{-NO})$, NH_3 and aerosol after four hours

Expt	Initial concentrations				Change in concentration at 4 hours			
	MEA/ NOx	MEA (ppbv)	NO (ppbv)	NO_2 (ppbv)	Δ(MEA) (ppbv)	$\Delta(O_3\text{-NO})$ ppbv	$\Delta(NH_3)$ (ppbv)	Δ(Aerosol) (µg m^{-3})
723	24.2	424	15	2.5	291	91	63	165.9
748	12.0	289	21	3	219	94	58	217.9
750	9.4	412	40	4	373	123	77	359.0
727	6.6	283	35	8	210	87	50	161.0
688	4.7	427	80	11	184	65	33	61.9
746	4.5	109	18	6	89	39	20	45.2
691	3.1	444	121	21	189	58	32	58.4
731	2.8	251	81	9	121	56	33	88.7
736	2.4	119	41	8	56	35	16	28.7
733	1.9	261	120	21	120	65	30	59.1
725	1.0	464	410	53	137	80	21	26.0
738	1.3	127	10	90	93	18	17	120.3

6.8.2 MECHANISM PERFORMANCE

An example of the mechanism predictions relative to experimental data for the highest MEA/NOx experiment is shown in Figure 33, and for the lowest MEA/NOx experiment in Figure 34.

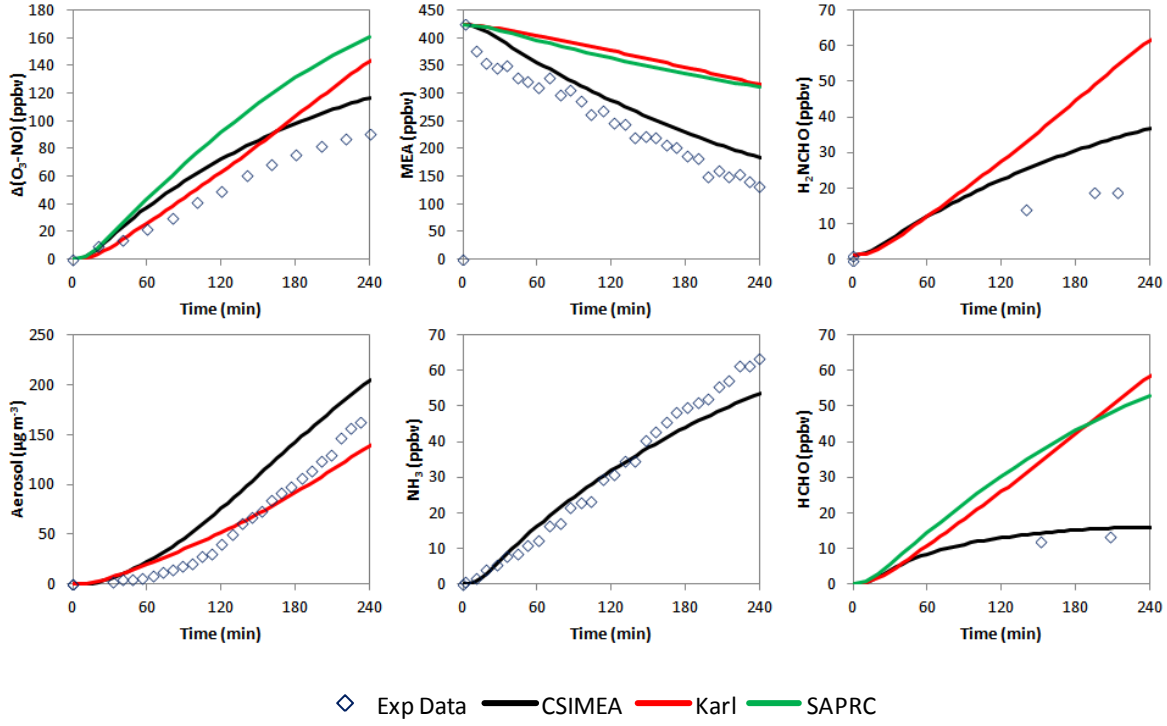

Figure 33. Model simulations of gas phase species and aerosol for E723

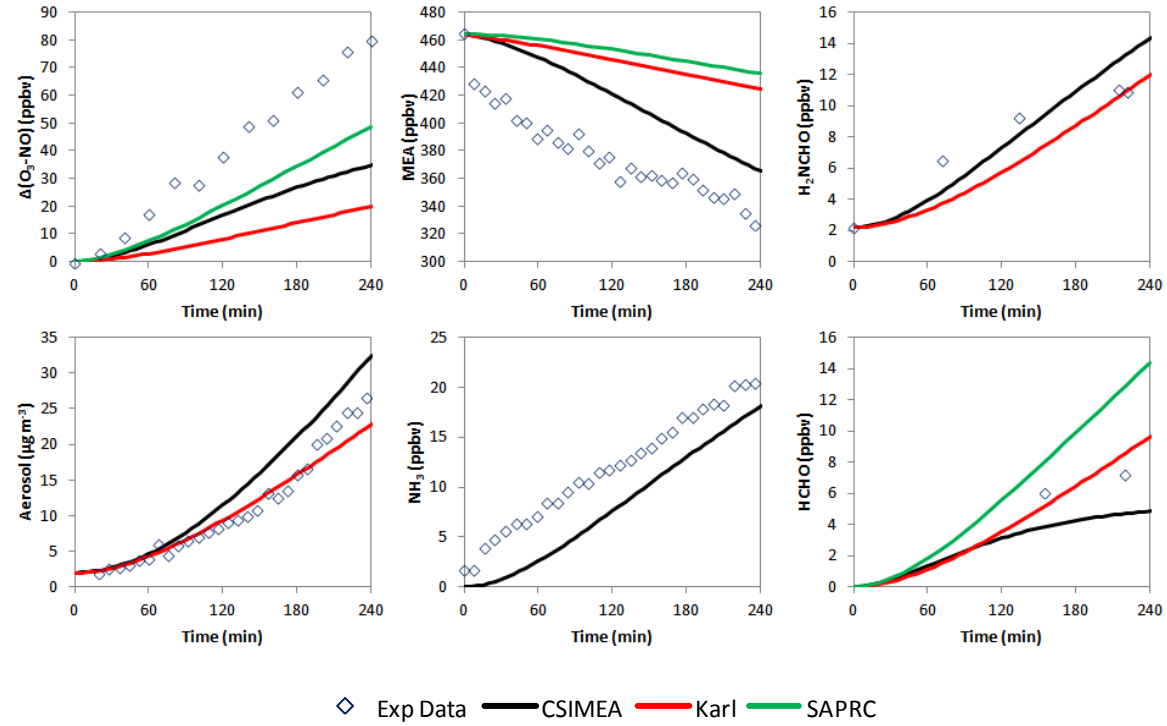

Figure 34. Model simulations of gas phase species and aerosol for E725

The most obvious improvement in the CSIMEA mechanism relative to the Karl and SAPRC mechanisms is in the prediction of MEA loss. In the Karl mechanism, it was assumed that a large amount of MEA was lost to the walls of the EUPHORE chamber based on measurements of the loss of MEA before the lights were turned on. In this chamber, the rate of MEA loss to the walls was calculated as being much lower than that used in their work, and while incorporated into the model it made only a small difference in MEA predictions.

For the two examples chosen, the CSIMEA mechanism provides reasonable fits for most of the key products. The one exception is in the prediction of $\Delta(O_3\text{-NO})$ for the high NOx experiment E725, where the SAPRC mechanism was more accurate. It should be noted that a wall loss rate was not included into SAPRC for these experiments, so the higher accuracy observed in the simulation for E725 may be a coincidence. For this experiment, the change in ozone was less than 2 ppbv, so the majority of the change in $\Delta(O_3\text{-NO})$ was attributed to loss of initial NO. Of this initial 80 ppbv change in NO, the corresponding change in NOy-NO was 30 ppbv, with the remaining 50 ppbv lost as NOy (Figure 35). If it is assumed that NOy-NO is entirely NO_2, then the predictions of CSIMEA are accurate for the NO to NO_2 conversion. If so the poor predictions for NOy and NO indicate a NOx sink which is currently unaccounted for in the mechanism. It is possible that this NOy loss is related to aerosol formation, although the amount of aerosol observed (26 µg m^{-3}) is lower than the mass of NO lost (63 µg m^{-3}).

No possible mechanism pathways or observed products could be identified which could describe this observation within the time frame of this project. As no additional NOx sink was required to improve predictions for low NOx experiments, it is hypothesised that this NOy loss arises from reactions of MEA under high NOx conditions. Therefore it is unlikely to be a major loss pathway in the atmosphere, where the concentration of NOx is typically considerably lower than 450 ppbv.

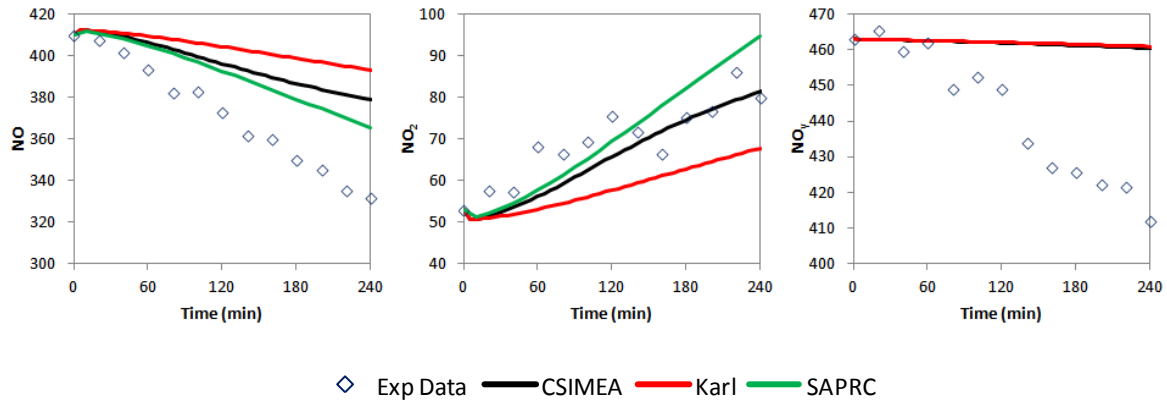

Figure 35. Comparison of NO, NO_y-NO and NO_y for E725. The mechanism predictions of 'NO_y' is equal to NO + NO_2, with 'NO_y-NO' equal to NO_2 only

Ozone

The $\Delta(O_3\text{-NO})$ model errors for 11 MEA/NOx experiments are shown for 2 hours (Figure 36) and 4 hours (Figure 37).

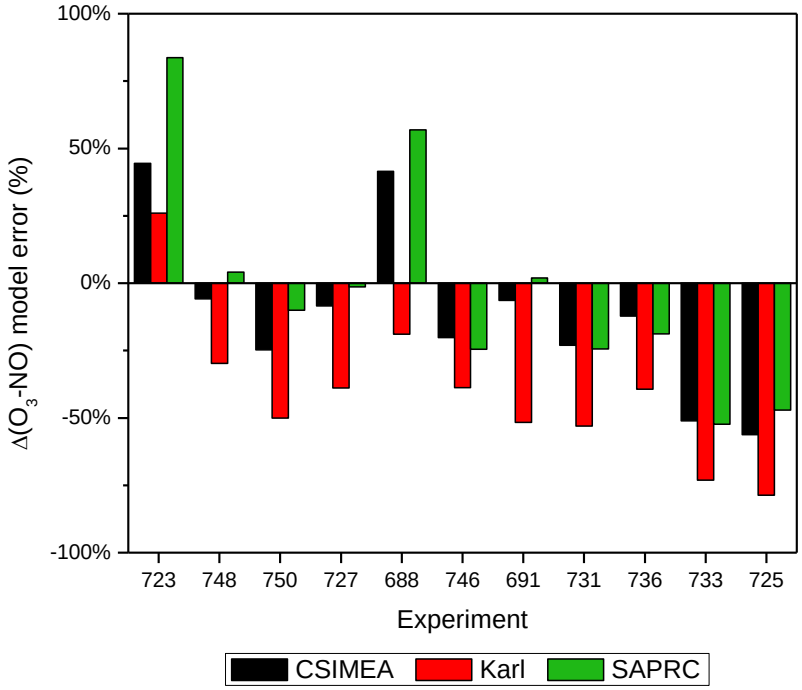

Figure 36. $\Delta(O_3\text{-NO})$ model error for MEA/NOx experiments after 2 hours

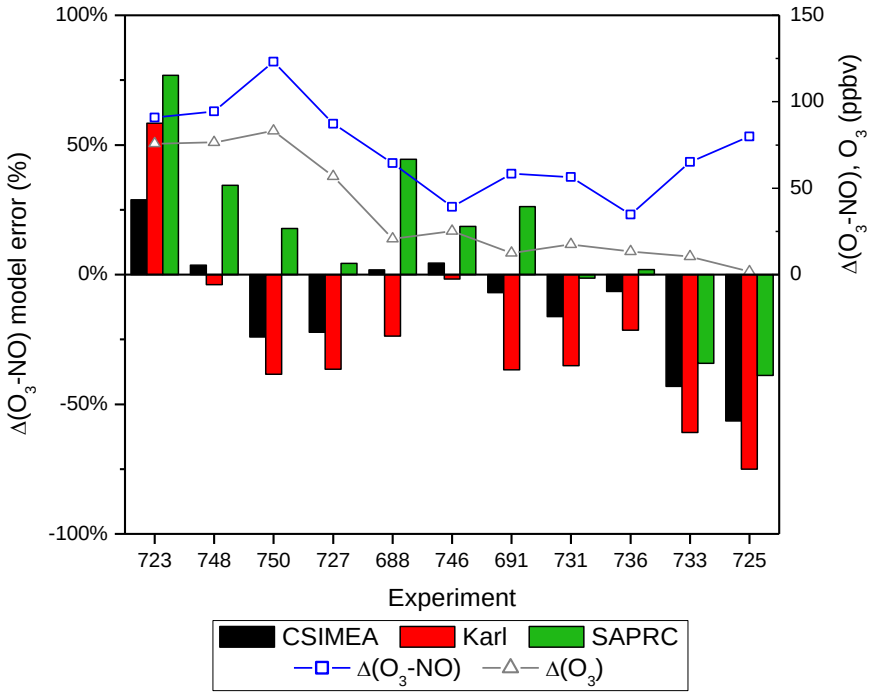

Figure 37. $\Delta(O_3\text{-NO})$ model error and experimental values for $\Delta(O_3\text{-NO})$ and O_3 for MEA/NOx experiments after 4 hours

The CSIMEA mechanism has predicted $\Delta(O_3\text{-NO})$ to within 25% for seven out of eleven experiments at 2 hours, and eight experiments after 4 hours. After 4 hours, four experiments were predicted to within 25% by the Karl mechanism, and five experiments for the SAPRC mechanism. For the three experiments that were not accurately predicted at 4 hours by CSIMEA, two of these (E733 and E725) were low reactivity experiments. As explained above, most of the change in $\Delta(O_3\text{-NO})$ for these experiments was due to loss of NO with minimal changes in ozone concentration. The other experiment not predicted to within 25% was the high reactivity experiment E723, with a positive model error of 29%.

Most importantly for their relevance to the atmosphere was the performance of the mechanisms against the experiments with low NOx with less than 25 ppbv (E723, E746 and E748). The Karl mechanism was accurate for two of these experiments (E746, E748), and over-predicted for the high MEA experiment (E723). For the SAPRC mechanism the low NOx experiments were over-predicted between 19% and 77%. Once these three experiments are excluded, the average $\Delta(O_3\text{-NO})$ model error at 4 hours was between -24% and -75% for the Karl mechanism, and between -39% to 45% for the SAPRC mechanism.

MEA predictions

Predictions of the change in MEA mixing ratio (ΔMEA) from the start of the experiment are shown at 4 hours in Figure 38. The predictions at 2 hours are approximately equivalent to those shown at 4 hours, and therefore are not shown. The predictions for the CSIMEA mechanism (average model error of -22%) are more accurate than the Karl (average -71%) or SAPRC mechanisms (average -70%). This can be attributed to two key differences between the CSIMEA mechanism and the other two mechanisms:

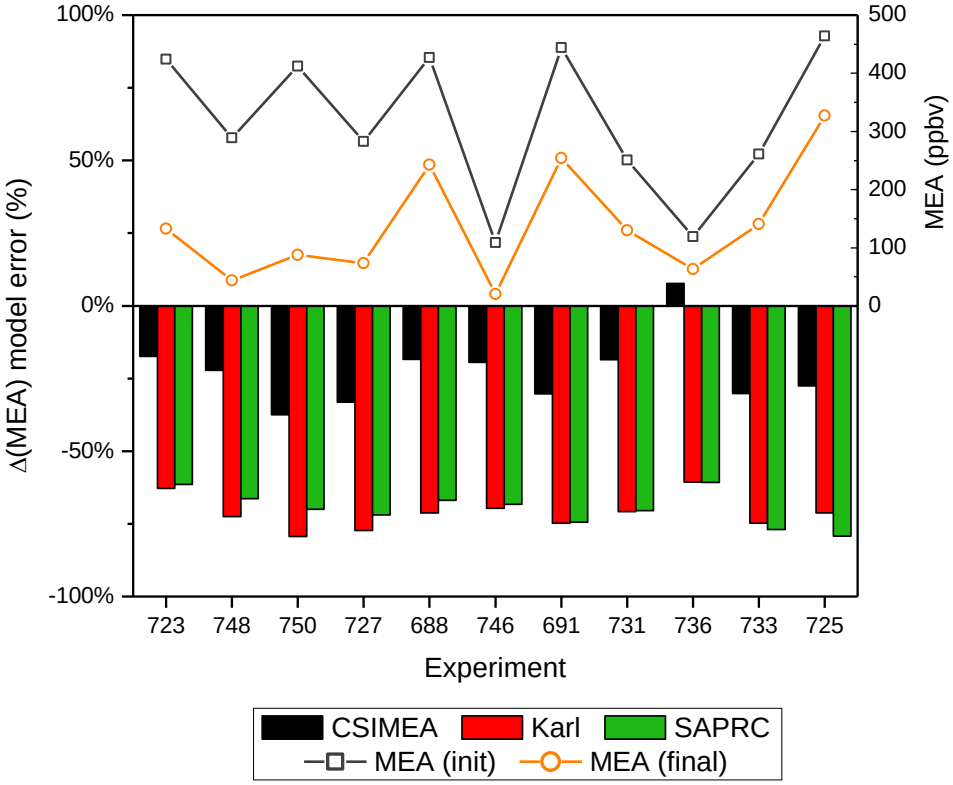

Figure 38. Δ(MEA) model error and experimental values for initial and final MEA concentrations for MEA/NOx experiments after 4 hours

The reaction rate of MEA with OH was set to the rate recently determined by Onel *et al.* (2012) (7.67 x 10^{-11} cm^3 $molecule^{-1}$ s^{-1} at 298 K), compared with that calculated using structure-activity relationships (SAR) (3.58 and 4.41 x 10^{-11} cm^3 $molecule^{-1}$ s^{-1}). Using the faster k_{OH} in the Karl or SAPRC mechanisms resulted in over-predictions of ozone. This is logical as yields of key products in these mechanisms were tuned in order to simulate reactivity accurately, based on the k_{OH} used.

Condensation reactions of MEA were included in the CSIMEA mechanism, which as shown in Figure 33 improved the predictions of MEA.

Ammonia

The ammonia model error for the CSIMEA mechanism at 4 hours is shown in Figure 39. No ammonia predictions were made by the other two mechanisms. All experiments under-predicted ammonia production, with an average model error at 4 hours of -21%.

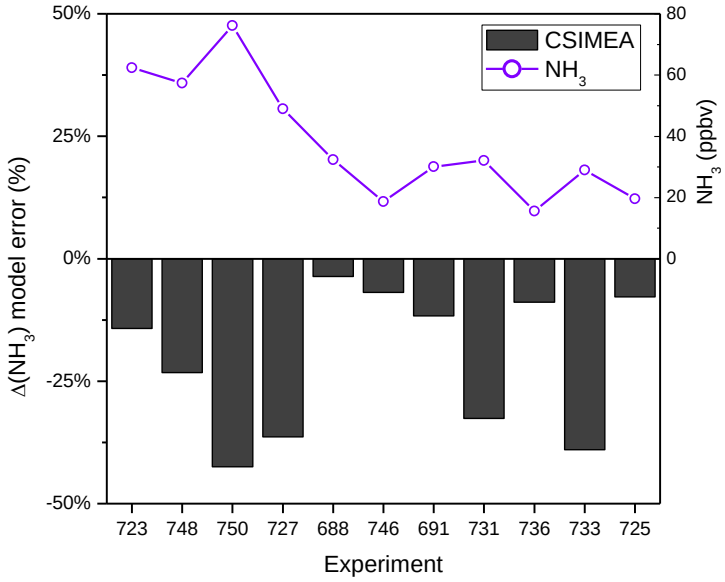

Figure 39. NH_3 model error and experimental NH_3 mixing ratios for MEA/NOx experiments after 4 hours

Of the eleven experiments evaluated here, seven were found to have ammonia predictions within 25% at 4 hours. The four experiments where the ammonia model error was greater than -25% correspond to the four of the five experiments where the $\Delta(O_3\text{-NO})$ predictions at 4 hours were lower than -10% (E727, E731, E733 and E750). Therefore in these experiments, some under-prediction in the reactivity is responsible for the negative model errors, and is not reflective of a problem with the ammonia yield from MEA photooxidation.

The one exception to this rule was the high NOx E725, where the ammonia concentration was accurately predicted but the $\Delta(O_3\text{-NO})$ model error was not, for reasons explained above.

Aerosol

The aerosol model error is shown for 2 hours (Figure 40) and 4 hours (Figure 41) for the CSIMEA and Karl mechanisms. In general the aerosol predictions are poorer than the prediction of gas phase products, with only four of the 11 experiments having an aerosol model error within 25% at 4 hours. The four experiments with aerosol model error greater (more negative) than -40% are E727, E731, E733 and E750, which are the same four experiments with ammonia model error lower than -25%. As with ammonia, some of this model

error can be attributed to lower simulated reactivity with these four experiments, but the reason why these particular experiments are more poorly predicted is not obvious, and cannot be linked to differences in measured initial conditions.

While the aerosol predictions are not satisfactory at this stage, in the absence of accurate measurements on organic aerosol composition and the difficulty in accounting for condensation reactions, it is difficult to make more concrete assertions as to organic aerosol yields.

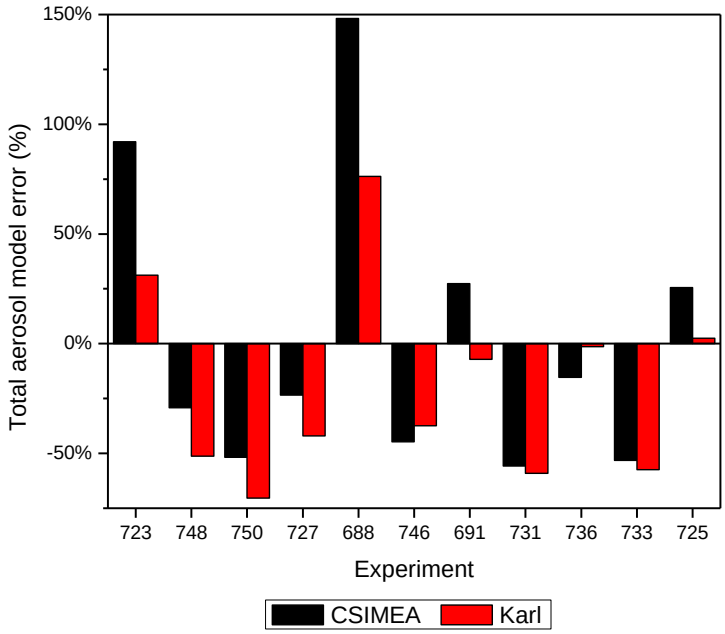

Figure 40. Aerosol model error for MEA/NOx experiments after 2 hours

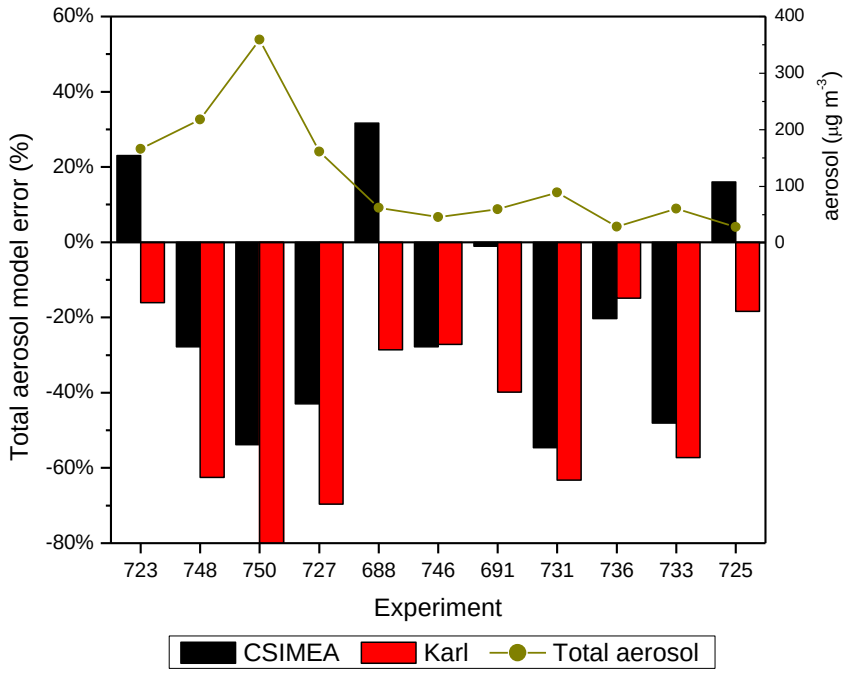

Figure 41. Aerosol model error and experimental values for aerosol concentrations for MEA/NOx experiments after 4 hours.

The composition of the aerosol as calculated by the CSI-MEA mechanism is shown in Table 11. Aerosol in the model is the combination of that formed by the two-product Odum approach (OH-1 and OH-2), the organic aerosol assumed from the reaction of MEA with NO3 (NO_3), the background aerosol as measured by the SMPS (BGOA) and the inorganic component resulting from the reaction of MEA and HNO_3 (MEANTR).

Table 11. Composition of aerosol at 4 hours calculated by CSIMEA mechanism and background aerosol present in each experiment

Experiment Number	Inorganic	Organic				Experimental
	MEANTR	OH-1	OH-2	NO_3	BGOA	Background (µg m^{-3})
723	1.4%	22.5%	56.7%	19.4%	0.0%	0.1
748	3.1%	24.1%	52.5%	20.3%	0.1%	0.1
750	2.8%	22.8%	51.1%	23.2%	0.1%	0.1
727	4.7%	28.8%	44.4%	21.9%	0.2%	0.15
688	4.9%	32.8%	46.4%	15.8%	0.1%	0.1
746	11.4%	44.4%	29.2%	13.5%	1.5%	0.48
691	6.5%	38.5%	42.3%	10.8%	1.9%	1.1
731	9.1%	44.8%	35.7%	9.3%	1.1%	0.43
736	15.1%	51.1%	23.9%	9.1%	0.8%	0.18
733	11.6%	47.4%	29.9%	7.2%	4.0%	1.25
725	11.8%	46.8%	30.3%	5.0%	6.2%	2.0*
738	11.4%	13.9%	11.2%	48.1%	15.5%	6.5

* Assumed due to SMPS error

The calculated amount of inorganic aerosol is no greater than 15.1% (for E736), so the model predicts a high concentration of organic aerosol for all experiments. The proportion of inorganic aerosol appears to increase with decreasing initial MEA/NOx, although this is reflective of lower Δ(MEA) in the lower MEA/NOx experiments, which corresponds to lower organic aerosol production. The proportion due to the OH reaction and Odum approach is consistent, between 73% and 81% of the total predicted aerosol volume for the 11 experiments with high initial NO, although the proportion attributable to each product varies across the experiment subset.

The calculated mass of aerosol arising from the reaction of MEA with NO_3, albeit it at a rapid $k_{NO3+MEA}$ reaction rate, comprises between 5% and 23% of the calculated aerosol from the experiments with initial $NO:NO_2$ ratios of ~9:1. For E738, the single experiment performed at high NO_2, the proportion of aerosol resulting from the NO_3 reaction was 48.1%. The aerosol model error for this experiment was -67%, so the model was not able to account for a large proportion of the aerosol growth from this experiment.

Aerosol formed from the reaction of MEA under high NO_2 conditions has been identified as comprising inorganic amine salt aerosol in high proportions (Murphy *et al.* 2007; Nielsen *et al.* 2010). As E738 contains NO_2 concentrations greater than 60 ppbv throughout the experiment, it is possible that the aerosol formed in this experiment also contains a higher inorganic component than the other experiments with higher initial $NO:NO_2$ ratios. This model suggests that the formation of increased nitrate aerosol under high NO_2 conditions could be the result of the MEA + NO_3 reaction, either by direct formation after the reaction, or by the formation of HNO_3 as a result of abstraction by the NO_3 radical.

Formamide and formaldehyde

Predictions for formamide and formaldehyde for each experiment are shown in Appendix D. In general, both the CSIMEA and Karl mechanisms over-predict formamide concentrations, with formamide not included as an explicit product in the SAPRC mechanism. The average model error for formamide at the last obtained measurement (between 200-230 minutes) across the 11 experiments is 37% for CSIMEA, and 56% for Karl. The differences between the average mechanism errors are due to poorer predictions by the Karl mechanism in the three low NOx experiments only (< 25 ppbv). For the remaining eight higher NOx experiments, the average model predictions and errors were effectively the same, at 25% for the CSIMEA mechanism and 28% for the Karl mechanism. The difference due to initial NOx is shown for three examples in Figure 42, the low NOx experiment E723 and two higher NOx experiments.

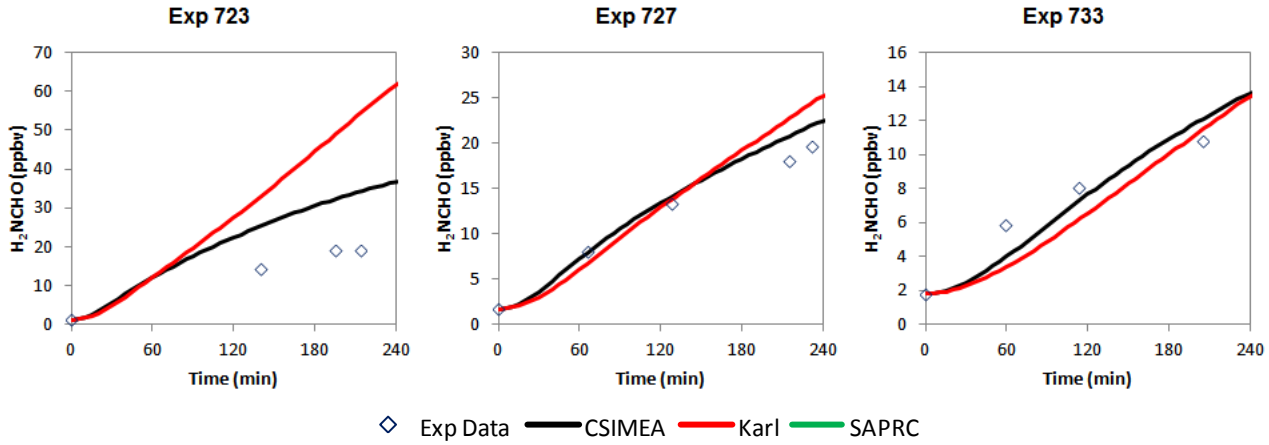

Figure 42. Formamide predictions for E723, E727 and E733.

Part of the over-prediction in formamide yields is related to the fitting for the yields from the MEA reaction with OH. In order to generate sufficient radical production to allow accurate ozone predictions, the yield of the C2-formamide channel relative to the C2-imine channel had to be increased to a level slightly higher than that required to minimise formamide model error. Further improvements to the yields from this reaction cannot be performed within the time frame of this project.

The average formaldehyde model errors at the time of the last DNPH cartridge measurement (assuming no initial formaldehyde concentration) are -5% for the CSIMEA mechanism, 89% for the Karl mechanism and 133% for the SAPRC mechanism. The differences between these average errors can be attributed to the gas phase reaction of MEA with formaldehyde, which has been included in the CSIMEA mechanism but not the other two mechanisms. This provides much more accurate measurements for formaldehyde, while also representing a small improvement in MEA concentrations (Figure 33).

Nitramine predictions

The concentration of the nitramine arising from MEA photooxidation (*N*-nitro-2-aminoethanol) could not be determined in this study. Modelled concentrations at 4 hours using the CSIMEA mechanism were between 0.02 and 0.13 ppbv, compared to concentrations between 0.08 and 0.34 ppbv for the Karl mechanism. As stated previously, uncertainty with regards to the reaction of the aminyl radical mean that no certainty can be provided for these values, and therefore no further analysis of modelled nitramine concentrations was undertaken in this study.

This page is intentionally blank

Part III Discussion and Conclusion

This page is intentionally blank

7 Fate of MEA and PZ emissions into the atmosphere

7.1 Tropospheric lifetime

The lifetime of any species emitted into the atmosphere is defined as that time required for concentration of the species to fall to $1/e$ of its initial value (Finlayson-Pitts and Pitts 1999). If the species is removed by a dominant reaction then the lifetime is dependent upon the rate of that reaction. An important reaction that dictates the lifetime of many volatile organic compounds (VOCs) that are emitted into the atmosphere is their initial reaction with the hydroxyl radical. The lifetime for a second order reaction as typified by a reaction with a VOC and the hydroxyl radical can be calculated using:

$$\tau_{OH} = \frac{1}{k_{\mathrm{OH}}[OH]}$$

Where τ_{OH} is the lifetime, k_{OH} is the rate constant and $[OH]$ is the hydroxyl radical concentration for which a typical 12 hour daytime average of 1.5 x10^6 radicals cm^{-3} has been used (Seinfeld and Pandis 2006).

Since there are other reaction processes that may compete with the OH reaction, it may be necessary to account for those reactions when calculating the lifetime of a VOC. The tropospheric lifetime of many VOCs, such as *n*-butane (5.7 days), benzene (12 days) and acetone (66 days) is dominated by the OH radical. However, for cases such as isoprene where the lifetime controlled by the OH radical is 1.7 hours, it may be necessary to consider reactions with O_3 (1.3 days) and the NO_3 radical (0.8 hours) when calculating tropospheric lifetime.

The k_{OH} rate constant determined for MEA by Onel *et al.* (2012) was 7.67 x 10^{-11}cm^3 molecule^{-1} s^{-1} and that estimated using the SAR method of Nielsen *et al.* (2012a) for PZ was ~1.6 x 10^{-10} cm^3 molecule^{-1} s^{-1}. Using the these rate constants, the OH radical-dependent lifetimes calculated for MEA and PZ were ~2.4 hours and ~1.2 hours, respectively, which are close to that of isoprene (1.7 hours).

7.2 Ozone formation with MEA and PZ

In daytime hours, some VOC reactions with the OH radical may lead to significant excursions in the ozone concentration if NOx is present. The rate in which ozone is produced in these reactions is initially dependent upon the VOC+OH rate constant. For example, the k_{OH} for isoprene is 10.1 x 10^{-11} cm^3 molecule^{-1} s^{-1} which is considered to be fast when compared to, say, *n*-butane which is 0.24 x 10^{-11} cm^3 molecule^{-1} s^{-1} (Seinfeld and Pandis 2006).

It is evident from the results of this study that the MEA/NOx system will produce ozone under lights and that PZ will react with ozone both in the dark and under lights. The relationship between ozone production and consumption of MEA and PZ is compared with modelled scenarios using similar conditions in Figure 43.

SAPRC-11 (Carter and Heo 2013) was used to produce a simulation for the VOCs propene, 1,3-butadiene, *m*-xylene, ethene, toluene and isoprene, with same initial conditions as MEA experiment 750 (MEA: 412 ppbv, $NO:NO_2$, 40:4 ppbv). The simulations were plotted in Figure 43 as change in ozone from start versus change in VOC from start. The simulations are compared to amine results obtained from MEA experiment 750 and PZ experiment 789. The initial conditions for E789 were PZ: 389 ppbv and $NO:NO_2$ = 38:4 ppbv.

It can be seen in Figure 43 that the production of ozone is more pronounced for the VOCs than for the amines, even though the amine+OH rate constants are comparable to that of isoprene.

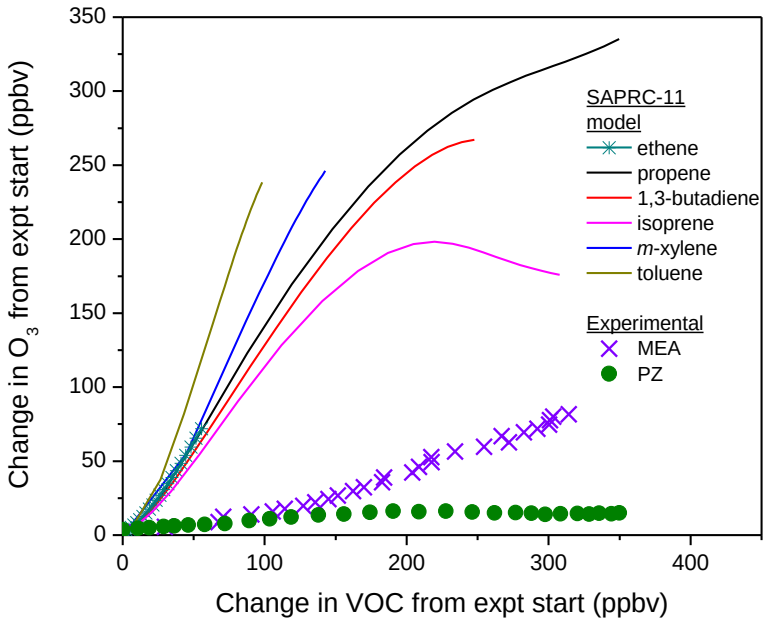

Figure 43. Comparison of SAPRC-11 model simulations of ozone against VOC loss for hydrocarbons, plotted against experimental values for MEA and PZ

7.3 MEA and PZ removal pathways

The results shown in Figure 43 clearly demonstrates that compared to VOCs, other reaction pathways are at play in the atmospheric chemistry of MEA and PZ that are competitive with OH reactions and/or competitive with the RO_2 to RO channel that occurs after the OH reaction.

Table 12 summarises reaction pathways that are believed to be responsible for the removal of MEA from the atmosphere.

In the atmosphere, gas phase MEA can be removed by a number of processes. Reaction with the OH radical provides three opportunities for this to occur. MEA is removed via the RO_2 pathway which is also responsible for the removal of NO to form NO_2. Significant products formed as a result of this pathway include ozone, formamide and predominantly, organic aerosol. This pathway is active during daylight and is liable to be more efficient at removing MEA closer to a NOx source.

In competition with the RO_2 pathway is the aminyl radical pathway which is more effective at removing MEA at low NOx than the RO_2 pathway. This pathway forms imines which have been linked to the formation of organic aerosol and the concomitant production of ammonia. This pathway is the dominant pathway post OH initiation at low NOx although it will also occur, when NO is readily available, in

competition with the RO_2 pathway. This pathway is active during daylight. An important characteristic of this pathway is the immediate cessation of ammonia formation after the light source is removed.

Table 12. Summary of MEA removal pathways.

	Removal (and pathway)		Products	Day/Night	Notes
MEA	OH	RO_2 (NO to NO_2)	O_3 H_2NCHO aerosol	Day	Reactive environments, especially near emission source containing NOx
		NOx uptake	nitramines	Day	NO_2 required, as above.
		aminyl radical / low NOx pathway	imines aerosol NH_3	Day	Dominant low NOx pathway for OH. Will also occur in readily available NOx as well, but competitive with RO_2/NO to NO_2 channel
	HNO_3		MEA-HNO_3 aerosol	Both	Requires HNO_3.
	NO_3		aerosol NH_3 HNO_3 (gas)	Night	Major night time reaction pathway. Expected high aerosol yield.
	Carbonyls		secondary amines	Day	Dependent upon carbonyl mixing ratio. May also occur with other oxygenated VOCs.
	Gas/particle partitioning		aerosol	Both	Direct uptake to aerosol/ aqueous phase.

A minor daylight pathway initiated by OH is NO_2 uptake by MEA to form nitramines. In this study we were not able to prove conclusively, using the methods available, that any nitramines, principally nitraminoethanol, were formed. The formation of this compound has been reported by Nielsen *et al.* (2010).

Another efficient MEA removal pathway is the direct reaction of MEA with nitric acid. This reaction rapidly produces inorganic aerosol and can occur in the day or the night. A similar reaction is expected to occur with sulphuric acid.

During the night, the NO_3 radical is at its highest concentration, especially after an active day influenced by above average ozone readings and NOx. The results presented in this study clearly demonstrate the reactivity of this MEA removal pathway which will produce ammonia and aerosol in high yield. This pathway is the major pathway at night which will also produce nitric acid which is expected to reinforce inorganic aerosol formation.

Primary amines have a propensity to react with carbonyls to form condensation products or Schiff Bases. Dependent upon the carbonyl, in the MEA case, a re-arrangement can occur to form an oxazolidine which in the MEA+HCHO case is called 1,3-oxazolidine. These products are secondary amines the fate of which requires further study since they could undergo further condensation with carbonyls to form stable enamines.

Glycolaldehyde, which is a product of MEA photo-oxidation, reacts with MEA faster than HCHO, probably in a third order reaction. It is possible that this or similar reactions may catalyse the formation of ring products from two MEA molecules. The extent to which MEA will react with other carbonyls present in the atmosphere will be dependent on the total carbonyl concentration, which at the end of a day, in an urban and some regional environments, is expected to be higher in concentration than at the beginning of the day. This complexity is a challenge when accounting for MEA removal in the troposphere as well as for most primary and secondary amines.

The last MEA removal process identified in Table 12 is the direct partitioning of gas phase MEA into aerosol which is composed mainly of water, that is, droplets. The extent to which this may occur is dependent upon the conditions and Henry's Law coefficients.

Consequently, in comparison to a base case without MEA, it is expected that the most obvious effect from an MEA emission during the day will be no increase in ozone formation, possibly a decrease, accompanied by an increase in aerosol formation. As the MEA concentration increases it is likely that the magnitude of these effects would increase. At night, an increase in aerosol production would likely be accompanied by an increase in ammonia formation. Both of these processes would be enhanced if the MEA concentration increased.

More study of the PZ system is required but the removal pathways in Table 12 are likely to operate with the following modifications. Unlike MEA, NO_2 uptake to form nitramines and nitrosamines is of greater importance.

There is a direct reaction with ozone and PZ which during the daytime will scavenge O_3 effectively resulting in the formation of aerosol directly from this reaction. It is likely that this would reduce the removal of NO which will keep the RO_2 pathway open. During the night, it is expected that residual ozone will be scavenged and aerosol will be formed by this reaction.

A more complete understanding of the fate of PZ requires further study. However, it is important to note that nitrosamines and nitramines are formed during its photo-oxidation in the presence of NOx.

The possibility that aerosol formation is enhanced by MEA and PZ emissions warrants further study since the effect that such aerosol would have regional climates is unknown. In addition, the composition of the aerosol is also of concern given that not all products have been indentified and that nitramines and/or nitrosamines are formed. It is also possible, that in the case of MEA, an unidentified pathway initiated by OH occurs. A product that may be formed from this pathway is HNCO (Borduas *et al.* 2013).

An accurate lifetime calculation requires a more complete understanding of the reaction of MEA, PZ and amines in general. The upper limit of the lifetime of MEA and PZ determined by consideration of the OH radical chemistry for MEA is ~2.4 hours and for PZ, is estimated to be ~1.2 hours.

8 Final Comments

8.1 Summary

Sampling, analytical and instrumental methodologies were investigated for the determination of priority compounds in chamber samples and implementation of a number of these methods provided valuable quantitative and qualitative information for evaluation of chamber experiments.

Sorbent collection techniques enabled frequent sampling over the period of the chamber experiment and also served to stabilise reactive analytes and/or concentrate trace species without the requirement for additional isolation techniques. Liquid chromatography (HPLC) of derivatised analytes provided highly sensitive analysis of polar and reactive compounds and gas chromatography using both chemical ionisation and electron ionisation modes of mass spectrometry provided a highly selective and sensitive tool for quantitative analysis and qualitative characterisation of a range of photolysis products.

The compounds generated in photochemistry experiments of this kind, and the gas phase environment under test, are of a nature that is not necessarily amenable to conventional methods of sampling or of analysis. Certain challenges were encountered and overcome and new techniques were implemented. Certain other aspects of both sampling and analysis require significant further effort in their optimisation or in the investigation into alternative techniques. Overall the suite of methods generated during this project provided a powerful basis for studies of this kind.

MEA/NOx experiments were performed over a range of MEA and NOx concentrations. The results generated from these experiments were used to investigate product and ozone formation from MEA photooxidation and to provide data to assist in the development of a chemical mechanism for MEA. Supplementary experiments were performed with MEA in the presence of HNO_3, NO_3, O_3, HCHO and glycolaldehyde. Results from these experiments, along with findings from published works, were also used in the development of the MEA mechanism. Additionally, reaction rate constants were calculated for the reaction of MEA with formaldehyde and glycolaldehyde.

Based on the MEA experiments performed, and given the time left available in the project, a restricted set of piperazine (PZ) experiments were completed. In comparison with MEA photooxidation, PZ generated higher yields of aerosol, reacted rapidly with ozone and generated nitrosamines and nitramines. For the conditions used in these experiments, both MEA and PZ produced high aerosol yields.

A chemical mechanism was developed for MEA (CSIMEA) which combines existing knowledge and results from this study. To ensure that photooxidation products of interest were simulated accurately across the MEA/NOx experiments, yields from important reactions were representatively fitted. This mechanism improves ozone and MEA predictions, includes generation of ammonia from MEA and includes an HO_2/RO_2 mechanism, which is considered to be more relevant under atmospheric conditions. This mechanism was used in the regional dispersion study performed as deliverable 4.3.

The upper limit of the lifetime of MEA and PZ determined by consideration of the OH radical chemistry for MEA is ~2.4 hours and for PZ, is estimated to be ~1.2 hours.

8.2 Recommendations

As a result of this study, the following recommendations are made.

This study has highlighted the differences in the atmospheric degradation of two amines intended to be used in the PCC process: MEA and PZ. In order to understand more completely the rates of degradation and formation of by-products of other amines, additional smog chamber experiments and analytical procedures are needed in order to be able to identify and quantify their potential air quality impacts. This data should be used to validate appropriate chemical mechanisms for other amines, which can be coupled with air quality models.

The measurement of nitrogenous compounds requires further investigation in order to more effectively address the range of compounds and experimental conditions encountered in studies of this kind. Factors associated with gas phase sampling, analytical preparative techniques and instrumental analysis combine to produce an efficient method and various approaches can be taken in each aspect. Alternative sampling techniques are of utmost importance in this area to better address the activity of most nitrogenous compounds on collection media and in the environment under test. For example, solid phase microextraction (SPME) is a novel technique which would be worth investigation, and can be combined with derivatisation to further its potential, particularly for active compounds. For amenable compounds it combines direct gas phase collection with GCMS analysis.

On-line instrumental techniques can obviate the collection aspect but can also be affected by the test environment or a lack of specificity; they are however an effective tool. For polar, basic and thermally labile compounds liquid chromatography is most suitable and the use of mass spectrometry provides qualitative information. The LCMS technique is complex and not without limitation when obtaining quantitative data from complex matrices. Further study is recommended in providing a robust and systematic approach to analytical studies into the products of PCC-amine photo-oxidation.

Given the high aerosol yields observed for MEA and PZ photooxidation in this study, a better understanding of the composition of the aerosol is required, as this probably represents the major fate of amines and their reaction products in the atmosphere. The effect that amines have on the ambient PM burden and potential impacts on human health requires further study. In addition, the role that aerosol formed from amines might have on the role of the formation of condensation nuclei and subsequent impact on urban and regional climate is unknown.

To be able to adequately account for the fate of amines in the atmosphere, an improved understanding of the role of condensation products, such as those formed by the reaction of MEA and formaldehyde, is required. Reactions such as those observed in this study can stabilise the amine group in a different form, and the fate of these products is unknown. Consequently, it is recommended that the impact of emissions of PCC-amines on existing VOC/NOx systems be under taken.

For the chemical mechanism, it is recommended that further research leading to an improved representation of aerosol formation is required, including experimental and simulated characterisation of the aerosol phase. In addition, a deeper understanding of the fundamental reactions of imines and aminyl radicals are required for amine mechanism generation. It is also important that the dark chemistry of amines be studied in greater depth.

Appendix A Development of Techniques for GCMS Analysis

Development, validation and implementation of sampling and GCMS instrumental methodologies for the collection, characterisation and quantification of priority reactant and nitrogenous product species from photochemical studies of amine and related reactant systems is described. Specifically the results from investigations into analysis of MEA, piperazine, formamide, 2-nitroaminoethanol and the characterisation of other minor nitrogenous and oxygenated products are described.

A.1 Florisil-liquid extraction GCMS technique

It was considered that the stage of development reached for this technique, as described in the interim report, was sufficient for current requirements and that emphasis be placed on further development of the thermal desorption technique.

A.2 Thermal desorption (TD) GCMS technique

A Markes Unity 2™ desorption unit and Ultra 2™ autosampler (Markes International Ltd) were interfaced to a Varian 450-GC gas chromatograph and 240—MS ion trap mass spectrometer (Varian Corporation, now Agilent Technologies Ltd). Chamber air was drawn through sorbent tubes containing the selected sorbent (Markes International) at a calibrated mass flow controlled flow rate for the required time period, generally 100 ml min^{-1} for 15 minutes. Samples were taken in order to monitor at least four phases of each experiment, from dark through to the UV.

Determination of MEA was deprioritised as a candidate for the thermal desorption GCMS technique after issues encountered and described in the interim report could not be efficiently or effectively overcome. The successful development of a HPLC methodology for measurement of MEA using *in-situ* derivatisation, as described in Appendix B, was implemented for quantitation of MEA in chamber samples.

Priority was given to furthering the TD-GCMS technique to the collection and analysis of other compounds of interest. Particular attention was given to the quantitative analysis of formamide, as this is a key product in the evaluation of results from the current program of photochemical experiments. The identification of minor components formed during photolysis experiments was also implemented, along with investigation of the viability of the method for determination of piperazine. The use of headspace TD-GCMS has provided information on the identity of trace components in the pure MEA liquid, which is important in determining the origin of compounds observed in chamber collected samples.

The use of electron ionisation mass spectrometry (EI-MS) for structural elucidation of unknowns, supported by methanol positive ion chemical ionisation (CI-MS) for MW confirmation has proved useful in the characterisation of photochemically derived products formed during the chamber experiments. The higher selectivity and sensitivity of CI-MS meant that this mode was used for all quantitative analyses and it

proved invaluable in the determination of isotopic distribution in products from experiments using isotopically labelled components.

Developments which were undertaken in sampling, analytical and instrumental aspects of the sorbent collection and TD-GCMS technique, and the validation of the methodology for formamide and other compounds relevant to the chamber monitoring program are described in the following points.

Sorbent Selection and Desorption Parameters

- Chamber collections of model compound atmospheres were made using three sorbents of different selectivity, namely; Tenax TA®, Tenax TA®/Unicarb® and Tenax TA®/Carbograph 1TD®/Carboxen 1000® (Markes International Ltd) to determine their efficiency in collection and desorption of analytes. These sorbents differ in their chemical and physical characteristics and hence the range of compounds for which they are best suited. For example; Carboxen is a carbonised molecular sieve which is a strong sorbent that is more efficient for collection of very volatile, low boiling point compounds which may have minimal adsorption on, or high partitioning through, Tenax or Carbograph sorbents. The mixed sorbent beds extend the range of compounds which can be collected, however they also require more stringent sampling and desorption protocols due to their ability to co-collect water and their potential for oxidation if heated in the presence of co-collected air. They also require higher temperatures in order to release collected compounds from the sorbent.
- Tenax sorbent was selected on the basis that this sorbent performed equally to the others for collection of diethylamine (as described in the interim report), and also in this work for the collection of formamide. As these are the two most volatile of the priority species it is expected that the method will also be efficient in the collection of less volatile species including those for which qualitative analysis will be undertaken, such as oxygenated and nitrated products formed during photolysis. Tenax is also the more inert sorbent and requires lower desorption temperatures which is advantageous due to the inherent reactivity and thermal lability of certain compounds targeted in this study. Tenax/Unicarb® showed higher adsorption efficiency for certain organic classes (such as oxazoline and oxazoles) but similar or lower affinity for others. The requirement for higher desorption temperatures and its higher background levels translated to lower sensitivity for overall trace product characterisation. Its use for application to specific compounds of interest will be pursued in future applications in this area.
- Two sorbents used for secondary cold-trapping in the thermal desorption system, namely Tenax TA® and Tenax TA® with carbonised molecular sieve, were tested for their efficiency in cold-trapping and desorption of priority analytes. No significant difference in performance was observed and the Tenax trap was selected due to mainly to its more inert nature which minimises possible reactivity issues.
- A base-deactivated capillary transfer line was installed between the thermal desorption and gas chromatograph to minimise surface activity and improve efficiency of analysis for highly basic compounds. A highly inert GC column was also used (RXi-624Sil MS 30m, 0.25mmID, 1.4µm df) to minimise peak broadening and tailing that is common in the chromatography of these compounds.
- Temperature and flow parameters controlling the efficiency of primary desorption, secondary trapping and desorption and transfer to the GC were optimised for priority analytes. Residuals from a second desorption of the sampling tube were < 1% of the original mass collected. The formamide

peak shows relatively good resolution with some minor tailing expected from a compound of this kind.

- The recollection system was tested for efficiency in transfer of analytes to the recollection tube. Recollection enables tube samples to be reanalysed and is useful in method development and in more thorough evaluation of actual samples. To date the recollection system is still showing 10 – 20% loss on transfer of analytes to the recollection tube despite rigorous testing of all parameters likely to impact on the efficiency of the recollection. The manufacturers have not found a resolution to this problem which is suspected to be associated with split valving and flow control. It was envisaged that reactants at high concentration could be run from the same sample tube as the analysis of minor compounds using recollection to alter the split ratio and hence allowing optimisation of the mass to the MS detector. This was preferable to altering sampling parameters and duplicating collections to accommodate large differences in concentration. As this option was unavailable, the way forward was to run the initial desorption for quantitative analysis by CI-MS and use the recollection for qualitative analysis by EI-MS.

Monoethanolamine (MEA)

- Resolution and identification of MEA was achievable from GCMS analysis of pure compound desorbed from the sorbent tube but the overall method proved quantitatively inefficient when applied to chamber sampling. The basicity and activity of this compound is known to be problematic and exposure to untreated silica and silanol surfaces causes adsorption effects. In consideration of this, sorbent tubes were Silco® treated to render the surface inert and base deactivation of TD and GC components was incorporated. The ion-trap of the MS was also purchased with Silco® treatment. Reactivity of MEA on the sorbent, and in the presence of NOx, and under thermal desorption conditions are all considerations associated with its loss. Accordingly the HPLC method, described in Appendix B was implemented for quantitative analysis. The TD-GCMS method was used for qualitative monitoring of MEA to assess its progress relative to product formation in samples from the chamber experiments.

MEA Purity

- The TD technique was also applied to the analysis of pure MEA used in the preparation of the chamber for photolysis experiments. This provided information on the identity of trace impurities or decomposition products present in the bulk MEA, which was important in determining the origin of compounds in chamber collected samples. The sorbent tube was directly exposed to the headspace of the MEA liquid, allowing MEA and associated components which have partitioned to the gas phase to be collected. Analysis by CI and EI-MS found a number of compounds in the MEA headspace which also occur as photolysis products. These include formamide, oxazoline (4,5-dihydro-oxazole), 1,3-oxazolidine, 2-methyloxazolidine, and pyrazine. As MEA cannot be quantitatively determined using this technique, the concentration of these compounds in the bulk liquid cannot be deduced. However their relative intensity compared to MEA can be assessed and the impact of their presence in the chamber can be ascertained, as discussed in Section 4. In all cases these compounds were at significantly lower concentration, relative to the MEA, in the headspace than in chamber samples indicating minimal concentration as artefacts in the pure MEA used for chamber experiments.

Formamide

- The efficiency of formamide sampling was assessed using a standard chamber atmosphere prepared from syringe injection and analysed against liquid standard tube preparations. Sampling parameters and collection efficiency were assessed using chamber mixing ratios in the range 75 ppbv to 300 ppbv. Optimisation of flow rate, sampling volumes, collection mass, sorbent capacity and breakthrough volume was performed. The efficiency of collection was also assessed using a nitrogen purge of spiked standard tubes to simulate high volume low concentration sampling conditions and breakthrough monitoring of the chamber atmosphere using a thermal emissions analyser (TEA) and the analysis of secondary back-up tubes was undertaken.
- Optimisation of the various parameters produced a sampling method showing a collection efficiency of 90-100% recovery with odd deviation within an experiment of 70% recovery. The use of back-up tubes to monitor possible breakthrough of formamide showed up to 10% carryover onto the second tube, under certain flow and mass conditions. Under all conditions the formamide calibration across the mass range representing the sample collection has remained linear, indicating efficiency in analyte desorption. Further work was undertaken to optimise and limit the collection variables to achieve consistently >90% recovery as collection and desorption efficiency.
- Tests to determine if the presence of co-collected MEA on the efficiency of collection and desorption of formamide was undertaken. A model atmosphere containing low concentration of formamide (60 ppbv) was sampled and compared to that which included a high MEA concentration of MEA (300 ppbv) to simulate conditions of collection under photochemical experiments. The test was also undertaken under laboratory conditions using collection of MEA headspace onto the tube before and after introduction of a formamide spike. These tests indicated that, under the conditions of collection, the presence of co-collected MEA did not affect the quantitative collection of formamide.
- Test to determine the chamber holding capacity for formamide in the presence of MEA were undertaken and showed no loss in concentration over a 2-hour period.
- The GCMS was optimised for chromatographic resolution across the expected compound range. The mass spectrometer was operated under both chemical ionisation (CI-MS) and electron ionisation modes (EI-MS). Formamide run under EI-MS shows concentration dependent hydrogen donation and a consequent shift in relative mass intensity across the peak, between the molecular ion m/z45 and m/z46. Integration by total ion count is therefore used if quantification is performed in this mode. This will reduce the selectivity and sensitivity of the analysis however and quantitative analysis was therefore undertaken using CI-MS. This mode has inherently higher sensitivity due to the mechanism of ion formation and detection. Reduction in background noise due to non-detection of non-ionisable compounds also increases sensitivity and selectivity. This is of particular advantage for analysis from sorbent tubes where sorbent artefact related background can be problematic for trace analysis when undertaken using the EI-MS mode.
- System calibration was verified using the external standard method from liquid standard spikes onto sorbent tubes. The standard tube preparations were optimised for parameters such as analyte mass, solvent volume, temperature and nitrogen purge time. Duplication of better than 2% RPD was achieved from tube preparations.

- Quantitative analysis was undertaken using methanol positive ion CI-MS using area integration of the extracted ion (M+1, m/z 47 for formamide). External standard calibration was linear over the mass range 450 to 10,000pg to the MS detector with correlation coefficient $r^2 > 0.99$ and a RSD on the response factor of < 10%. This is equivalent to a mass to the sorbent tube of 5 to 100ng at 10:1 outlet split ratio and a chamber concentration of 1.8 to 40 ppbv for nominal 1.5 litre sample volume. Higher mass calibrations, through to 1500ng, have also shown linearity after appropriate manipulation of inlet and/or outlet split ratios.
- The detection limit for formamide was 45pg to the detector using CI-MS mode. Under nil split conditions this would equate to a best case quantitation limit of 0.045ng as mass collected to the tube, or 0.02 ppbv for 1.5 litre collection volumes (e.g. 15 mins at 100ml min^{-1}). A minimum split of at least 10:1 is preferred to optimise secondary trapping and hence a detection limit of 0.2 ppbv is considered nominal under these conditions. Sensitivity of formamide by CI-MS is around 5-fold higher than EI-MS, and other compounds, such as nitrosamines have been previously verified at up to 60x higher sensitivity under CI mode of analysis. Methanol positive ion CI-MS of formamide suffers lower sensitivity than higher molecular weight molecules due to the requirement to monitor at low mass and a consequent decrease in signal:noise due to the presence of m/z 47 in the background from ionisation of the methanol reagent.
- Stability of formamide standard solutions in methanol and of standards stored on tubes has shown nil loss over a period of 2-month in solution and 1-week on-tube. Longer term tube stability tests will be undertaken using both liquid standards and tubes sampled in the presence of MEA.
- Under the sampling and instrumental protocols validated above, quantitative analyses was undertaken to monitor formamide in all experiments performed in this project during stages from clean chamber, through dark and UV. The results are discussed in Section 4.

Piperazine

- The validation protocols used for formamide were applied for the instrumental aspects of piperazine analysis by Tenax® sorbent tube TD-GCMS. Unfortunately project constraints did not allow full validation involving the sampling aspects using standard chamber atmospheres, as was validated for formamide.
- Piperazine was adequately resolved by TD-GCMS however it showed a non-linear response over the required concentration range. The chromatographic behaviour it exhibited indicated that this was due to reactivity and adsorption effects more likely associated with GC transfer and column components than the desorption process. Despite this, the response was reproducible at each concentration level and calibration was therefore possible using a trend line obtained from a power equation. This provided adequate quantitation; provided certain conditions around the standard and sample data set were upheld. Piperazine measurements were made on all PZ experiments to provide a semi-quantitative comparison to data obtained from the FTIR result.

Nitroaminoethanol

- The evaluation of 2-nitroaminoethanol (NAE) for its determination by TD-GCMS was evaluated by liquid injection onto the sorbent bed and by headspace analysis. Whilst a chromatogram exhibiting a major compound was evident in both cases, along with a number of minor compounds, none of these presented with a volatility, molecular weight or mass spectrum indicative of NAE. It is evident

therefore that this compound was either already degraded in its bulk form or degraded under the processes of gas chromatography. The analysis of this compound, likely to be formed during the UV phases of MEA experiments, was therefore unable to be achieved. The chromatograms were examined for the major degradation product seen from analysis of pure compound as an indicator of NAE, but this compound was not found.

Minor Photolysis Products

- Qualitative analysis for minor products associated with MEA, MEA related systems and of piperazine photolysis were undertaken using CI and EI-MS modes. Recollection of desorbed analytes from each sample tube allowed subsequent re-analysis under EI-MS mode immediately after its CI-MS analysis. The knowledge of a compound's molecular weight, obtained from CI-MS, together with its EI mass spectra allowed structural elucidation and characterisation of organic class or specific identity for each compound found in the chamber samples. Mass spectral search software assisted in this process, for those compounds included in the NIST database. The ability of the ion-trap mass spectrometer to run both CI and EI-MS modes simultaneously, which cannot be achieved using quadrupole MS instrumentation, provided a power tool for characterisation of nitrated and oxygenated compounds relevant to this project.
- Certain experiments were fully examined for minor compounds and this report includes the results from that assessment for Experiments 750 MEA, E807 ^{13}C isotopically labelled MEA, E753 MEA/Formaldehyde, E773 MEA/Formaldehyde, E785 MEA/Glycolaldehyde and piperazine experiments E787 and E789. In general the process of determining minor compounds first looked at the CI-MS mass and then EI-MS spectra associated with each of the chromatographic peaks. Peaks associated with Tenax® sorbent artefacts were determined and discarded. The CI-MS chromatograms were also searched, using extracted ion, for masses relevant to compounds expected as photolysis products from mechanistic studies and with reference to various relevant publications, such as Neilson *et al.* (2010). Mass hits by CI-MS were then checked against the EI analysis and the mass spectra used to characterise the compound. As CI is significantly more sensitive than EI and as system background effects EI more significantly it was not always possible to discern an EI spectrum when intensities were very low.
- This process yielded up to 40 nitrogenous and oxygenated organics as photolysis products including oxazolines, oxazolidines and related compounds, amides, aldehydes, nitrosamines and nitramines, from around 80 compounds searched.
- CI-MS was used to monitor experiments where isotopically labelled ^{13}C-MEA or PZ/^{15}NO was used. The ability to use CI data to determine molecular weight and hence the proportion of native and labelled component for each compound proved invaluable in evaluating the distribution of the label in the reactant and its products.

Appendix B Development of Techniques for HPLC Analysis

Investigations made into sorbent sampling and HPLC instrumental methodologies for the collection and quantification of MEA, piperazine and NAE from photochemical studies of amine and related reactant systems are described. The methodology for carbonyl compounds has been validated for routine use in our laboratory and as such detail is not described here and an outline of its implementation is included in the main body of this report.

B.1 MEA analysis using *in-situ* NITC derivatisation

The aim of this work was to assess the use of adsorbent tubes containing XAD-2 coated with 10% of 1-naphthylisothiocyanate (1-NITC) to derivatise and trap monoethanolamine (MEA) at parts per billion levels from a reaction chamber gas sample. This technique was to be used to verify the confirm concentrations of MEA determined by FTIR measurements within the chamber.

The methodologies developed were based on OSHA method PV2111 (1988) and that published by Levin *et al.* (1989). These both use the NITC/HPLC techniques for determination of MEA in ambient air and to date the OSHA method is only partially validated. A known volume of air is drawn through glass tubes containing an 80mg primary sorbent bed and 40mg back-up bed separated by a glass wool plug. Such tubes are now commercially available (SKC). The derivative is desorbed using dimethylformamide (DMF) and the solution is analysed by HPLC with UV detection at 254 or 280 nm. OSHA used both normal phase and reversed phase HPLC, the reversed phase being C18 column and acetonitrile (ACN)/water solvent. The Levin *et al.* (1989) method is similar except they used 5% 1-NITC on a 200mg bed and acetonitrile to desorb the derivative.

These methodologies were used as a basis for further development and were optimised and validated for the requirements of this project, as described in detail in the sections that follow. It has been confirmed that MEA can be readily derivatised with 1-NITC when dissolved in ACN and separated by reversed phase HPLC on a C8 column with a solvent mix of 30% ACN in water at a flow of 1.5 ml min^{-1}. The NITC-MEA derivative gives UV absorptions at λ_{max} = 222 nm with ε_{max} = 6056 L mol^{-1} cm^{-1} and a less intense peak at λ_{max} = 285 nm. Four point calibrations had very linear fits for Conc = α x Peak Area.

It was found that sampling efficiency of MEA collection was improved by reducing the collection flow from 0.1 litres min^{-1} to 0.05 litres min^{-1} and the optimum sampling time was found to be ~60 minutes. Even so the amount of MEA adsorbed was low and recoveries indicated that some NITC-MEA may be irreversibly absorbed (recoveries 60-90%). This adds a level of uncertainty to the measurements. DMF was less suitable than ACN as the desorption solvent, due to chromatographic disturbances and greater extraction efficiency. Of the other extraction variables examined, higher temperature or longer time had small but negative impacts on recovery while the use of PTFE or nylon as the filter material had virtually no effect.

The effect of humidity on the reaction of MEA with the 1-NITC on the XAD-2 adsorbent should be examined to determine if this is the reason for lower collection efficiency in chamber air.

The developments which were undertaken in sampling, analytical and instrumental aspects of the NITC sorbent collection and HPLC technique are described in more detail under the following points.

Analytical and Instrumental Parameters

- The instrumental methodology incorporated a standard HPLC system (Agilent 1200 series) which comprised a vacuum degasser, a quaternary pump, an autosampler, a diode array detector and a computer for data acquisition and integration. A Restek Ultra C8 column (4.6 mm id x 250 mm, 5 µm) column was selected over a more conventional C18 column due to its higher polarity in likely higher efficiency in the separation of the various small polar entities likely to be present in samples from photolysis experiments. A Zorbax Eclipse guard column (4.6 mm id x 12.5 mm, 5 µm) was placed ahead of the analytical column. The chromatography was optimised under reverse phase conditions and used a 20µl sample injection under a solvent regime of 1.5 ml min^{-1} isocratic elution in 30% ACN/water followed by 100% ACN to flush the column of residual materials.
- Standard MEA solutions were prepared in ACN and standard NITC-MEA solutions were prepared with the addition of an excess of 1-NITC. Since one MEA molecule reacts with one NITC molecule and considering that the ratio of molecular weights is 3.033, for 95% purity NITC the ratios of NITC used to that required stoichiometrically were 1.12 to 1.78. Workings standards were prepared to cover the range of 0.10 to ~16 µg ml^{-1}.
- Initial tests were made to optimise the HPLC system with solutions of NITC only and NITC-MEA. Figure B.1 shows a chromatogram for NITC alone with 1 ml min^{-1} flow rate before the ACN flush was introduced. The strong peak at ~15.8 minutes gave the spectrum shown in Figure B.2 with two peaks, the first had λ_{max} = 222 nm and an absorption of ~2.13 mAu and the second was broader and less intense with λ_{max} = 286 nm and an absorption of ~0.26 mAu. The peaks between 1 minute and 2.5 minutes are due to the injection disturbance and very polar compounds and are ignored in this work. All chromatograms taken were recorded at 230 nm which was close to the λ_{max} but slightly above to lessen the effects of strong absorptions at shorter wavelengths.
- Figure B.3 shows the chromatogram of a blank tube analysed with the flow rate at 1.5 ml min^{-1} and the ACN flush from 18-21 min. There are several features to note. Firstly the strong NITC peak has moved earlier to ~10.3 minutes. Secondly the significant shift in baseline at ~19 minutes and the two strong peaks (not shown) that occur after 20 minutes obviously caused by the solvent programme with the 100% ACN flush. Also of note are the 4 small peaks between 5 and 9 minutes. These four peaks appear in all samples contacted with XAD-2 but not in the standards or solvent blank. The NITC-MEA peak, when present, always overlays the third peak but has a slightly lower retention time. If the NITC-MEA peak is very large it may overlay the second and fourth peaks as well. It was decided to use the third peak as the blank area not because it was NITC-MEA but because it would always contribute to the area of small NITC-MEA peaks. Larger peaks would not be significantly affected by including the second and fourth peaks and there were very few times the 4th peak could not be separated.

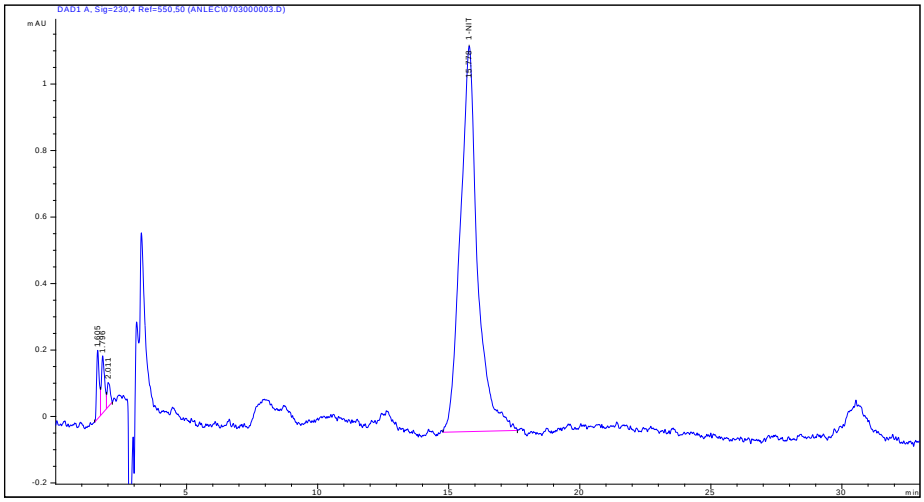

Figure B.1. Initial chromatogram of 1-NITC in ACN

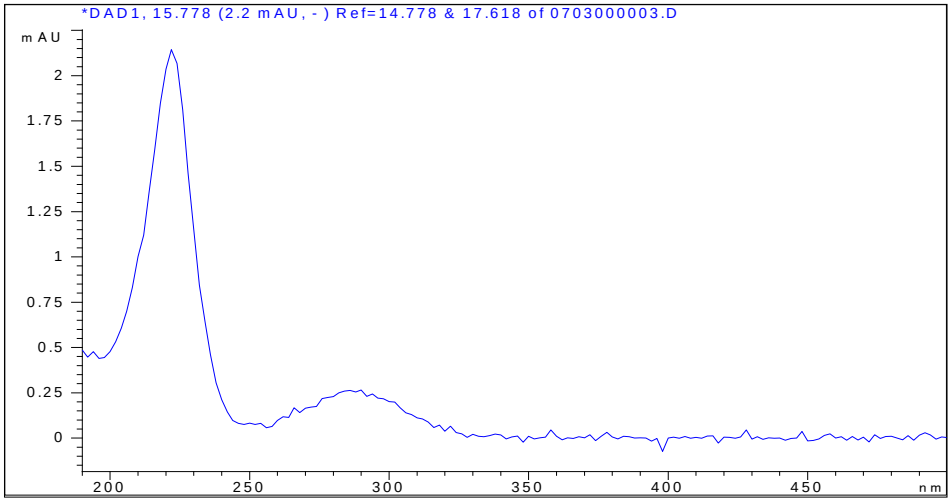

Figure B.2. Spectrum of peak with ~15.8 min retention time

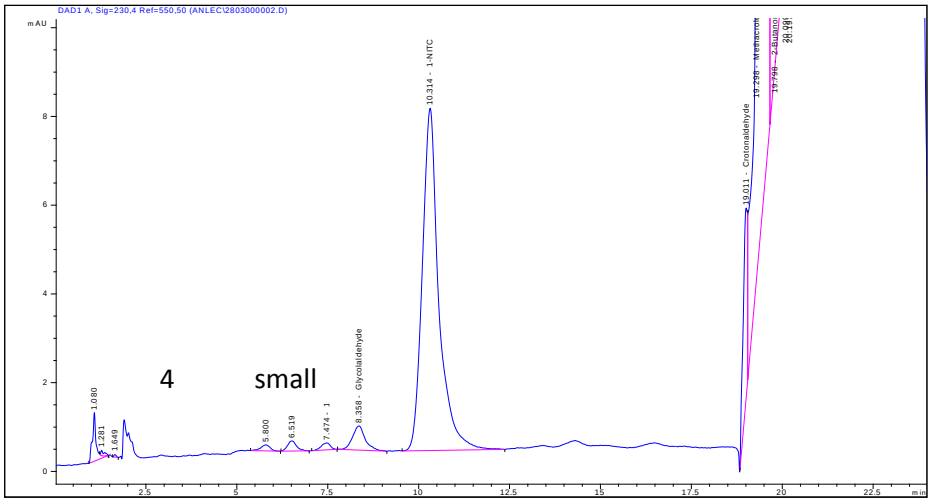

Figure B.3. Chromatogram of blank sample at 1.5 ml min^{-1} with ACN flush

- Various batches of NITC-MEA standards were prepared over the period of this work. All gave very linear results for 4 point calibrations for concentration being directly proportional to peak area (i.e. Conc = α x Area) with R^2 varying from 0.99984 to 0.999995. The slopes varied from 0.002760 to 0.003171 indicating the batches of standard were quite consistent. Figure B.4 gives the spectrum of a 1.20±0.05 µg ml^{-1} standard of NITC-MEA. The two peaks due to the 1-NITC are evident as well as a broader peak from 190 to ~260 nm which is an effect of the MEA on the absorption. The strongest peak has λ_{max} = 222 nm and an absorption of 29.5 mAu which corresponds to a molar absorptivity ε_{max} = 6056 L $mol^{-1}cm^{-1}$. The second broader and less intense peak had λ_{max} = 285 nm and an absorption of ~4 mAu. Observations indicate that the 1-NITC reacts readily and completely with MEA dissolved in ACN and the complex appears to be quite stable when stored in a fridge for up to 6 weeks.

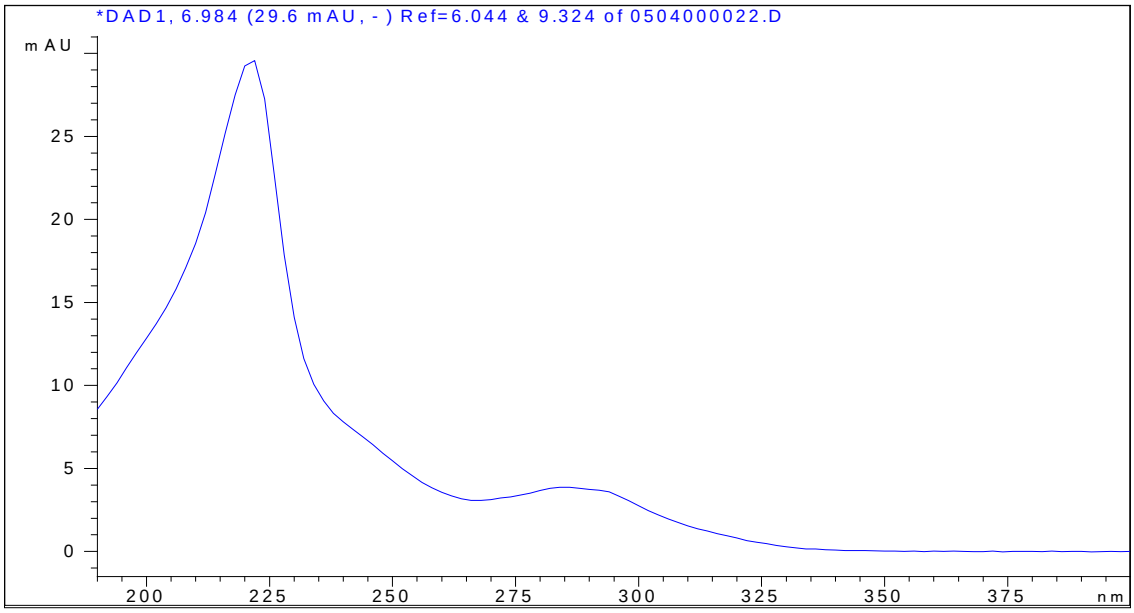

Figure B.4. Spectrum of 1-NITC+MEA derivative from a 1.20±0.05 µg ml^{-1} standard

Chamber Sampling Parameters

- An MEA atmosphere was prepared in the experimental chamber at a concentration of ~500 ppbv to determine the effect of various sampling parameters on the recovery of MEA.
- OSHA PV2111 recommends a sampling gas flow of 0.1 litres min^{-1} to sample 10 litres of air over a sampling time of 100 minutes. Levin *et al.* (1989) used a flow of 0.2 litres min^{-1} to sample 5 litres over a sampling time of 25 minutes. The front section of the SKC adsorption tube, with 80 mg of coated XAD-2, should have been able to react with ~2638 µg of MEA and similarly the rear sections react with ~1319 µg of MEA. Sampling 500 ppbv MEA at 0.1 litres min^{-1} for 60 minutes corresponds to 7.5 µg of MEA so there should have been plenty of capacity to absorb the MEA on either section by a factor of >350. In this work, samples were initially taken with a flow rate of 0.1 litres min^{-1} for 60 minutes but results from the tube rear sections indicated there were significant amounts of MEA reaching these sections.

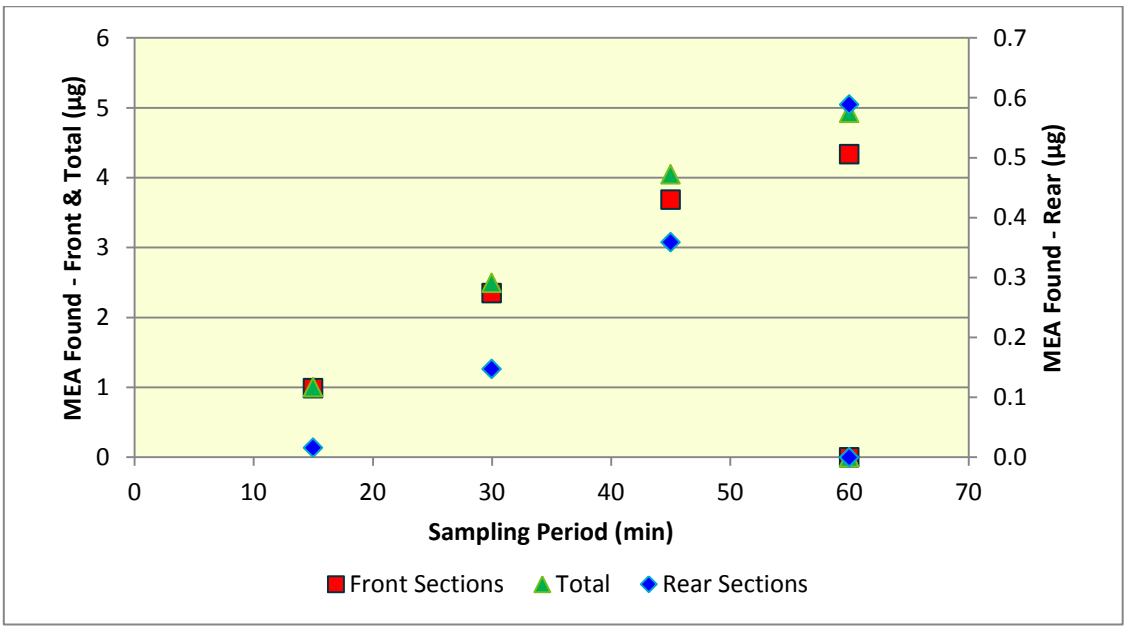

Figure B.5. MEA found in sample tubes with various sampling times

- Tests were conducted with 15, 30 45 and 60 minute sampling periods and for the 60 minute test a second tube was placed in series to determine if there was any material not being collected. The results in Figure B.5 show that the concentration in the front section increases linearly with collection time to 45 minutes but is slightly below expected at 60 minutes. The amount on the rear sections is much lower but not zero except for the second tube at 60 minutes. The front section of the second tube in series at 60 minutes showed a small amount of MEA confirming that carry-over occurs at this flow rate and absorption time. This indicates that the MEA does not have enough time to react with the NITC at 0.1 litres min^{-1} flow rate so the sampling flow rate was reduced to 0.05 litres min^{-1} and the sampling time kept at 60 minutes. This proved effective in improving the efficiency of MEA collection.

Recovery and Desorption Solvent

- Due to chamber samples giving values below 90% of the expected values, some samples were extracted with DMF (as used in OSHA PV2111) instead of ACN to see if this would improve recoveries. The results were actually worse recoveries as shown in Table B.1. The reason for this is clear from the chromatogram in Figure B.6. The DMF elutes from ~1.6 minutes and creates an intense peak overloading the detector and continues to elute until 6 minutes or later indicating the column is also overloaded. When the NITC-MEA peak elutes at ~7.5 minutes the baseline is still well above background and there appears to be a hump beneath it and the next few peaks, thus preventing accurate area determination. The OSHA method used shorter column (100 mm) than this work (250 mm) which may have helped with separation of the DMF peak and that of NITC-MEA. Also they show a chromatogram of 80.9 µg mL^{-1} NITC-MEA which is >20 times the concentration of our samples so the resolution is lower and disturbance of the baseline not clear. Tests for complete desorption with the ACN solvent were made by completing a second sequential extraction on two samples. After the initial extraction only 1 ml of the solvent was removed and filtered for analysis, the remaining 1 ml was left with the XAD-2 and glass wool in the vial in a fridge for 20 days. A further 1.0 ml of fresh ACN was added to the vial, which was then treated as a

normal sample. The results (Table B.2.) show that no significant amount of NITC-MEA was extracted with the extra contact time or fresh solvent since the expected ratio is 0.5.

Table B.1. Results for Samples Extracted with DMF compared to ACN

Sample	Amount Extracted with DMF (µg)	Amount Extracted with ACN (µg)
686/2 Front	1.67	2.88
686/2 Rear	0.04	0.05
693/4 Front	1.77	2.85
693/4 Rear	0.10	0.08
693/5 Front	2.90	3.52
693/5 Rear	0.21	0.29

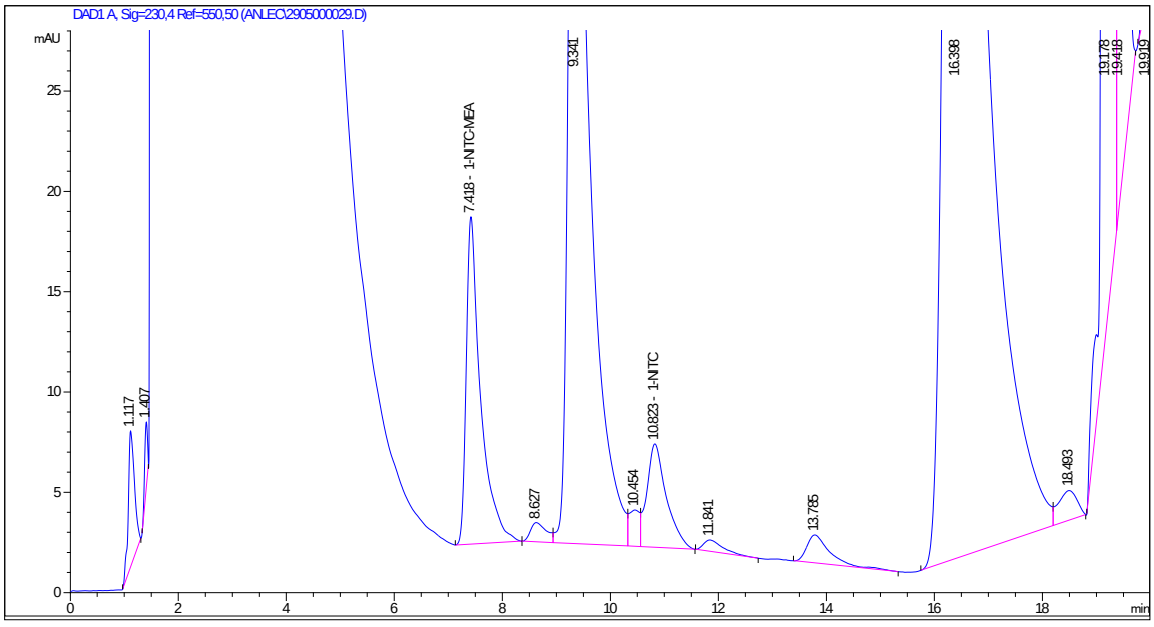

Figure B.6. Sample extracted with dimethylformamide

Table B.2. Results of ACN Re-extraction Tests.

Sample	Initial Concentration ($\mu g\ ml^{-1}$)	Re-extract Concentration ($\mu g\ ml^{-1}$)	Ratio Re-extract/Initial
688/1 Front	1.398	0.699	0.500
691/2 Front	1.527	0.779	0.511

- The OSHA method assessed tube recovery or desorption efficiency by spiking tubes with MEA then leaving them overnight and extracting them the next day. The method of spiking is not clear but presumed to be by liquid injection. Desorption into the DMF occurred over "30 minutes with occasional shaking". Six replicate tubes were spiked with 161.8, 80.9, 40.45 and 16.18 µg of MEA and the recoveries ranged from 95% to 103% with an average of 100% with a standard deviation of ±2.0%. However the levels of MEA recovered in this work have been around 1-4 µg for the tube front sections (<1 µg for the tube rear sections) which is of an order of magnitude less than the OSHA lowest levels. Levin *et al.* (1989) also measured recovery of liquid spiked tubes but passed 5 litres of air at either 20% or 85% humidity through the tubes after spiking them. Their spiking levels were 80, 40 and 4 µg of MEA and desorption was with ACN with 30 minutes of shaking then standing overnight. They report recoveries of 92-97% for the 40 and 80µg samples but only 75% for the 4 µg samples. This seems to correlate with the results achieved in this work, where recoveries of spiked tube samples have often been below 80%. There is the suggestion that a certain small amount of MEA may be irreversibly absorbed on the XAD-2 leading to low recoveries at low concentrations but not being significant at higher levels.

Sampling Time and Extraction Variables

- Longer sampling times, at the reduced flow rate, were considered as a way to increase the total amount of MEA adsorbed on the tubes and decrease the recovery error. Other extraction variables that were considered as possible contributions to the low recoveries were temperature of extraction, time allowed for desorption and the material used to filter the extracted solution. These were tested in a multivariable study with 8 tubes all sampled at virtually constant chamber conditions. Table B.3 gives the results for the sum of front and rear sections corrected for sampling time, temperature and pressure as ppbv in the chamber air.

- These results show, as mentioned before, that DMF (samples 4 and 5) gives poor results with our analytical system compared to ACN as the extraction solvent. It is also clear that sampling for 90 minutes (samples 6-8) gives slightly lower results than sampling for 60 minutes (samples 1-3). Samples 2 and 3 and samples 6 and 7 show the effect of extraction temperature. The higher extraction temperature of 40°C gave results that were slightly lower, ~3.6% lower, which is probably at or within the error of measurement. The effect of doubling the extraction time also seems to have a slight negative effect if sample 1 and 2 are compared and also samples 7 and 8 but again this is similar to the error of measurement. It is a little harder to deduce the effect of the filter material but the results indicate very little difference and if anything that nylon gives slightly higher results than PTFE which would be unlikely.

Table B.3. Effect of Sampling Time and Extraction Factors on the Concentration of MEA.

Sample #	Sample Time (min)	Extraction Solvent	Extraction Temp (°C)	Extraction Time (hrs)	Filter Material[1]	MEA Conc[2] (ppbv)
1	60	ACN	Room[3]	~42	PTFE	340
2	60	ACN	Room[3]	~20	Nylon	353
3	60	ACN	40°	~20	Nylon	340
4	60	DMF	Room[3]	~20	PTFE	223
5	90	DMF	Room[3]	~20	Nylon	267
6	90	ACN	40°	~20	PTFE	318
7	90	ACN	Room[3]	~20	PTFE	330
8	90	ACN	Room[3]	~42	Nylon	304

1. Both filters were 4mm diameter
2. Corrected for sampling time, temperature and pressure to 25°C and 760 mm Hg.
3. Daily maxima ≤20°C and minima ≥7°C.

- Despite the work done here recoveries of NITC-MEA from spiked samples remains variable, from 60-90%, which adds uncertainty to the measurements. One factor not examined so far is the role of humidity in the sampled air. All the samples taken in this work have been taken at very low humidity levels (<5%). The OSHA method is for sampling atmospheric air where the lowest humidity levels would be expected to be at least 20%. OSHA and Levin both describe tests on spiked tubes where humid air is drawn through the tubes, to show that the NITC-MEA is retained on the tubes but neither tests their methods with real samples in dry air. The effect of humidity on the adsorption of MEA and reaction with the 1-NITC on the XAD-2 should be examined.

B.2 Diethanolamine (DELA) using *in-situ* NITC derivatisation

An NITC method for determination of diethanolamine (DELA) is based on similar principles to that for analysis of MEA as outlined in OSHA method PV2018 (1988). This method has been only partially validated and provides some guidance. DELA was investigated for its analytical and instrumental efficiency using protocols as described for MEA, above. The full description of the development of the method for simultaneous determination of DELA using HPLC is therefore not repeated, but is available on request.

It has been confirmed that DELA can be readily derivatised with 1-NITC when dissolved in ACN and separated by reversed phase HPLC on a C8 column with a solvent mix of 30% ACN in water at a flow of 1.5 ml min^{-1}. The NITC-DELA derivative gave UV absorptions at λ_{max} = 220 nm with ε_{max} = 1933 L mol^{-1} cm^{-1} and a less intense peak at λ_{max} = 278 nm. The derivative elutes slightly later than the MEA derivative indicating they can be distinguished and quantified with the current system with the limitation that major concentration differences may impact on the accuracy of peak integration. An instrument detection limit of ~0.1 µg mL^{-1} has been estimated.

The validation of the method for gas phase chamber sampling was not within the scope of this project and the retention and desorption efficiency associated with this aspect of the methodology should be assessed before its implementation for DELA analysis.

B.3 Piperazine analysis using *in-situ* NITC derivatisation

An investigation of the analysis of piperazine concentration in the experimental chamber by *in-situ* derivatisation using 1-naphthylisothiocyanate (NITC) during sampling and measurement by HPLC was carried out. The method is based on the US OSHA in-house method for determining piperazine in ambient air, which to date is not validated and provides no details of the sampling parameters or analysis conditions. The method uses an adsorbent tube followed by HPLC analysis. The initial investigation followed an identical method to that used for MEA, as described above, using reversed-phase HPLC, and later a normal-phase HPLC condition was tested using dimethylformamide (DMF) as the desorption solvent. The latter is used by OSHA in their methods for MEA (PV2111), diethanolamine (PV2018) and aminomethylpropanol (PV2145).

In-situ derivatisation was performed by drawing gas from the experimental chamber through a sampling tube containing in 10% NITC on a polystyrene XAD-2 adsorbent (SKC Incorporated). The sampling flow rate was ~0.05 litres min^{-1} and the sampling time was ~60 minutes based on the work for MEA sampling.

The initial tube desorption followed the method used for MEA and the analysis system was identical except the solvent mix and flow rate was optimised for a piperazine-NITC standard. Analysis of initial piperazine samples, and also the blank, showed a doublet peak that interfered with the quantitation of small piperazine derivative peaks and the peak heights of the standards seemed low indicating poor sensitivity. Efforts were made to separate the interfering peaks from the piperazine peak but these were unsuccessful. The OHSA method was then investigated using a Zorbax Eclipse XDB-CN column (4.6 mm id x 250 mm, 5 µm). An isocratic isopropanol/isooctane mobile phase regime was used. It was found that while piperazine and NITC are both soluble in acetonitrile the derivative crystallises out from the mixture. The derivative is soluble in DMF, however DMF has a strong absorption in the low UV and the piperazine-NITC peak elutes on its tail. Samples were analysed using this method but a loss of peak height was observed over ~24 hour period.

Direct communication with OSHA has confirmed that they now use reversed-phase HPLC with an acetonitrile/water solvent. This method would require significant further development.

B.4 Nitroaminoethanol using underivatised and derivatised collection and HPLC analysis

An investigation was carried out to determine if 2-nitroaminoethanol (NAE) could be detected directly by HPLC without derivatisation and, if detected, to assess if it could be efficiently collected and quantified in chamber samples by HPLC. Additionally, whether *in-situ* derivatisation could be used for its determination was investigated.

The results clearly showed that underivatised NAE (Toronto Research Chemicals Incorporated and Chiron AS) was sufficiently chromaphoric and could be easily resolved and detected at concentrations down to ~0.2 µg ml^{-1} in standard solution by the HPLC system (absorption peak at λ_{max} = 230 nm and ε_{max} =

800 L mol^{-1} cm^{-1}). However the results from its collection onto, and desorption from, Florisil sorbent cartridges found poor recoveries, typically < 45%, indicating its adsorption or reaction with the collection media. A further series of tests could be performed with other more polar solvents to see if better recoveries could be obtained, however it is recommended that a different adsorbent be considered.

Other polar compounds present in samples collected from chamber experiments also interfered with the resolution of NAE, under the chromatographic parameters used. The retention time of NAE was very close to the injection pulse on a C8 column using ACN/THF/water phase, indicating that NAE is not retained under the current column and mobile phase system. Obviously the use of a more polar column, or one of different functionality, such as a CN column, would afford better retention and hence separation. The non-linear nature of the calibration standards may also be improved with better separation of polar components.

Tests were also undertaken to determine if derivatisation using NITC (using amine functionality) or DNPH (using NO_2 functionality) would be possible for this compound. Certain publications have indicated that DNPH is a possible agent (Nielson *et al.* 2010) however their methodology was not explained. Derivatised standard solutions were prepared and gas phase chamber collections were also examined. However, derivatisation was not successful using either agent under the various sampling and analytical conditions used.

From the investigation made, it is concluded that NAE was not observable in samples from chamber experiments using HPLC analysis.

Appendix C MEA+NOx Gas and Aerosol Profiles

MEA and NOx (18 to 24 ppbv) experiments (refer to Table 2)

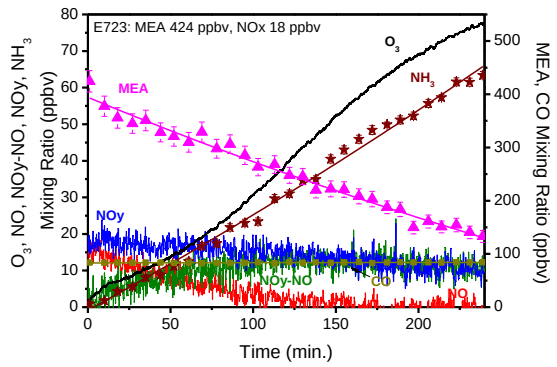

Figure C.1a. UV gas-phase profiles E723

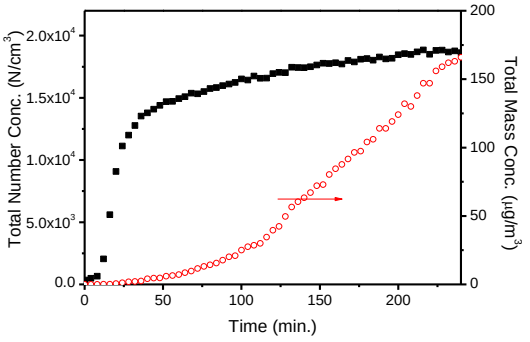

Figure C.1b. UV aerosol profile E723

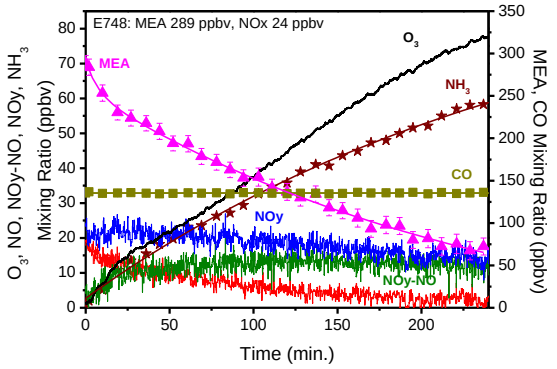

Figure C.2a. UV gas-phase profiles E748

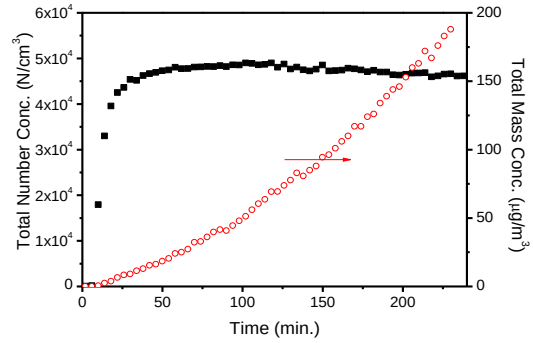

Figure C.2b. UV aerosol profile E748

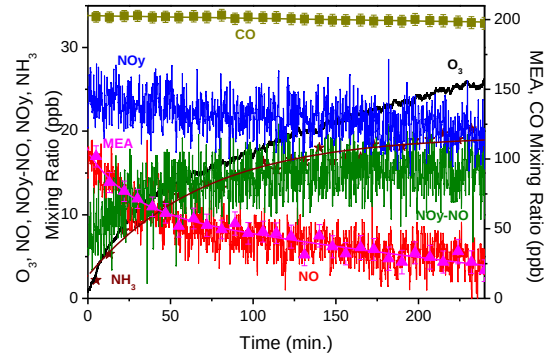

Figure C.3a. UV gas-phase profiles E746

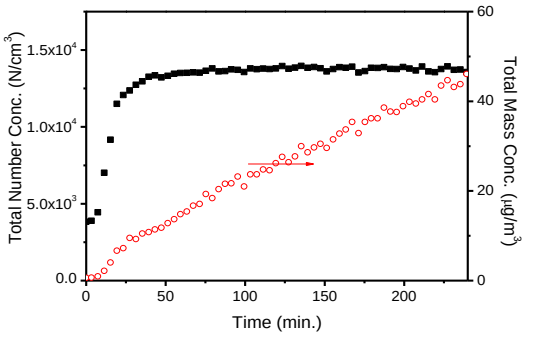

Figure C.3b. UV aerosol profile E746

MEA and NOx (43 to 49 ppbv) experiments (refer to Table 2)

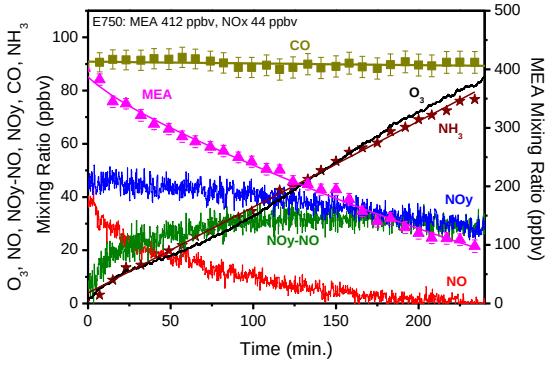

Figure C.4a. UV gas-phase profiles E750

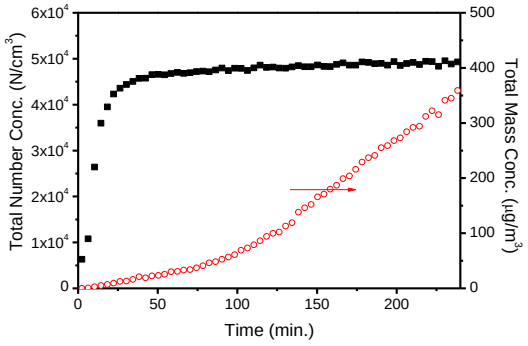

Figure C.4b. UV aerosol profile E750

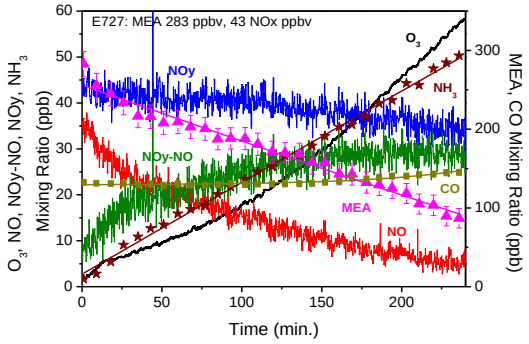

Figure C.5a. UV gas-phase profiles E727

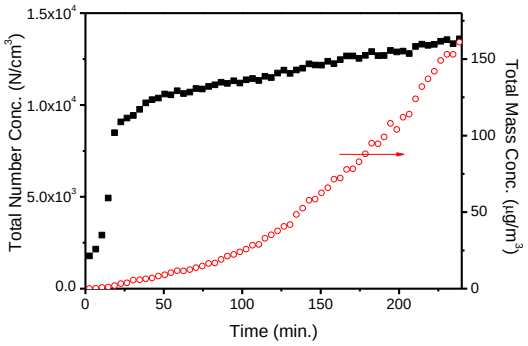

Figure C.5b. UV aerosol profile E727

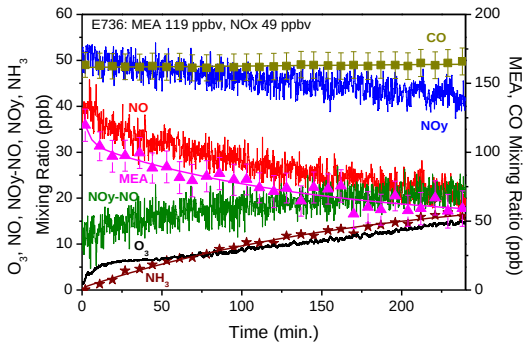

Figure C.6a. UV gas-phase profiles E736

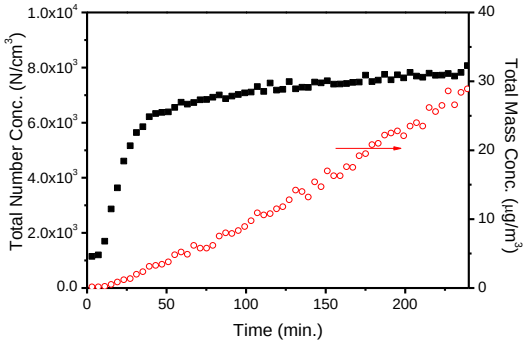

Figure C.6b.: UV aerosol profile E736

MEA and NOx (91 to 100 ppbv) experiments (refer to Table 2)

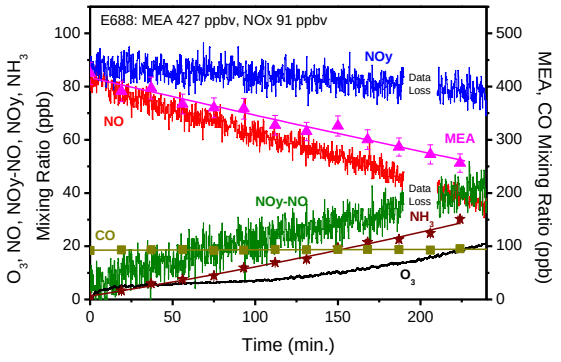

Figure C.7a. UV gas-phase profiles E688

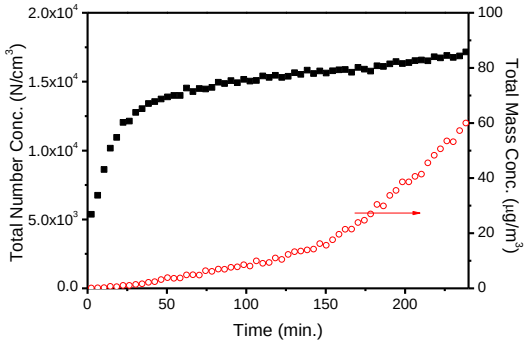

Figure C.7b. UV aerosol profile E688

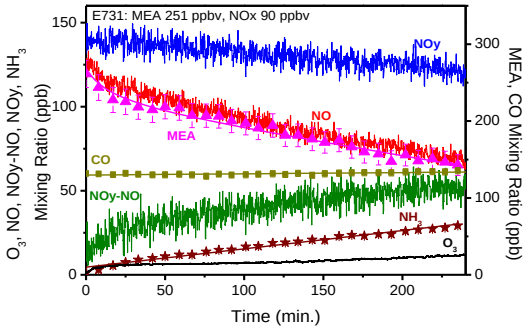

Figure C.8a. UV gas-phase profiles E731

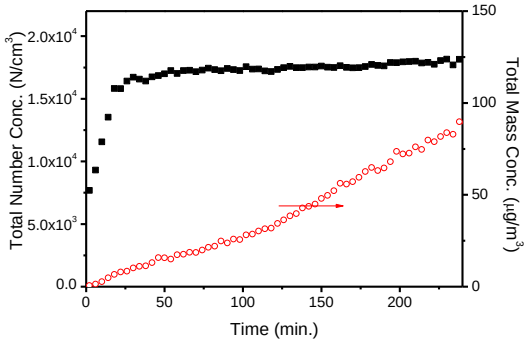

Figure C.8b. UV aerosol profile E731

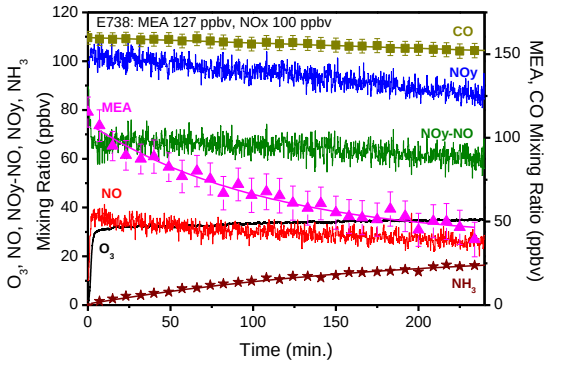

Figure C.9a. UV gas-phase profiles E738

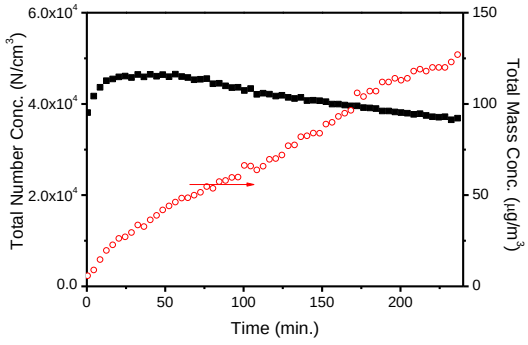

Figure C.9b. UV aerosol profile E738

MEA and NOx (~140 ppbv) experiments (refer to Table 2)

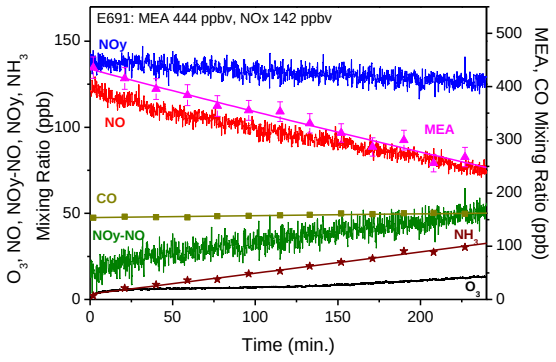

Figure C.10a. UV gas-phase profiles E691

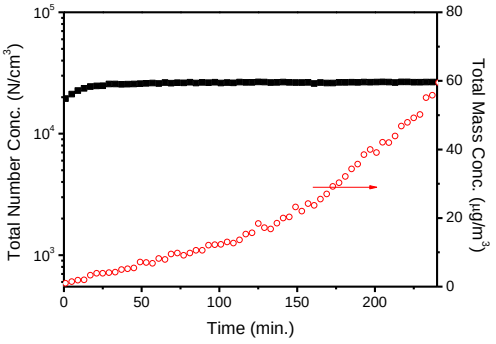

Figure C.10b. UV aerosol profile E691

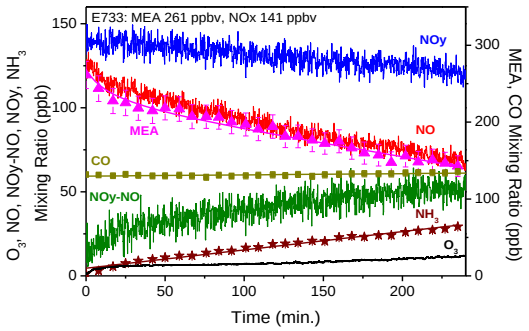

Figure C.11a. UV gas-phase profiles E733

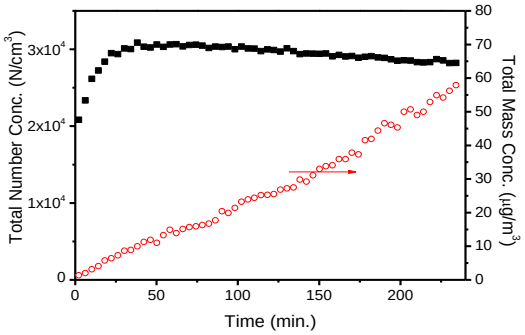

Figure C.11b. UV aerosol profile E733

MEA and NOx (463 ppbv) experiment (refer Table 2)

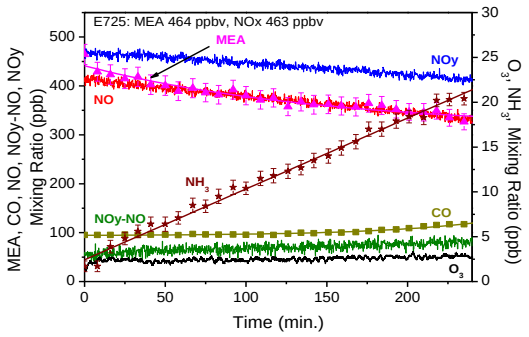

Figure C.12a. UV gas-phase profiles E725

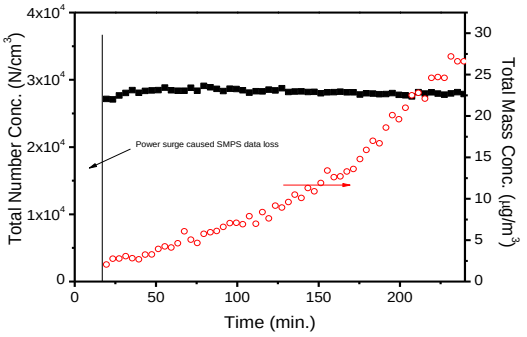

Figure C.12b. UV aerosol profile E725

Appendix D Modelling Results

The chemical mechanism results for the twelve MEA/NOx experiments in Table 10 are shown in Figures D.1 through D.12. Four major gas phase species (MEA, $CHONH_2$, NH_3 and HCHO), the $\Delta(O_3\text{-}NO)$ factor and aerosol predictions are shown for mechanisms which predict those products explicitly. The experiments are ordered by initial MEA/NOx ratio, with the high initial NO_2 experiment (E738) included at the end.

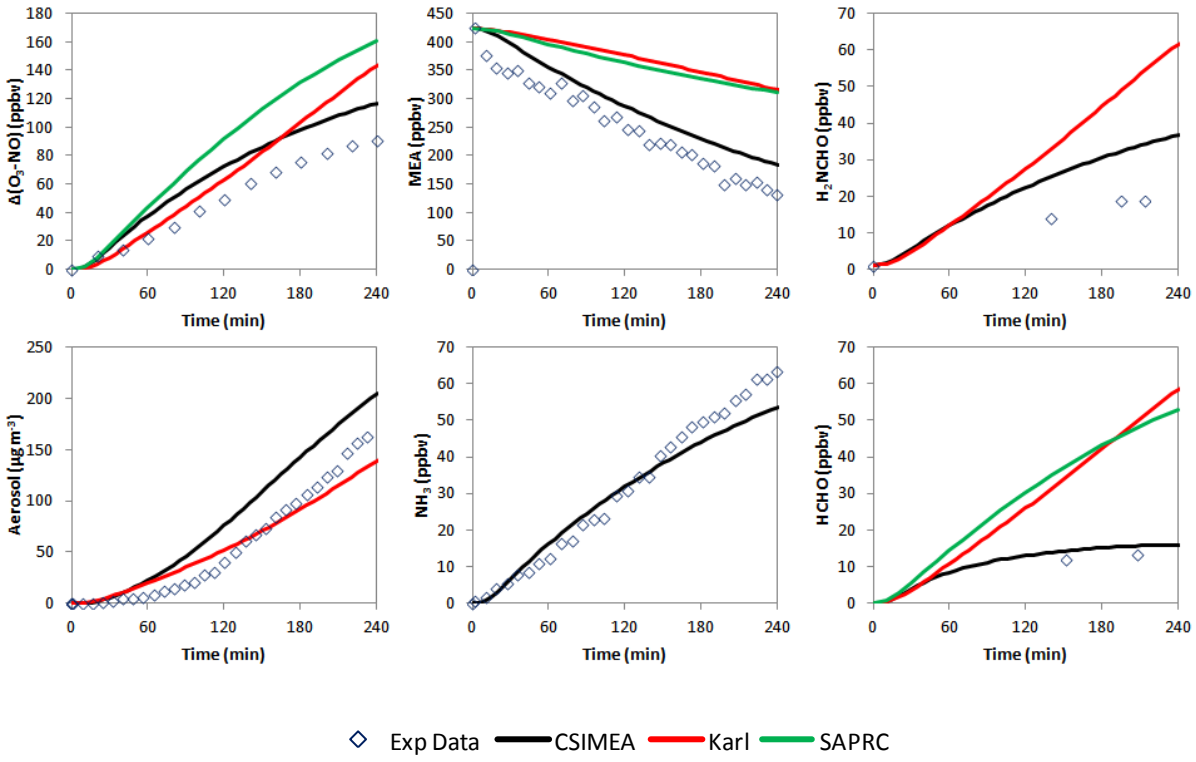

Figure D.1. Comparison of key species between CSIMEA, Karl and SAPRC-07 mechanisms for E723

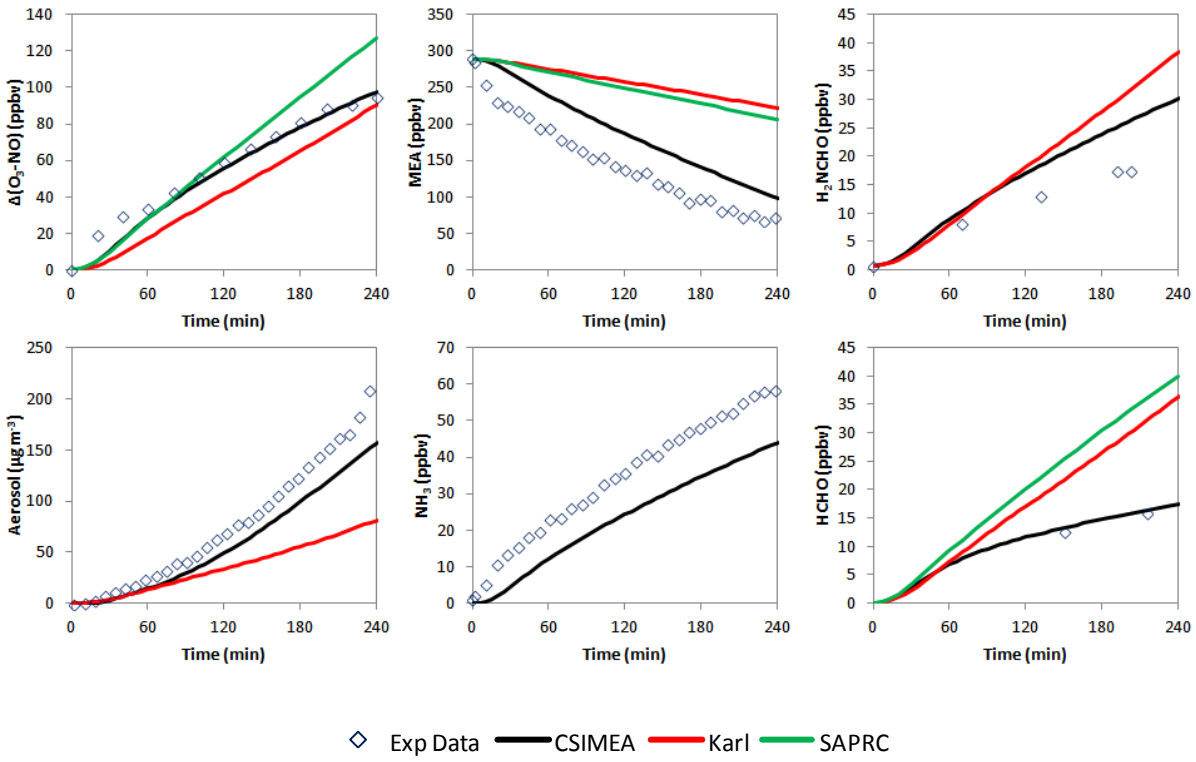

Figure D.2. Comparison of key species between CSIMEA, Karl and SAPRC-07 mechanisms for E748

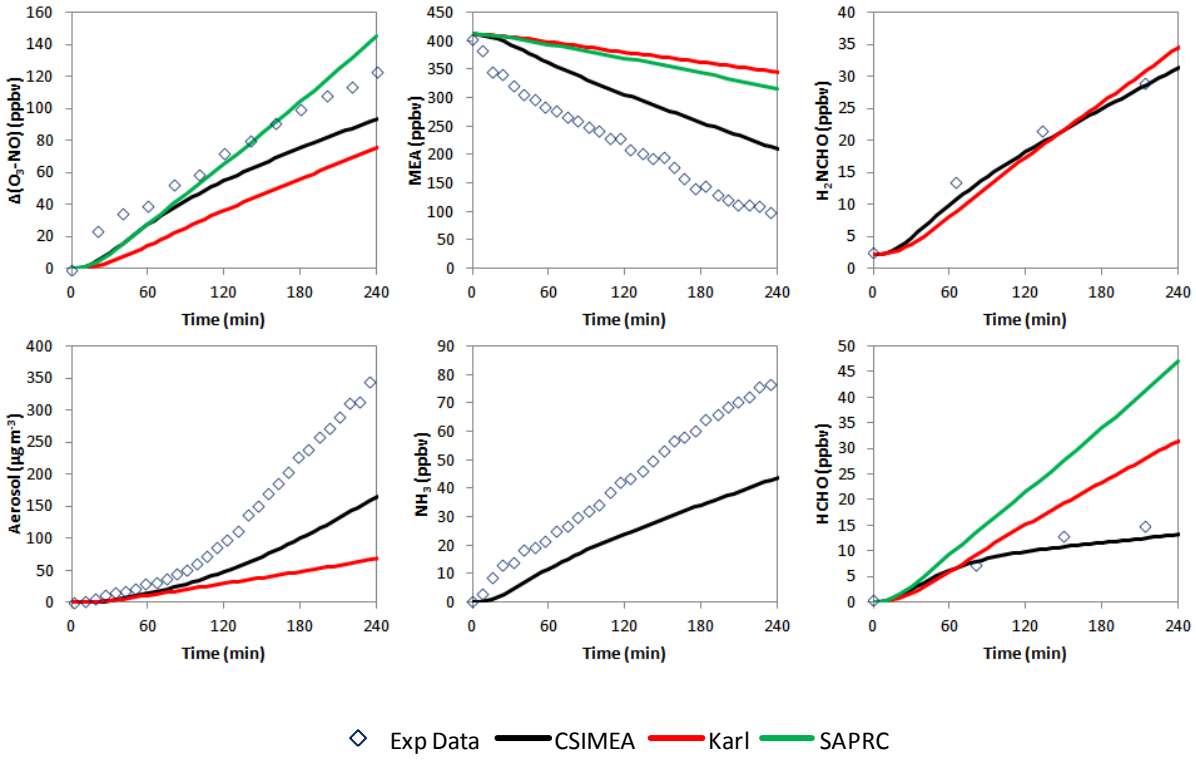

Figure D.3. Comparison of key species between CSIMEA, Karl and SAPRC-07 mechanisms for E750

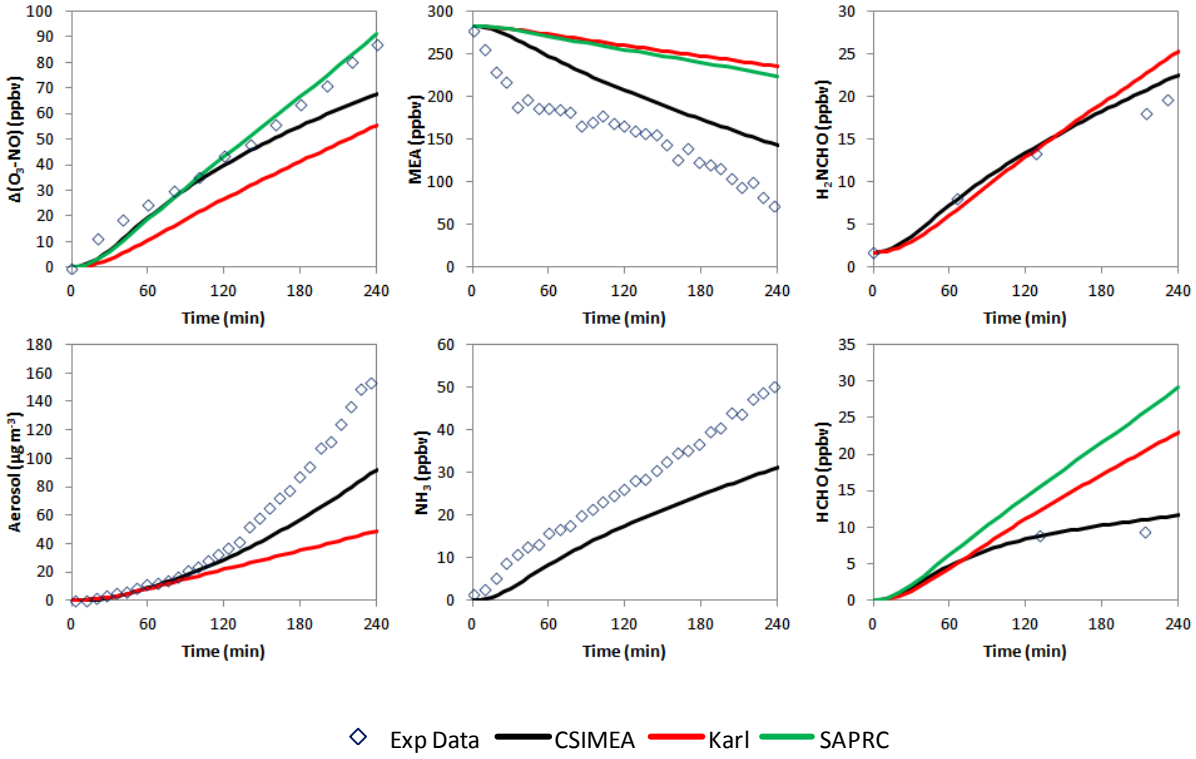

Figure D.4. Comparison of key species between CSIMEA, Karl and SAPRC-07 mechanisms for E727

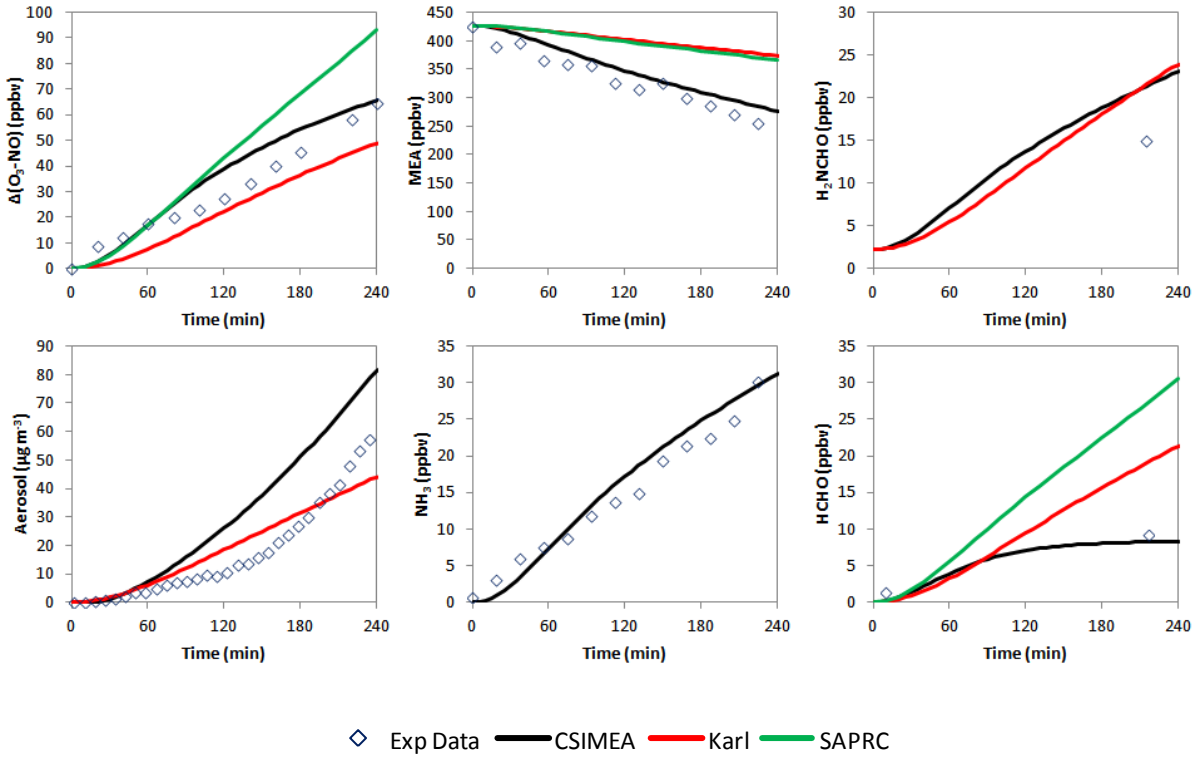

Figure D.5. Comparison of key species between CSIMEA, Karl and SAPRC-07 mechanisms for E688

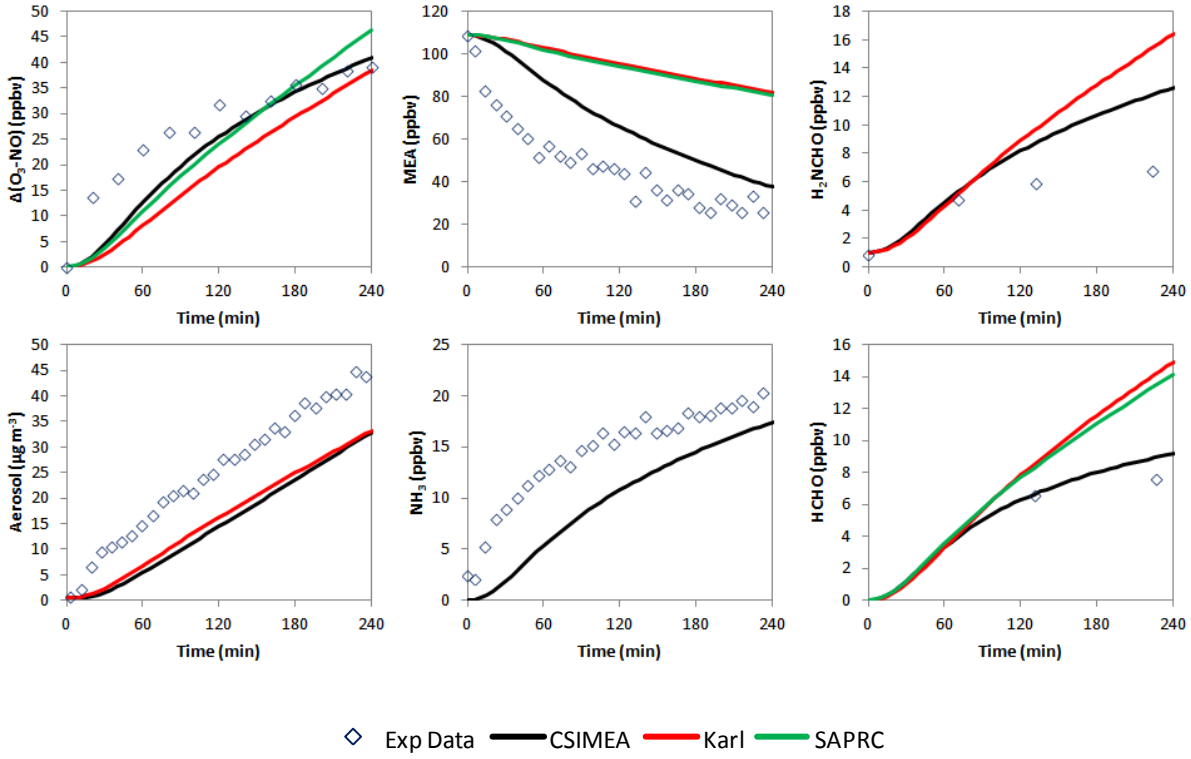

Figure D.6. Comparison of key species between CSIMEA, Karl and SAPRC-07 mechanisms for E746

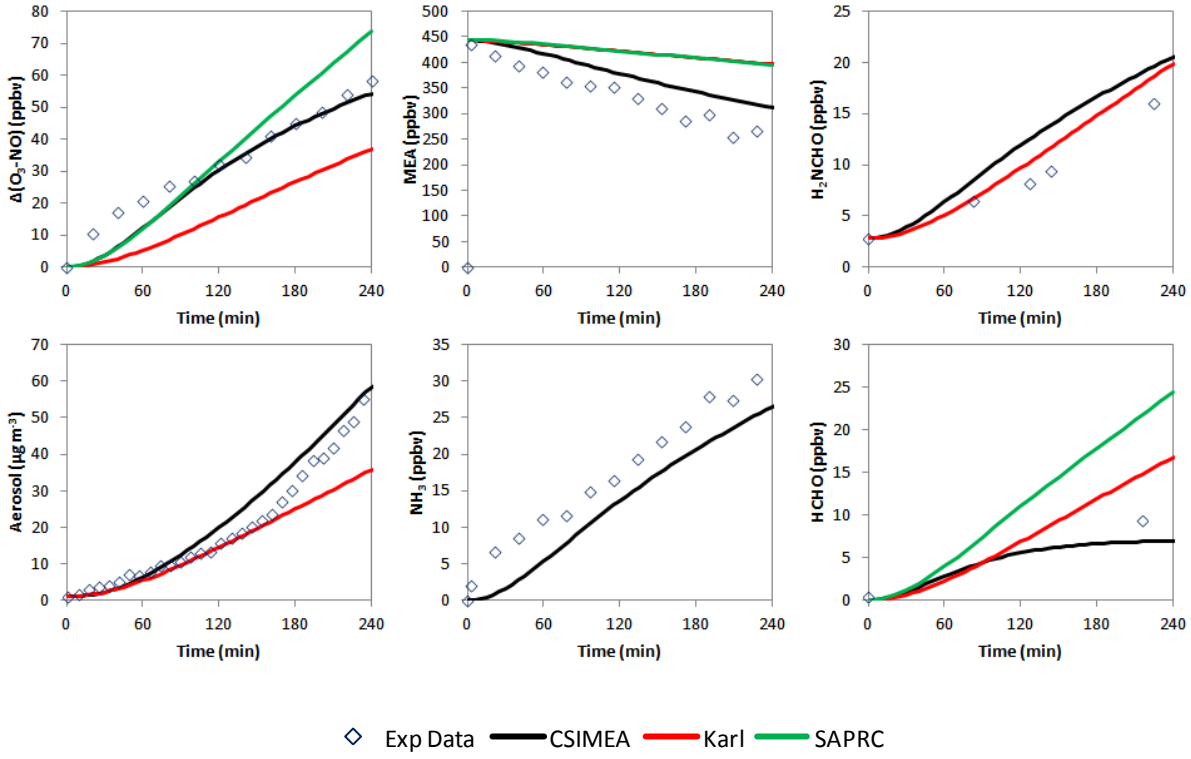

Figure D.7. Comparison of key species between CSIMEA, Karl and SAPRC-07 mechanisms for E691

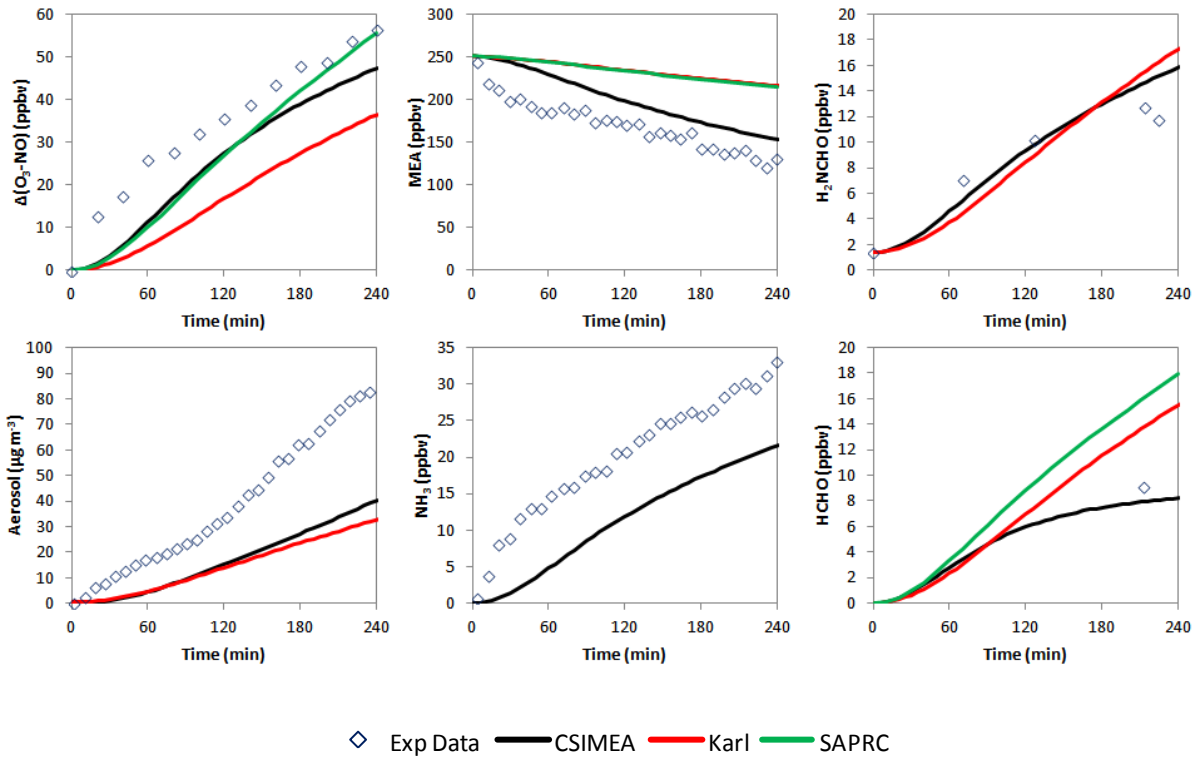

Figure D.8. Comparison of key species between CSIMEA, Karl and SAPRC-07 mechanisms for E731

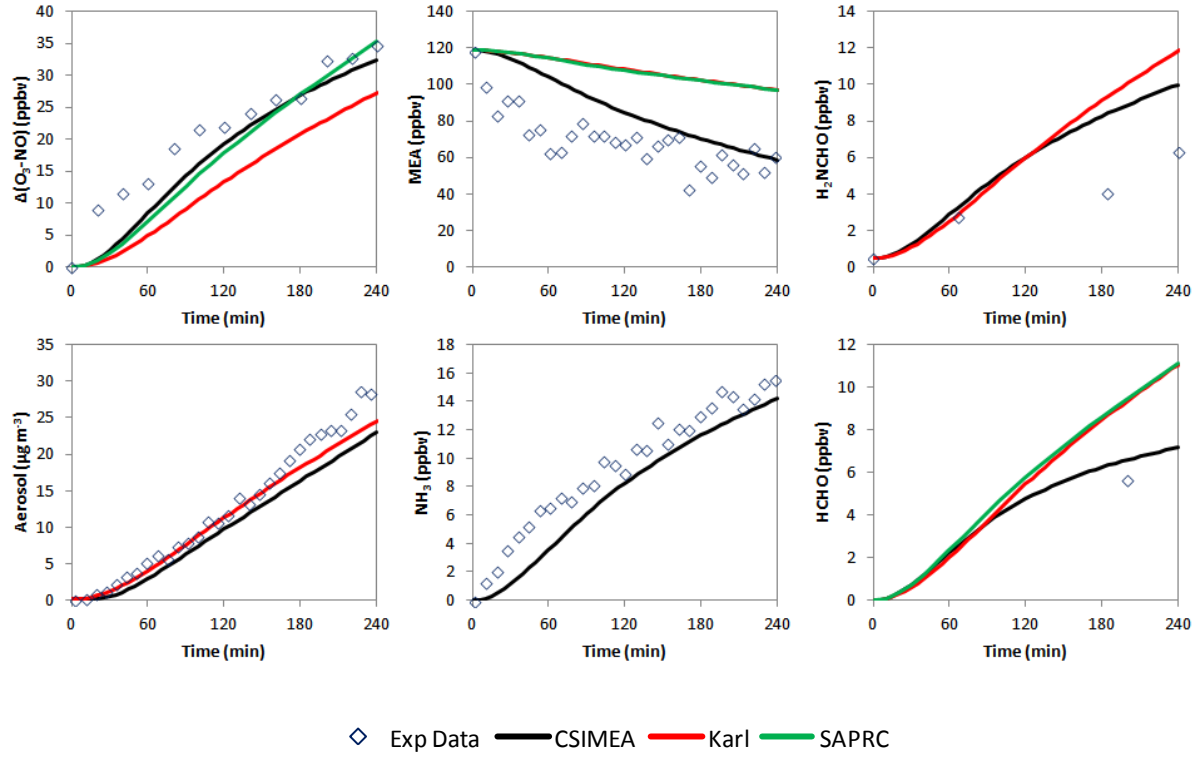

Figure D.9. Comparison of key species between CSIMEA, Karl and SAPRC-07 mechanisms for E736

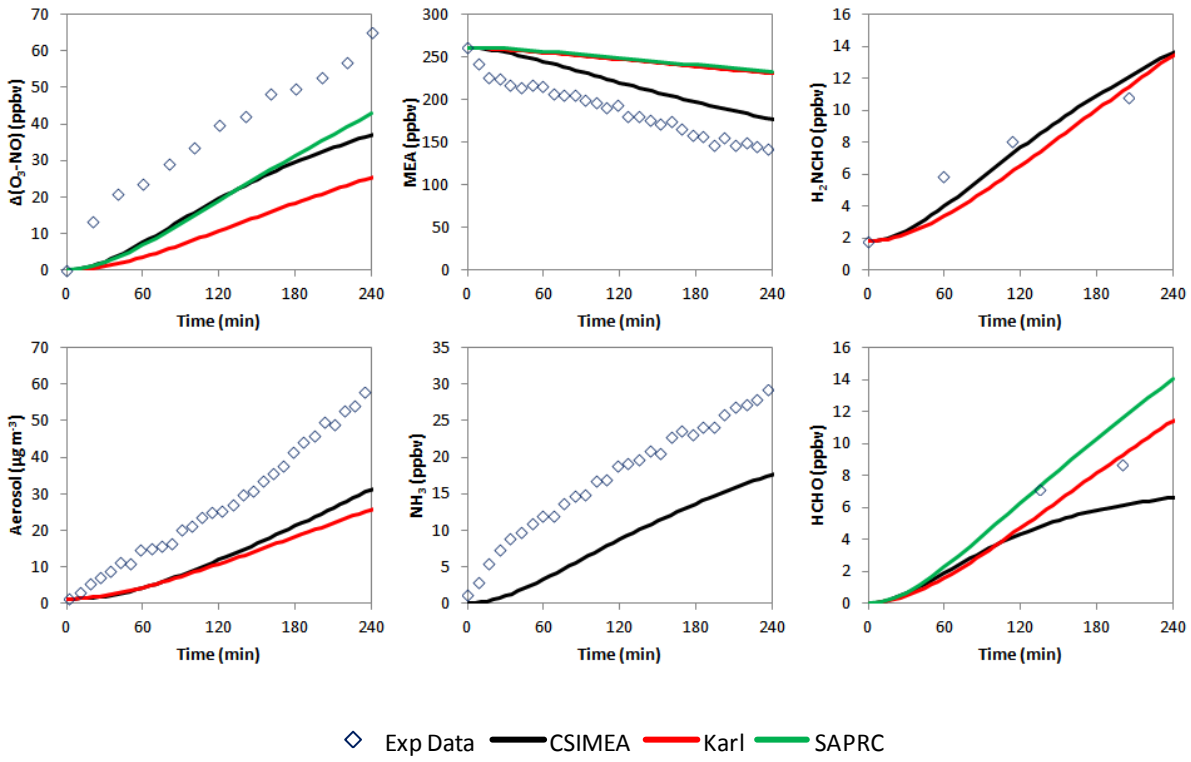

Figure D.10. Comparison of key species between CSIMEA, Karl and SAPRC-07 mechanisms for E733

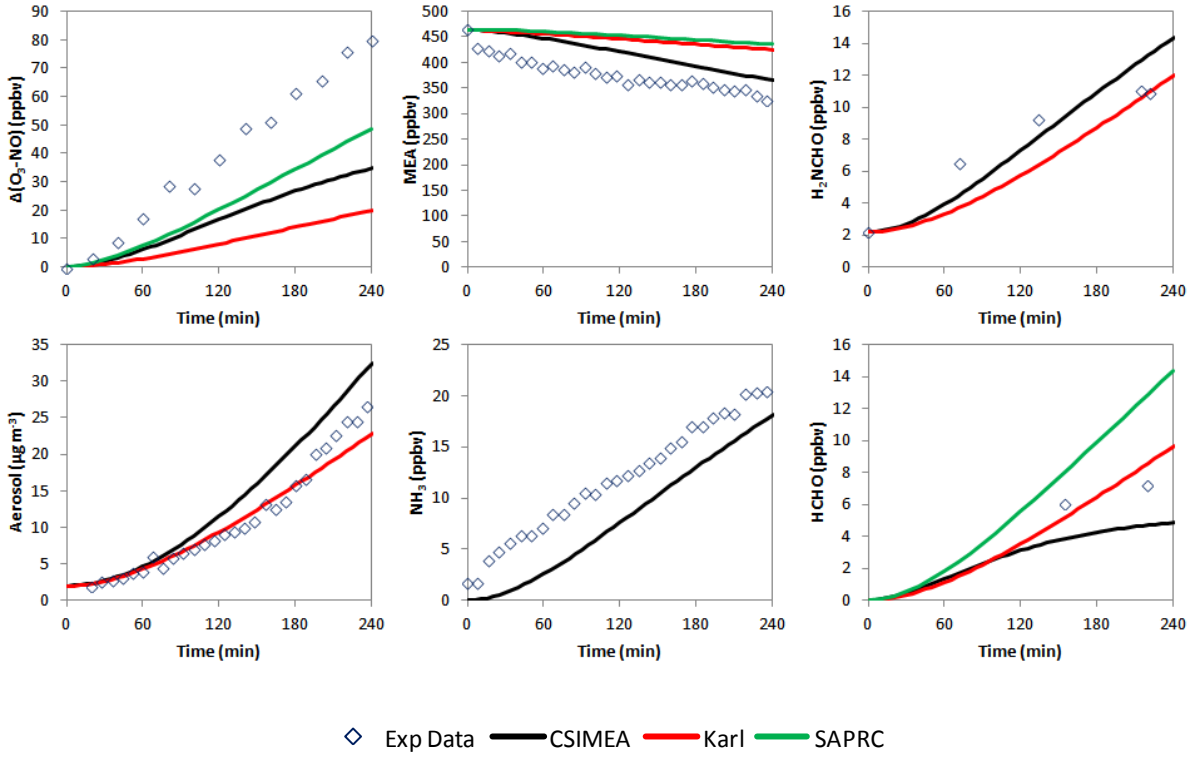

Figure D.11. Comparison of key species between CSIMEA, Karl and SAPRC-07 mechanisms for E725

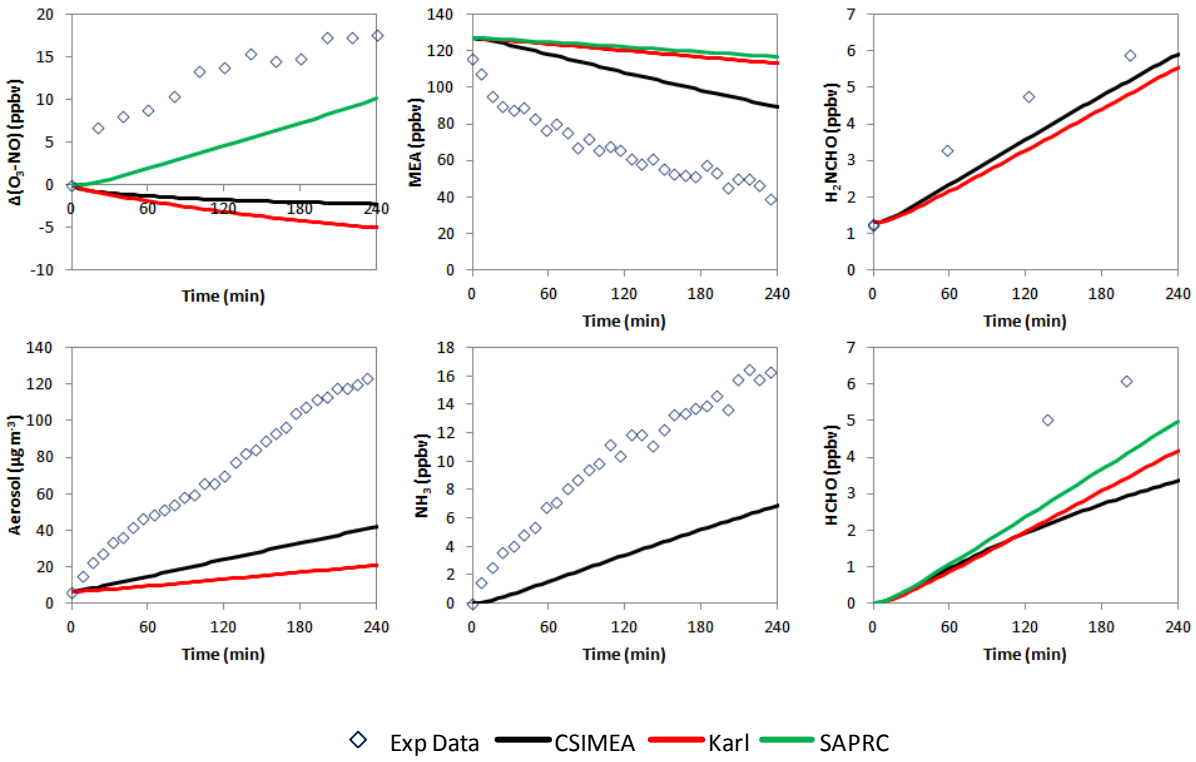

Figure D.12. Comparison of key species between CSIMEA, Karl and SAPRC-07 mechanisms for E738

References

Angove, D., Azzi, M., Tibbett, A., White, S., Cope, M., Lee, S. (2010a). *Investigation of the Atmospheric Photochemistry of the CO_2 Capture Solvent, Monoethanolamine (MEA) Under Controlled Conditions. Final Report for Norsk Energi and Gassnova.* CSIRO EP101723, Final Report to Norsk Energi and Gassnova.

Angove, D., Jackson, P., Lambropoulos, N., Azzi, M., Attalla, M. (2010b). *CO_2 Capture Mongstad – Project B: Theoretical evaluation of the potential to form and emit harmful compounds; Task 2: Atmospheric Chemistry. Final Report to Gassnova.* CSIRO. Available at: http://www.gassnova.no/co2-capture-storage/results-from-the-first-studies-of-the-health-and-environmental-issues-of-amines-used-in-co2-capture/. [Accessed 13 May 2013].

Angove, D., Azzi, M., Tibbett, A., Campbell, I. (2012). An Investigation into Photochemistry of Monoethanolamine (MEA) in NOx. In: Attalla, M. ed. *Recent Advances in Post-Combustion CO_2 Capture Chemistry.* ACS Symposium Series **1097**, 265-273. American Chemical Society: Washington, DC, 2012.

Barnes, I., Solignac, G., Mellouki, A., Becker, K.H. (2010). Aspects of the Atmospheric Chemistry of Amides. *ChemPhysChem*, **11** 3844-3857.

Bergmann, E.D., Gil-Av, E., Pinchas, S. (1953). The Structure of the Products of Condensation between primary β-Hydroxyamines and Aliphatic Carbonyl Compounds. *Journal of the American Chemical Society,* **75** 358-361.

Bergmann, E.D. (1953). The Oxazolidines. *Chemical Reviews*, **53** 309-352.

Borduas, N., Abbatt, J.P.D., Murphy, J.G. (2013). Gas Phase Oxidation of Monoethanolamine (MEA) with OH Radical and Ozone: Kinetics, Products, and Particles. *Environmental Science and Technology* **47** 6377-6383.

Bråten, H.B., Bunkan, A.J., Bache-Andreassen, L., Solimannejad, M., Nielsen, C.J. (2009). *Final report on a theoretical study on the atmospheric degradation of selected amines.* Kjeller, Norwegian Institute for Air Research (NILU), NILU OR 77/2008.

Carter, W.P.L. (2008). *Reactivity estimates for selected consumer product compounds. Final Report to the California Air Resources Board, Contract No. 06-408.* Available at: http://www.cert.ucr.edu/~carter/absts.htm. [Accessed 13 May 2013]

Carter, W.P.L. (2013). SAPRC Atmospheric Chemical Mechanisms and VOC Reactivity Scales. http://www.engr.ucr.edu/~carter/SAPRC/. [Accessed 13 May 2013].

Carter, W.P.L., Heo, G. (2013). Development of a revised SAPRC aromatics mechanism. *Accepted for publication in Atmospheric Environment*.

da Silva, G. (2012). Atmospheric Chemistry of 2-Aminoethanol (MEA): Reaction of NH_2•$CHCH_2OH$ Radical with O_2. *The Journal of Physical Chemistry A*, **116** 10980-10986.

da Silva, G., Kirk, B.B., Lloyd, C., Trevitt, A.J., Blanksby, S.J. (2012). Concerted HO_2 Elimination from α-Aminoalkylperoxyl Free Radicals: Experimental and Theoretical Evidence from the Gas-Phase NH_2•$CHCO_2^-$ + O_2 Reaction. *The Journal of Physical Chemistry Letters*, **3** 805-811.

Finlayson-Pitts, B. J., Pitts, J.N. (2000). *Chemistry of the Upper and Lower Atmosphere*, Academic Press, California, p969.

Gafarov, A.N., Punegova, L.N., Loginova, E.I., Novikov, S.S., Titov, N.K. (1978). Condensation of monoethanolamine with formaldehyde. *Bulletin of the Academy of Sciences of the USSR, Division of Chemical Science*. **27** 1938.

Ge, X., Wexler, A.S., Clegg, S.L. (2011). Atmospheric amines – Part II. Thermodynamic properties and gas/particle partitioning. *Atmospheric Environment*, **45** 561-577.

Gouedard, C., Picq, D., Launay, F., Carrette, P.-L. (2012). Amine degradation in CO_2 capture. I. A Review. *International Journal of Greenhouse Gas Control*, **10** 244-270.

Hanst, P.L., Spence, J.W., Miller, M. (1977). Atmospheric Chemistry of N-Nitroso Dimethylamine. *Environmental Science and Technology*, **11** 403-405.

Hynes, R.G., Angove, D.E., Saunders, S.M., Haverd, V., Azzi, M. (2005). Evaluation of two MCM v3.1 alkene mechanisms using indoor environmental chamber data. *Atmospheric Environment*, **39** 7251-7262.

Jenkin, M.E., Saunders, S.M., Pilling, M.J. (1997). The tropospheric degradation of volatile organic compounds: a protocol for mechanism development. *Atmospheric Environment*, **31** 81-104.

Johnson, G.M. (1983). Factors affecting oxidant formation in Sydney air. In: Carras, J.N., Johnson, G.M. eds. *The Urban Atmopshere – Sydney, a Case Study*. CSIRO, Melbourne. pp. 393-408.

Karl, M., Dye, C., Schmidbauer, N., Wisthaler, A., Mikoviny, T., D'Anna, B., Müller, M., Borrás, E., Clemente, E., Muñoz, A., Porras, R., Ródenas, M., Vásquez, M., Brauers, T. (2012). Study of OH-initiated degradation of 2-aminoethanol. *Atmospheric Chemistry and Physics*, **12** 1881-1901.

Kwok, E.S.C., Atkinson, R. (1995). Estimation of hydroxyl radical reaction rate constants for gas-phase organic compounds using a structure-reactivity relationship: An update. *Atmospheric Environment*, **29** 1685-1695.

Lazarou, Y.G., Kambanis, K.G., Papagiannakopoulos, P. (1994). Gas-Phase Reactions of $(CH_3)_2N$ Radicals with NO and NO_2. *Journal of Physical Chemistry*, **98** 2110-2115.

Lee, D., Wexler, A.S. (2013). Atmospheric amines – Part III: Photochemistry and toxicity. *Atmospheric Environment*, **71** 95-103

Lee, S.-B., Bae, G.-N., Moon, K.-C. (2009). Smog Chamber Measurements. In: Kim, Y.J., Platt, U., Gu. M.B., Iwahashi, H. eds *Atmospheric and Biological Environmental Monitoring*. pp. 105-136. Springer Netherlands.

Levin, J.O., Andersson K., Hallgren C. (1989). Determination of monoethanolamine and diethanolamine in air. *Annals of Occupational Hygiene*, **33**(*2*) 175-180.

Lindley, C.R.C., Calvert, J.G., Shaw, J.H. (1979). Rate studies of the reactions of the $(CH_3)_2N$ radical with O_2, NO, and NO_2. *Chemical Physics Letters*, **67** 57-62.

Magneron, I., Mellouki, A., Le Bras, G., Moortgat, G.K., Horowitz, A., Wirtz, K. (2005). Photolysis and OH-initiated Oxidation of Glycolaldehyde under Atmospheric Conditions. *Journal of Physical Chemistry A,* **109** 4552-4561.

Malloy, Q.G.J., Qi. L., Warren, B., Cocker III, D.R., Erupe, M.E., Silva P.J. (2009). Secondary organic aerosol formation from primary aliphatic amines with NO_3 radical. *Atmospheric Chemistry and Physics* **9** 2051-2060.

Murphy, S.M., Sorooshian, A., Kroll, J.H., Ng, N.L., Chhabra, P., Tong, C., Surratt, J.D., Knipping, E., Flagan, R.C., Seinfeld, J.H. (2007). Secondary aerosol formation from atmospheric reactions of aliphatic amines. *Atmospheric Chemistry and Physics* **7** 2313-2337.

Nielsen, C.J., D'Anna, B., Dye, C., George, C., Graus, M., Hansel, A., Karl, M., King, S., Musabila, M., Müller, M., Schmidbauer, N., Stenstrøm, Y., Wisthaler, A. (2010). *Atmospheric Degradation of amines (ADA); Summary report: Gas-phase photo-oxidation of 2-aminoethanol (MEA)*. CLIMIT project no. 193438. Kjeller, Norwegian Institute for Air Research (NILU).

Nielsen, C.J., D'Anna, B., Karl, M., Aursnes, M., Boreave, A., Bossi, R., Bunkan, A.J.C., Glasius, M., Hallquist, M., Hansen, A.-M.K., Kristensen, K., Mikoviny, T., Maguta, M.M., Müller, M., Nguyen, Q., Westerlund, J., Salo, K., Skov, H., Stenstrøm, Y., Wisthaler, A. (2011a). *Atmospheric Degradation of Amines (ADA); Summary Report: Photo-Oxidation of Methylamine, Dimethylamine and Trimethylamine*. CLIMIT project no. 201604. Kjeller, Norwegian Institute for Air Research (NILU) OR 2/2011.

Nielsen, C.J., D'Anna, B., Dye, C., Graus, M., Karl, M., King, S., Maguto, M.M., Müller, M., Schmidbauer, N., Stenstrøm, Y., Wisthaler, A., Pederson, S. (2011b). Atmospheric chemistry of 2-aminoethanol (MEA). *Energy Procedia*, **4** 2245-2252.

Nielsen, C.J., Hermmann, H., Weller, C. (2012a). Atmospheric chemistry and environmental impact of the use of amines in carbon capture and storage (CCS). *Chemical Society Reviews*, **41** 6684-6704.

Nielsen, C.J., D'Anna, B., Bossi, R., Bunkan, A.J.C., Dithmer, L., Glasius, M., Hallquist, M., Hansen, A.M.K., Lutz, A., Salo, K., Maguta, M.M., Nguyen, Q., Mikoviny, T., Müller, M., Skov, H., Sarrasin, E., Stenstrøm, Y., Tang, Y., Westerlund, J., Wisthaler, A. (2012b). *Atmospheric Degradation of Amines (ADA); Summary report from atmospheric chemistry studies of amines, nitrosamines, nitramines and amides*. CLIMIT project no. 208122. Kjeller, Norwegian Institute for Air Research (NILU).

Odum, J.R., Hoffmann, T., Bowman, F., Collins, D., Flagan, R.C., Seinfeld, J.H. (1996). Gas/Particle Partitioning and Secondary Organic Aerosol Yields. *Environmental Science and Technology*, **30** 2580-2585.

Onel, L., Blitz, M.A., Seakins, P.W. (2012). Direct Determination of the Rate Coefficient for the Reaction of OH Radicals with Monoethanol Amine (MEA) from 296 to 510 K. *The Journal of Physical Chemistry Letters*, **3** 853-856.

Pitts, Jr., J.N., Grosjean, D., Van Cauwenberghe, K., Schmid, J.P., Fitz, D.R. (1978). Photooxidation of Aliphatic Amines Under Simulated Atmospheric Conditions: Formation of Nitrosamines, Nitramines, Amides, and Photochemical Oxidant. *Environmental Science and Technology*, **12**, 946-953.

Schade, G.W., Crutzen, P.J. (1995). Emission of Aliphatic Amines from Animal Husbandry and their Reactions: Potential source of N_2O and HCN. *Journal of Atmospheric Chemistry*, **22** 319-346.

Seinfeld, J. J., Pandis, S.N. (2006). *Atmospheric Chemistry and Physics: From Air Pollution to Climate Change (2nd Ed.)*, Wiley & Sons Inc., New Jersey, pp. 1203.

Silva, P. J., Erupe, M.E., Price, D., Elias, J., Malloy, Q.G.J., Li, Q., Warren, B., Cocker III, D.R. (2008). Trimethylamine as Precursor to Secondary Organic Aerosol Formation via Nitrate Radical Reaction in the Atmosphere. *Environmental Science and Technology*, **42** 4689-4696.

Singh-Peterson, L. (2007). *Modelling secondary organic aerosol formation: from chemical mechanistic modelling to empirical modelling*. PhD Thesis, University of New South Wales.

Tang, Y., Hanrath, M., Nielsen, C.J. (2012). Do primary nitrosamines form and exist in the gas phase? A computational study of CH_3NHNO and $(CH_3)_2NNO$. *Physical Chemistry Chemical Physics*, **14** 16365-16370.

Tang, X., Price, D., Praske, E., Lee, S.A., Shattuck, M.A., Purvis-Roberts, K., Silva, P.J., Asa-Awuku, A., Cocker III, D.R. (2013). NO_3 radical, OH radical and O_3-initiated secondary aerosol formation from aliphatic amines. *Atmospheric Environment*, **72** 105-112.

Tuazon, E.C., Carter, W.P.L., Brown, R.V., Atkinson, R., Winer, A.M., Pitts, Jr. J.N. (1982). *Atmospheric Reaction Mechanisms of Amine Fuels*. Statewide Air Pollution Research Center, University of California, Riverside.

Tuazon, E.C., Atkinson, R., Aschmann, S.M., Arey, J. (1994). Kinetics and products of the gas-phase reactions of O_3 with amines and related compounds. *Research of Chemical Intermediates*, **20** 303-320.

US Dept of Labor OSHA Method PV2018 (1987). Available at: http://www.osha.gov/dts/sltc/methods/partial/pv2018/2018.html [Accessed 22 May 2013]

US Dept of Labor OSHA Method PV2111 (1988). Available at: http://www.osha.gov/dts/sltc/methods/partial/t-pv2111-01-8803-ch/t-pv2111-01-8803-ch.html [Accessed 22 May 2013]

US Dept of Labor OSHA Method PV2145 (1992). Available at: http://www.osha.gov/dts/sltc/methods/partial/pv2145/pv2145.html [Accessed 22 May 2013]

US EPA Method TO-11A (1999). Available at: http://www.epa.gov/ttnamti1/files/ambient/airtox/to-11ar.pdf [Accessed 22 May 2013]

Wang H., Zhang X., Chen Z. (2009). Development of DNPH/HPLC method for the measurement of carbonyl compounds in the aqueous phase: applications to laboratory simulation and field measurement. *Environmental Chemistry*, **6** 389–397.

White, S.J., Azzi, M., Angove, D.E., Jamie, I.M., 2010. Modelling the photooxidation of ULP, E5 and E10 in the CSIRO smog chamber. *Atmospheric Environment*, **44** 5375-538.

Wirtz, K. (2005). El Centro de Estudios Ambientales del Mediterráneo (CEAM). Personal communication to RG Hynes.

Zhou X., Gu H., Civerolo K., Schwab J. (2009). Measurement of Atmospheric Hydroxyacetone, Glycolaldehyde, and Formaldehyde. *Environmental Science and Technology*, **43** 2753-2759.

CONTACT US

t 1300 363 400
+61 3 9545 2176
e enquiries@csiro.au
w www.csiro.au

YOUR CSIRO

Australia is founding its future on science and innovation. Its national science agency, CSIRO, is a powerhouse of ideas, technologies and skills for building prosperity, growth, health and sustainability. It serves governments, industries, business and communities across the nation.

FOR FURTHER INFORMATION

CSIRO Energy Technology
Merched Azzi
t +61 2 9490 5307
e merched.azzi@csiro.au
w www.csiro.au/